UNIVERSITY OF NAPLES FEDERICO II

Department of structures
for engineering and architecture

PH.D. PROGRAMME IN
STRUCTURAL GEOTECHNICAL AND SEISMIC ENGINEERING
XXX CYCLE

ANDREA MIANO

PH.D. THESIS

PERFORMANCE BASED ASSESSMENT AND RETROFIT FOR EXISTING RC STRUCTURES

TUTORS PROF. FATEMEH JALAYER AND PROF. ANDREA PROTA

2017

Abstract

The scope of this thesis is to propose a journey through probabilistic performance based assessment and retrofit design based on nonlinear dynamic analysis tools. The thesis aims to address the performance-based assessment paradigm by developing seismic fragilities and earthquake loss estimation. The "Performance-based earthquake engineering" (PBEE) for design, assessment and retrofit of building structures seeks to enhance seismic risk decision-making through assessment and design methods that have a strong scientific basis and support the stakeholders in making informed decisions. The PBEE is based on a consistent probabilistic methodological framework in which the various sources of uncertainty in seismic performance assessment of structures can be represented. The methodology can be used directly for performance assessment, or can be implemented for establishing efficient performance criteria for performance-based design. In particular, the PBEE aims to maximize the utility for a building by minimizing the expected total cost due to seismic risk, including the costs of construction and the incurred losses due to future earthquakes.

The PBEE advocates substituting the traditional single-tier design against collapse and its prescriptive rules, with a transparent multi-tier seismic design, meeting more than one discrete "performance objective" by satisfying the corresponding "performance level" (referred to as the "limit state" in the European code) expressed in terms of the physical condition of the building as a consequence of an earthquake whose intensity would be exceeded by a mean annual rate quantified as the "seismic hazard level". In other words, PBEE distinguishes itself from the prescriptive requirements of the traditional building codes by envisioning explicit verification of satisfying various performance objectives. Last but not least, the PBEE is fundamental to seismic assessment of existing buildings, seen as an indispensable step in the seismic retrofit design process.

The principal elements of the PBEE procedure can be summarized as description, definition, and quantification of earthquake intensity measures, engineering demand parameters, damage measures, and decision variables. The process encompasses the following steps: (1) calculation of ground motion hazard

by representing the uncertainty in ground motion with a probabilistic model for a parameter (or vector of parameters) related to ground motion and known as the intensity measure (IM); (2) estimation of the uncertainty in structural response expressed as a group of engineering demand parameters EDP (e.g., force and deformation-related engineering parameters) conditioned on each IM level; (3) estimation of the uncertainty in damage measure DM (i.e., physical states of damage, that describes the condition of the structure and its components) conditioned on the EDP and IM; (4) estimation of the uncertainty in the decision variable DV expressing the decision-related consequences (e.g., financial losses, fatalities, business interruption, etc.) given DM, EDP and IM. One interesting and useful characteristic of the PBEE procedure is that any of the above-mentioned intermediate steps can be collapsed. For example, the damage measure DM can be conditioned directly on intensity measure IM by collapsing the intermediate step related to the engineering demand parameter EDP. It is important to note that the performance levels should ideally be described in terms of the decision variable(s) DV. However, many modern codes and guidelines express the various discrete performance levels in terms of the incurred damage (i.e., DM).

An important focus in this thesis is dedicated to the estimation of the conditional probability of exceeding a damage measure DM expressed as the critical demand to capacity ratio throughout the structure and a given ground motion time-history and relating it directly to IM (by collapsing the intermediate EDP step). The conditional probability of exceeding a given level of DM given IM can be expressed as the structural fragility for a given performance level. In fact, the assessment of analytic structural fragility for existing buildings is one of the fundamental steps in the modern performance-based engineering. In general, methods for assessing the structural fragility for a given performance level or limit state range from the simplest methods based on the response of an equivalent single-degree-of-freedom (SDOF) model to complex nonlinear dynamic analysis procedures performed for a structural model subjected to a set of ground-motion records.

In the past fifteen years, many research efforts have been dedicated to an in-depth study of the implementation, the nuances and the potential complications of non-linear dynamic analysis procedures. These efforts have led to different methodologies such as Incremental Dynamic Analysis (IDA), Multiple-Stripe

Analysis (MSA) with conditional mean spectrum, and Cloud Analysis. This work focuses on the non-linear dynamic analysis procedure known as the Cloud Analysis. This analysis is based on fitting a linear regression model in the logarithmic scale to the pairs of structural response parameter (e.g., maximum inter-story drift) and IM (e.g., first-mode spectral acceleration) for a suite of as-recorded ground motions. This method is well-known both for the simplicity of its underlying formulation and for the relatively small number of structural analyses required. However, the Cloud Analysis is also notorious for being based on a few simplifying assumptions (fixed standard error of regression, mean response varying linearly as a function of IM in the logarithmic scale, and structural response given IM being modeled as a Lognormal distribution), and for being sensitive to the selected suite of records.

A functional variation to the original Cloud Analysis is presented in order to take into account the cases leading to structural collapse. Moreover, to reduce record-selection-dependence of the results, a Bayesian version of the Cloud Analysis considering the "collapse-cases" is presented in which the uncertainty in the structural fragility model parameters is considered. This leads to a Robust Fragility estimate and a desired confidence interval defined around it. The entire method is based on the adoption of a normalized demand to capacity ratio as the damage measure/decision performance variable. Herein, as said, a normalized demand to capacity ratio coined as "critical demand to capacity ratio" and denoted as *DCR,* takes the structure closest to the onset of a prescribed limit state *LS*, is adopted. The adoption of DCR_{LS} as performance variable is also central to a new nonlinear dynamic analysis procedure referred to as "*Cloud to IDA*" that exploits the Cloud Analysis to perform IDA in a more efficient manner.

Evaluation of structural behaviour under seismic actions for an existing building encompasses the consideration of numerous sources of uncertainty associated with the seismic action and the structural modelling. In the past decades, significant research efforts have been carried out and substantial progress has been made towards the consideration of various sources of uncertainty into structural performance assessment and design frameworks. Several alternative methods have been proposed that combine reliability methods such as the first order second moment (FOSM and MVFOSM) methods, response surface methods, simulation-based methods (e.g., Monte Carlo, Latin Hypercube

Sampling) with non-linear dynamic procedures such as IDA based on recorded ground motions in order to take into account sources of uncertainties other than record-to-records variability.

This thesis aims to quantify the impact of structural modeling uncertainties on the seismic performance assessment for an existing case-study building. Herein, the proposed version of the Cloud Analysis, considering the collapse cases, is implemented to consider the record-to-record variability, the structural modeling uncertainties and also the uncertainties in the parameters of the adopted fragility model, through a Bayesian procedure. The presented procedure can lead to reliable results with a considerably lower computational effort in comparison to the methods available in literature.

Finally, the PBEE methodology is implemented for the case-study building in order to choose the most appropriate seismic retrofit design that maximizes the utility (by minimizing the expected costs) and satisfies the safety-checking for three different performance levels. To this end, the non-ductile older RC frame of the case-study is retrofit designed based on different strategies aimed to improve the seismic performance of the frame. The case-study moment resisting frame is modeled using structural elements with fiber sections in order to take into account the flexural-axial interactions. Furthermore, the flexural-axial-shear interactions and the fixed end rotations due to bar slip in the columns are considered by adding zero-length springs to column ends. The performance-based safety-checking procedure is based on the Demand and Capacity Factored Design (DCFD) format. Amongst the viable retrofit designs that satisfy the risk-related safety-checking DCFD criteria, the one that corresponds to the minimum expected loss over the life cycle of the building is identified.

Acknowledgments

Have the opportunity to attend a PhD program, meant for me to continue the study of the engineering topics learned during the master degree, to acquire the knowledge of new concepts and theories, to develop new methodologies and learn new instruments.

First of all, I express my thanks to Prof. Fatemeh Jalayer, the person that taught me what it means the research. Her suggestions and observations were fundamental for the development of the thesis.

I express my gratitude to Prof. Andrea Prota for the constant support and for the opportunity given to me to be part of the Department of Structures for Engineering and Architecture of the University of Naples Federico II and of his research group.

I express my thanks to Prof. Halil Sezen for the crucial support in the understanding of the structural modeling issues, during my research exchange period at Ohio State University under his supervision. Moreover, he reviewed the thesis, contributing to improving the work.

I express my acknowledgements to Dr. Paolo Castaldo for reviewing the thesis and contributing to enriching the work.

Sincere gratitude to Dr. Hossein Ebrahimian for sharing with me his experience and knowledge, essential for the success of the present study.

Thanks to all my department colleagues for their sincere friendship and because they gave me the opportunity to work in a very pleasant and cooperative environment.

Thanks to Anna and to my family, for their understanding and support, without which I would not have reached my objective today.

Naples, December 2017

Table of Contents

List of Figures

List of Tables

Chapter 1

INTRODUCTION

1.1 GENERAL OVERVIEW

Major earthquakes that hit developed countries in the past years, causing relatively few casualties but very large damage to property and economic losses, led, in response to this, to the origin of "Performance-based earthquake engineering" (PBEE) for design, assessment and retrofit of building structures, based on the work developed by the "Pacific Earthquake Engineering Research Center" (PEER; [1-3]). PBEE seeks to enhance seismic risk decision-making through assessment and design methods that have a strong scientific basis and support the stakeholders in making informed decisions. In fact, the PEER developed a robust and efficient methodology for performing PBEE, in which the performance design, assessment and retrofit processes are divided into logical elements that can be studied and solved in a rigorous manner. Moreover, the PBEE is based on a consistent probabilistic methodological framework in which the various sources of uncertainty in seismic performance assessment of structures can be represented. The methodology can be used directly for performance assessment, or can be implemented for establishing efficient performance criteria for performance-based design.

It's to note that PBEE aims to maximize the utility from the use of a building by minimizing its expected total cost, including the short-term cost of the work and the expected value of the loss in future earthquakes (in terms of casualties, cost of repair or replacement, loss of use, etc.). It's possible to take into account all possible future seismic events with their annual probability and carry out a convolution with the corresponding consequences during the design working life of the building, but under some circumstances, this is not practical. Therefore, at

present the PBEE advocates substituting the traditional single-tier design against collapse and its prescriptive rules, with a transparent multi-tier seismic design, meeting more than one discrete "performance objective" by satisfying the corresponding "performance level" (referred to as the "limit state" in the European code) expressed in terms of the physical condition of the building as a consequence of an earthquake whose intensity would be exceeded by a mean annual rate quantified as the "seismic hazard level". In other words, PBEE distinguishes itself from the prescriptive requirements of the traditional building codes by envisioning explicit verification of satisfying various performance objectives. However, the definition of explicitly probabilistic performance objectives has found its way into design codes and guidelines as early as 1983 [4-7] and today there is a widespread of this procedure in the codes (e.g. [8-11]). Last but not least, the PBEE is fundamental to seismic assessment of existing buildings, seen as an indispensable step in the seismic retrofit design process [11-12]. In fact, also the seismic retrofit can be seen as the design of measures to improve the seismic performance of structural or nonstructural components of a building by correcting deficiencies identified in a seismic evaluation relative to a selected performance objective [8,11,13].

The principal elements of the PBEE procedure can be summarized as description, definition, and quantification of earthquake intensity measures, engineering demand parameters, damage measures, and decision variables [3-14]. The process encompasses the following steps:

(1) calculation of ground motion hazard by representing the uncertainty in ground motion with a probabilistic model for a parameter (or vector of parameters) related to ground motion and known as the intensity measure (IM). IM defines in a probabilistic sense the salient features of the ground motion hazard that affect structural response;

(2) estimation of the uncertainty in structural response expressed as a group of engineering demand parameters EDP conditioned on each IM level. In particular, the EDP describes structural response in terms of force and deformation-related engineering parameters, calculated by simulation of the building to the input ground motions;

(3) estimation of the uncertainty in damage measure DM (i.e., physical states of damages, that describe the condition of the structure and its components) conditioned on the EDP and IM;

(4) estimation of the uncertainty in the decision variable DV expressing the decision-related consequences (e.g., financial losses, fatalities, business interruption, etc.) given DM, EDP and IM. So, DV translate the damage into quantities that enter into risk management decisions.

Each stage of the process is performed and executed (more-or-less) independently, and then linked back together, as expressed in the following integral form:

$$\lambda(DV) = \iiint G[DV \mid DM] \cdot \left| \frac{dG[DM \mid EDP]}{dDM} \right| \cdot \left| \frac{dG[EDP \mid IM]}{dEDP} \right| \cdot \left| \frac{d\lambda[IM]}{dIM} \right| \cdot dIM \cdot dEDP \cdot dDM \quad (1.1)$$

where G[Y|X] denotes generically the conditional Complementary Cumulative Density Function (CCDF) of Y given a certain value of X, and λ(Y) denotes the mean annual exceedance rate (mean annual frequency) of Y. As it can be observed from Equation 1.1, the PEER framework enjoys a modular structure and benefits from the assumed conditional independence between the main parameters (i.e., the conditional independence of *DV*|*DM* from *EDP* and *IM* and other ground motion parameters, *DM*|*EDP* from *IM* and other ground motion parameters, and *EDP*|*IM* from other ground motion parameters, such as but not limited to, magnitude and distance).

One interesting and useful characteristic of the PBEE procedure is that any of the above-mentioned intermediate steps can be collapsed. For example, the damage measure *DM* can be conditioned directly on intensity measure *IM* by collapsing the intermediate step related to the engineering demand parameter *EDP*. It is important to note that the performance levels should ideally be described in terms of the decision variable(s) DV. However, many modern codes and guidelines express the various discrete performance levels in terms of the incurred damage (i.e., DM, [8, 11, 13]).

An important focus in this thesis is dedicated to the estimation of the conditional probability of exceeding a damage measure *DM* expressed as the

critical demand to capacity ratio throughout the structure and a given ground motion time-history and relating it directly to *IM* (by collapsing the intermediate *EDP* step). The conditional probability of exceeding a given level of *DM* given *IM* can be expressed as the structural fragility for a given performance level. In fact, the assessment of analytic structural fragility for existing buildings is one of the fundamental steps in the modern performance-based engineering [2]. This consideration is based on the fact that many existing reinforced concrete (RC) moment-resisting frame buildings in regions with high seismicity were built without adequate seismic-detailing requirements and are particularly vulnerable to seismic excitation. Identifying accurately the level of performance can facilitate efficient seismic assessment and classification of these buildings.

In general, methods for assessing the structural fragility for a given performance level or limit state range from the simplest methods based on the response of an equivalent single-degree-of-freedom (SDOF) model to complex nonlinear dynamic analysis procedures performed for a structural model subjected to a set of ground-motion records [15]. In the past fifteen years, many research efforts have been dedicated to an in-depth study of the implementation, the nuances and the potential complications of non-linear dynamic analysis procedures. Initial versions of procedures later called Incremental Dynamic Analysis (IDA [16]), Multiple-Stripe Analysis (MSA, [17-18]), and Cloud Analysis [19] could be seen in works such as Bertero ([20], IDA), Singhal and Kiremidjian ([21], MSA), Bazzurro et al. ([22], MSA, Cloud), Shome et al. ([23], Cloud), and Luco and Cornell ([24], Cloud). Both MSA and IDA involve the prediction of structural performance (often measured in terms of maximum inter-story drift) over the height of structure, over the entire time-history for a suite of ground motions, and based on increasing linear scaling of ground motion records in amplitude. The two methods are practically the same, if the suite of records remains invariant during the scaling. However, the MSA has the potential of using different suites of ground motion at different intensity levels. The IDA has been widely used by researchers to capture the record-to-record variability in structural response to ground motion. IDA is based on a fixed suite of records scaled successively to higher intensity levels. The Conditional Mean Spectrum (CMS) [25-26], instead, “anchors” the acceleration response spectra to the first-mode spectral acceleration value. The CMS provides a useful instrument for careful

record selection based on mean spectral shape considerations adopting the first-mode spectral acceleration as the IM. Baker and Cornell [25] have selected, using CMS, different suites of ground motion records for various intensity levels and have implemented them to perform MSA. They have shown that coupling careful record selection using the CMS with MSA leads to results analogous to those obtained based on record selection considering the expected distribution of epsilon at various intensity levels.

The work of this thesis focuses on the non-linear dynamic analysis procedure known as the Cloud Analysis. This analysis is based on fitting a linear regression model in the logarithmic scale to the pairs of structural response parameter (e.g., maximum inter-story drift) and IM (e.g., first-mode spectral acceleration) for a suite of as-recorded ground motions. This method is well-known both for the simplicity of its underlying formulation and for the relatively small number of structural analyses required. It has had a relatively wide use among researchers, e.g., [27-30]. However, the Cloud Analysis is also notorious for being based on a few simplifying assumptions (fixed standard error of regression, mean response varying linearly as a function of IM in the logarithmic scale, and structural response given IM being modeled as a Lognormal distribution), and for being sensitive to the selected suite of records [31].

A functional variation to the original Cloud Analysis, is proposed in this thesis in order to take into account the cases leading to structural collapse (and/or dynamic instability due to large deformations, [32]). The proposed method, apart from resolving the frequently-encountered problem of the "collapse cases", leads to a more realistic mathematical model for the structural response given IM. Moreover, to reduce record-selection-dependence of the results, a Bayesian version of the Cloud Analysis considering the "collapse-cases" is presented in which the uncertainty in the structural fragility model parameters is considered. This leads to a Robust Fragility estimate and a desired confidence interval defined around it.

The entire method is based on the adoption of a normalized demand to capacity ratio as the damage measure/decision performance variable. Herein, liberally inspired from the code-based definition of demand to capacity ratios evaluated at the local level [33] for safety-checking purposes, a normalized demand to capacity ratio coined as "critical demand to capacity ratio" and denoted

as *DCR,* that takes the structure closest to the onset of a prescribed limit state *LS*, is adopted. This performance variable has been proposed as an effective and rigorous way of mapping the local structural behavior to the global level [34]. It has been shown [31-32, 35-39] that adopting DCR_{LS} as structural damage measure/performance variable facilitates the determination of the onset of a given limit state. DCR_{LS} is --by definition-- equal to unity at the onset of the limit state.

The adoption of DCR_{LS} as performance variable is also central to a new nonlinear dynamic analysis procedure referred to as "*Cloud to IDA*" that exploits the Cloud Analysis to perform IDA in a more efficient manner [39]. In fact, plotting the IDA curves in terms of such variable facilitates the identification of intensity values corresponding to the onset of limit state as the intensity values corresponding to a DCR_{LS} equal to unity through the IDA curves. Based on these assumptions, an IDA curve can be obtained with only two data points consisting of pairs of intensity versus critical DCR_{LS}. It is most desirable that the interval of values covered by the two points includes the demand to capacity ratio equal to one --to avoid extrapolation for estimating the intensity level corresponding to the onset of the limit state. Based on such a consideration, the simple linear (logarithmic) regression predictions, made based on the results of the structural analysis to the un-scaled registered records (a.k.a., Cloud Analysis), can be exploited to identify the range of intensity values near DCR_{LS} equal to unity. Definitively, "*Cloud to IDA*" procedure delivers *IM*-based fragility curves by exploiting IDA curves constructed with minimum amount of scaling and minimum number of analyses strictly necessary.

Evaluation of structural behaviour under seismic actions for an existing building encompasses the consideration of numerous sources of uncertainty associated with the seismic action and the structural modeling. Traditionally, seismic-design codes have addressed the uncertainties by allowing some degree of conservatism in evaluating demand and capacity at the level of structural components; nevertheless, the link to the overall performance of the structure remains unclear. Strictly speaking, the reliability of the structure to withstand future events remains more-or-less unknown to the designer while employing various established code-based approaches. Therefore, in the past decades, significant research efforts have been carried out and substantial progress has been made towards the consideration of various sources of uncertainty into

structural performance assessment and design frameworks. Several alternative methods have been proposed that combine reliability methods such as the first order second moment (FOSM and MVFOSM, see for example [40]) methods, response surface methods [41], simulation-based methods (e.g., Monte Carlo, Latin Hypercube Sampling) with non-linear dynamic procedures such as IDA based on recorded ground motions in order to take into account sources of uncertainties other than record-to-records variability [42-45].

This thesis aims to quantify the impact of structural modeling uncertainties on the seismic performance assessment for an existing case-study building. The large amount of uncertainty present in determining the structural modeling parameters is investigated. Considering the partial information available related to material properties, construction details and also the uncertainty in the capacity models, the impact of modeling uncertainties on the seismic performance assessment can be relevant. This work wants to highlight that, for existing buildings, explicit consideration of modeling uncertainty in the process of the assessment of structural performance can lead to more accurate results. In particular, herein, the proposed version of the Cloud Analysis considering the collapse cases, is implemented to consider the record-to-record variability, the structural modeling uncertainties and also the uncertainties in the parameters of the adopted fragility model, through a Bayesian procedure [37].

Finally, the PBEE methodology is implemented for the case-study building in order to choose the most appropriate seismic retrofit design that maximizes the utility (by minimizing the expected costs) and satisfies the safety-checking for three different performance levels. This type of works has been a persistent research theme over the past decade within the earthquake engineering community in the context of the performance-based assessment and retrofit of existing buildings in order to develop seismic fragilities [28, 46-47] and earthquake loss estimation [48-50].

A non-ductile older RC frame of the case-study is retrofit designed based on different strategies aimed to improve the seismic performance of the frame. The case-study moment resisting frame is modeled using structural elements with fiber sections in order to take into account the flexural-axial interactions [see [37, 51] for more details]. Furthermore, the flexural-axial-shear interactions and the

fixed end rotations due to bar slip in the columns are considered by adding zero-length springs to column ends [52-53].

A nonlinear performance-based methodology is used to evaluate the different retrofit methods applied to the bare frame, considering hazard level, target performance levels, and also life cycle cost estimates. The performance-based safety-checking procedure is based on the Demand and Capacity Factored Design (DCFD) format [17-19]. At the end of the procedure, after the verification of the structural safety through risk-related safety-checking criteria (DCFD), the performance-based retrofit design leads to the optimal retrofit strategy by comparing the expected loss during the service life of the structure for each viable retrofit option. Amongst the viable retrofit designs that satisfy the risk-related safety-checking DCFD criteria, the one that corresponds to the minimum expected loss over the life cycle of the building is identified.

1.2 ORGANIZATION AND OUTLINE

The dissertation is organized into seven chapters with the following contents:

Chapter 2 presents the modeling strategies adopted in the thesis. It is clear that, for existing building, it is necessary to accurately model materials and column members and to choose the most suitable shear capacity model for assessment in order to capture the flexure, shear and flexure-shear failure modes in columns and the potential collapse of the building. Based on these considerations, a detailed modeling strategy is presented in order to explicitly capture the flexure-shear-axial interaction of structural members and the bar slip phenomenon. Initially, analytical models and theories developed in the past years are presented. Therefore, a suitable procedure is proposed to address critical modeling issues while predicting the response accurately and keeping overall computational process simple with easy implementation. This procedure, based on the single modeling of flexural, shear and bar slip behaviors and using specific rules in order to combined them, predicts the total lateral response of the members.

Chapter 3 proposes a journey through probabilistic performance based assessment and design based on nonlinear dynamic analysis tools. Cloud Analysis is used to perform fragility assessment using un-scaled ground motion records

and the results are compared with those obtained from the IDA and MSA with conditional mean spectrum. A functional variation to the original Cloud Analysis is presented in order to take into account the cases leading to structural collapse (and/or dynamic instability due to large deformations). The proposed method, apart from resolving the frequently-encountered problem of the "collapse cases", leads to a more realistic mathematical model for the structural response given IM. Moreover, to reduce record-selection-dependence of the results, a Bayesian version of the Cloud Analysis considering the "collapse-cases" is presented in which the uncertainty in the structural fragility model parameters is considered. This leads to a Robust Fragility estimate and a desired confidence interval defined around it.

Chapter 4 proposes a new nonlinear dynamic analysis procedure referred to as "*Cloud to IDA*" that exploits the Cloud Analysis to perform IDA in a more efficient manner. Incremental dynamic analysis (IDA) is a procedure in which a structure is subjected to a suite of ground motion records that are linearly scaled up to multiple levels of intensity. This leads to curves of structural response/performance variable usually expressed in terms of maximum inter-story drift ratio versus intensity, commonly known as the IDA curves. It is known that implementation of IDA usually involves a significant computational effort. Employing a performance variable expressed in terms of the critical demand to capacity ratio throughout the structure, which is equal to unity at the onset of the limit state, facilitates the implementation of the IDA procedure. An efficient solution for performing IDA, in which the intensity levels to scale to are chosen strategically to perform the minimum number of analyses and minimum amount of scaling strictly necessary, is presented. To this end, one can exploit the simple linear (logarithmic) regression predictions made based on the results of the structural analysis to the un-scaled registered records (a.k.a., Cloud Analysis) to identify the range of intensity values near to the of structural response/performance equal to unity. Definitively, "*Cloud to IDA*" procedure delivers *IM*-based fragility curves by exploiting IDA curves constructed with minimum amount of scaling and minimum number of analyses strictly necessary.

Chapter 5 deals with the quantification of the impact of structural modeling uncertainty on the seismic performance assessment for existing building. The

large amount of uncertainty present in determining the structural modeling parameters is investigated. Considering the partial information available related to material properties, construction details and also the uncertainty in the capacity models, the impact of modeling uncertainties on the seismic performance assessment can be relevant. This chapter shows that, for this existing structures, explicit consideration of modeling uncertainty in the process of the assessment of structural performance can lead to more accurate results. The proposed version of the Cloud Analysis considering the collapse cases, is implemented to consider the record-to-record variability, the structural modeling uncertainties and also the uncertainties in the parameters of the adopted fragility model, through a Bayesian procedure. The presented procedure can lead to reliable results with a considerably lower computational effort in comparison to the other methods available in literature.

Chapter 6 presents a nonlinear performance-based methodology to evaluate different retrofit methods considering hazard level, target performance levels, and also life cycle cost estimates. The methodology is illustrated using three retrofit strategies (with different options for each strategy, based on an iterative process) for a case study building, used to improve the seismic performance of the frame. The performance-based retrofit design leads to the optimal retrofit strategy by comparing the expected loss during the service life of the structure for each viable retrofit option, based on risk-related safety-checking criteria. In summary, the performance-based procedure implemented in this chapter identifies the most economic retrofit solution that satisfies structural safety requirements for a given performance level. The process has been developed with reference only to the record to record variability, while at the end of the chapter a brief insight about the consideration of the impact of structural modeling uncertainty on the seismic performance assessment is proposed with reference to the case study building.

Chapter 7 presents the conclusions from the present research along with suggestion for future research.

1.3 OBJECTIVES

The scope of this thesis is to propose a journey through probabilistic performance based assessment and retrofit design based on nonlinear dynamic analysis tools. This paragraph aims to synthesize the main objectives achieved in this thesis. As conceptual goal, the thesis aims to address the performance-based assessment paradigm by developing seismic fragilities and earthquake loss estimation. In general, in order to achieve this goal, it starts from an overall comparison and discussion about the results from the main known nonlinear dynamic procedures. The target analysis in this work is the Cloud Analysis, performed based on the use of unscaled ground motions, with a low computational effort. The results of Cloud Analysis lead to reasonable and efficient fragility estimates. This objective is shown by comparing the Cloud Analysis results with those obtained from the other main known nonlinear dynamic procedures, that are IDA and MSA with conditional mean spectrum.

In particular, a functional variation to the original Cloud Analysis is proposed in order to take into account the cases leading to structural collapse. Moreover, to reduce record-selection-dependence of the results, a Bayesian version of the Cloud Analysis considering the "collapse-cases" is presented in which the uncertainty in the structural fragility model parameters is considered. This leads to a Robust Fragility estimate and a desired confidence interval defined around it.

Another new propose of the thesis is a new nonlinear dynamic analysis procedure referred to as "*Cloud to IDA*" that exploits the Cloud Analysis to perform IDA in a more efficient manner. This procedure performs IDA based on the consideration that the intensity levels to scale should be chosen strategically to scaling in a strictly necessary manner the records.

The following critical point of the thesis aims to quantify the impact of structural modeling uncertainty on the seismic performance assessment for existing building. Herein, the proposed version of the Cloud Analysis considering the collapse cases, is implemented to consider the record-to-record variability, the structural modeling uncertainties and also the uncertainties in the parameters of the adopted fragility model, through a Bayesian procedure.

As final application, the modified version of the Cloud Analysis, is used as basis for presenting a nonlinear performance-based methodology to evaluate

different retrofit methods considering hazard level, target performance levels, and also life cycle cost estimates, identifying the most economic retrofit solution that satisfies structural safety requirements for a set of given limit states/performance levels.

1.4 CASE STUDY

One of the longitudinal frames and one of the transverse frames of the seven-story hotel building in Van Nuys, California, are modeled and analyzed in this study [37, 51, 54-55]. The building is located in the San Fernando Valley of Los Angeles County (34.221° north latitude, 118.471° west longitude). The frame building was constructed in 1966 according to the 1964 Los Angeles City Building Code. The building was damaged in the M6.7 1994 Northridge earthquake. After the 1994 earthquake, the building was retrofitted with addition of new RC shear walls. Figure 1.1 shows the Holiday Inn hotel building and some photos of the damages in the building after Northridge earthquake (1994) in the longitudinal direction.

Figure 1.1: (a) Holiday Inn hotel building [56] and (b) photos of the damages in the building after Northridge earthquake, 1994, in the longitudinal direction [57].

Columns in the longitudinal and in the transverse frames are 356 mm wide and 508 mm deep, i.e., they are oriented to bend in their weak direction when resisting lateral forces in the plane of the longitudinal frame. Spandrel beams in the north frame are typically 406 mm wide and 762 mm deep in the second floor,

406 mm wide and 572 mm deep in the third through seventh floors, and 406 mm by 559 mm at the roof level. Column concrete has a compressive nominal strength f'_c of 34.5 MPa in the first story, 27.6 MPa in the second story, and 20.7 MPa in other floors. Beam and slab concrete strength f'_c is 27.6 MPa in the second floor and 20.7 MPa in other floors. Grade 60 (nominal f_y=414 MPa) reinforcing steel is used in columns. The specified nominal yield strength, f_y, is 276 MPa (Grade 40) for the steel used in beams and slabs.

Figure 1.2 a and 1.2 b show the longitudinal and the transverse frames modeled in this research.

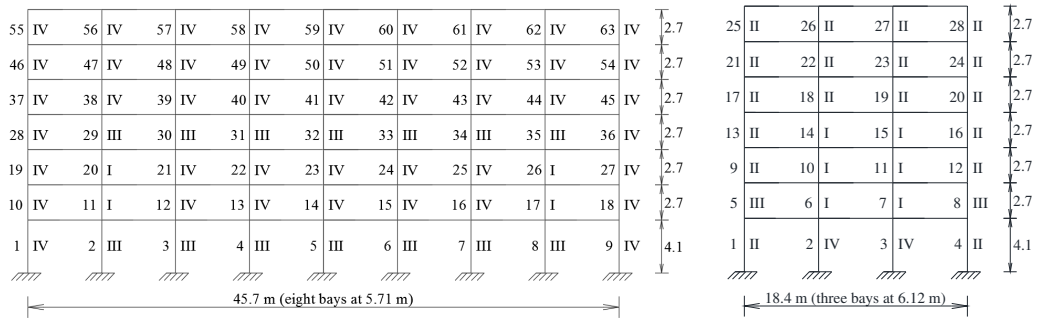

Figure 1.2: (a) Geometric configuration of the longitudinal frame and (b) geometric configuration of the transverse frame.

The column and beam reinforcement details are provided in Krawinkler [54]. In the longitudinal frame (Figure 2a), end columns include eight No.9 longitudinal bars between ground and second floors and six No.7 bars in other stories. The column ties are No.3 spaced at 310 mm on center between ground and second floors and No.2 spaced at 310 mm on center above the second floor level. All middle columns are reinforced with ten No.9 longitudinal bars between ground and second floors, six No.9 bars between second and fourth floors and six No.7 bars above the fourth floor (with the exception of columns 11, 17, 20, 26, reinforced with eight No.9 bars between second and fourth floors). The No.3 and No.2 column ties are spaced at 310 mm below and above the fourth floor level, respectively. Beams are reinforced with two No.6 longitudinal bars at the bottom and anywhere from two No.8 to three No.9 at the top. The stirrups are No.3 spaced at 310 mm on center above the ground.

In the transverse frame (Figure 2b), end columns include eight No.9 longitudinal bars between ground and second floors and six No.7 bars in other stories. The column ties are No.3 spaced at 310 mm on center between ground and second floors and No.2 spaced at 310 mm on center above the second floor level. Middle columns are reinforced with twelve No.9 longitudinal bars between ground and second floors, eight No.9 bars between second and fourth floors, six No.9 bars between fourth and fifth floors and six No.7 bars above the fifth floor. The No.3 and No.2 column ties are spaced at 310 mm below and above the fifth floor level, respectively. Beams are reinforced with two No.6 longitudinal bars at the bottom and anywhere from two No.8 to three No.9 at the top. The stirrups are No.3 spaced at 310 mm on center above the ground.

1.5 REFERENCES

[1] Krawinkler, H., 1999. Challenges and progress in performance-based earthquake engineering. International Seminar on Seismic Engineering for Tomorrow-In Honor of Professor Hiroshi Akiyama, Tokyo, Japan, November 26, 1999.

[2] Cornell, C.A., and Krawinkler, H., 2000. Progress and challenges in seismic performance assessment. PEER Center News; 3 (2): 1-2

[3] Moehle, J., and Deierlein., G.G., 2004. A framework methodology for performance-based earthquake engineering; 13th world conference on earthquake engineering.

[4] Hickman, J.W., 1983. PRA procedures guide: a guide to the performance of probabilistic risk assessments for nuclear power plants. NUREG/CR-2300, U.S. Nuclear Regulatory Commission, Washington, DC.

[5] Kennedy, R.P., Short, A.S., McDonald, R.R., McCann, M.W., Murray, R.C., Hill, J.R., and Gopinath, V., 1994. Natural phenomena hazards design and evaluation criteria for department of energy facilities. DOE-STD-1020–94, U.S. Department of Energy, Washington, DC.

[6] FEMA-350 Recommended Seismic Design Criteria for New Steel Moment-Frame Buildings. Federal Emergency Management Agency: Washington, DC, 2000.

[7] FEMA P-58-1 Seismic Performance Assessment of Buildings Volume 1-Methodology. Federal Emergency Management Agency: Washington, DC, 2012.

[8] ASCE/SEI 41-13. Seismic Evaluation and Retrofit of Existing Buildings. American Society of Civil Engineers: Reston, VA, 2014.

[9] FEMA P440A. Effects of strength and stiffness degradation on seismic response. Washington (DC): Federal Emergency Management Agency; 2009.

[10] FEMA P695. Quantification of Building Seismic Performance Factors. Washington (DC): Federal Emergency Management Agency; 2009.

[11] CEN. Eurocode 8: Design of structures for earthquake resistance, Part 3: Assessment and retrofitting of buildings. EN 1998-1 CEN Brussels, April 2004.

[12] FEMA P-58-1. Seismic assessment performance of buildings, Volume 1-Methodology. Washington (DC): Federal Emergency Management Agency; 2012.

[13] FEMA 356. Prestandard and Commentary for the Seismic Rehabilitation of Buildings. Washington (DC): Federal Emergency Management Agency; 2000.

[14] Ebrahimian, H., and De Risi R.., 2014. Seismic reliability assessment, alternative methods for. Encyclopedia of Earthquake Engineering: 1-29.

[15] Villaverde, R., 2007. Methods to assess the seismic collapse capacity of building structures: State of the art. Journal of Structural Engineering; 133 (1): 57-66.

[16] Vamvatsikos, D., and Cornell, C.A., 2002. Incremental dynamic analysis. Earthquake Engineering and Structural Dynamics; 31 (3): 491-514.

[17] Jalayer, F., and Cornell, C.A., 2003. A Technical Framework for Probability-Based Demand and Capacity Factor Design (DCFD) Seismic Formats. Pacific Earthquake Engineering Center (PEER) 2003/08.

[18] Jalayer, F., and Cornell, C.A., 2009. Alternative non-linear demand estimation methods for probability-based seismic assessments. Earthquake Engineering and Structural Dynamics; 38 (8): 951-972.

[19] Cornell, C.A., Jalayer, F., Hamburger, R.O., and Foutch, D.A., 2002. Probabilistic basis for 2000 SAC federal emergency management agency steel moment frame guidelines. Journal of Structural Engineering (ASCE); 128 (4): 526-533.

[20] Bertero, V.V., 1980. Strength and deformation capacities of buildings under extreme environments. In Structural engineering and structural mechanics, A Volume Honoring Edgar P. Popov, Pister K (ed.). Prentice-Hall: Englewood Cliffs, N.J.; 188-237.

[21] Singhal, A., and Kiremidjian, A.S., 1996. Method for probabilistic evaluation of seismic structural damage. Journal of Structural Engineering; 122 (12): 1459-1467.

[22] Bazzurro, P., Cornell, C.A., Shome, N., and Carballo, J.E., 1998. Three proposals for characterizing MDOF nonlinear seismic response. Journal of Structural Engineering (ASCE); 124 (11): 1281-1289.

[23] Shome, N., Cornell, C.A., Bazzurro, P., and Carballo, J.E., 1998. Earthquakes, records, and nonlinear responses. Earthquake Spectra; 14 (3): 469-500.

[24] Luco, N., and Cornell, C.A., 1998. Seismic drift demands for two SMRF structures with brittle connections. Structural Engineering World Wide; Elsevier Science Ltd., Oxford, England, Paper T158-3.

[25] Baker, J.W., and Cornell C.A., 2006. Spectral shape, epsilon and record selection. Earthquake Engineering and Structural Dynamics; 35 (9): 1077-1095.

[26] Baker, J.W., 2011. Conditional Mean Spectrum: Tool for ground motion selection. Journal of Structural Engineering (ASCE); 137 (3): 322–331.

[27] Ellingwood, B.R, Celik, O.C., and Kinali, K., 2007. Fragility assessment of building structural systems in Mid - America. Earthquake Engineering and Structural Dynamics; 36 (13): 1935-1952.

[28] Celik, O.C., and Ellingwood, B.R., 2010. Seismic fragilities for non-ductile reinforced concrete frames–Role of aleatoric and epistemic uncertainties. Structural Safety; 32 (1): 1-12.

[29] Elefante, L., Jalayer, F., Iervolino, I., and Manfredi. G., 2010. Disaggregation-based response weighting scheme for seismic risk assessment of structures. Soil Dynamics and Earthquake Engineering; 30 (2): 1513-1527.

[30] Jeong, S.H., Mwafy, A.M., and Elnashai, A.S., 2012. Probabilistic seismic performance assessment of code-compliant multi-story RC buildings. Engineering Structures; 34: 527-537.

[31] Jalayer, F., De Risi, R., and Manfredi, G., 2015. Bayesian Cloud Analysis: efficient structural fragility assessment using linear regression. Bulletin of Earthquake Engineering; 13 (4): 1183-1203.

[32] Jalayer, F., Ebrahimian H., Miano A., Manfredi G. and Sezen H., 2017. Analytical fragility assessment using un-scaled ground motion records. Earthquake Engineering & Structural Dynamics; https://doi.org/10.1002/eqe.2922.

[33] ASCE/SEI 41-13. Seismic evaluation and retrofit of existing buildings. American Society of Civil Engineers: Reston, VA, 2014.

[34] Jalayer, F., Franchin, P., and Pinto, P.E., 2007. A scalar damage measure for seismic reliability analysis of RC frames. Earthquake Engineering and Structural Dynamics; 36(13): 2059-2079.

[35] Miano, A., Jalayer, F., and Prota, A., 2016. Cloud to IDA: a very efficient solution for performing Incremental Dynamic Analysis. AICAP 2016 Congress, Italian concrete days, Rome, Italy, 27-28 October 2016.

[36] Ebrahimian, H., Jalayer, F., and Manfredi, G., 2015. Seismic retrofit decision-making of bridges based on life-cycle cost criteria. In: Proceedings of the 5th ECCOMAS Thematic Conference on Computational Methods in Structural Dynamics and Earthquake Engineering (COMPDYN 2015), M. Papadrakakis, V. Papadopoulos, V. Plevris (eds.), Crete Island, Greece, 25-27 May 2015.

[37] Miano, A., Sezen, H., Jalayer, F., and Prota, A., 2017. Performance based comparison of different retrofit methods for reinforced concrete structures. In: Proceedings of the 6th ECCOMAS Thematic Conference on Computational Methods in Structural Dynamics and Earthquake Engineering (COMPDYN 2017), Rhodes, Greece, 15-17 June 2017.

[38] Miano, A., Jalayer, F., and Prota, A., 2017. Considering Structural Modeling Uncertainties usign Bayesian Cloud Analysis. In: Proceedings of the 6th ECCOMAS Thematic Conference on Computational Methods in Structural Dynamics and Earthquake Engineering (COMPDYN 2017), Rhodes, Greece, 15-17 June 2017.

[39] Miano. A., Jalayer. F., Ebrahimian, H., and Prota, A., 2017. Cloud to IDA: Efficient Fragility Assessment with Limited Scaling. Earthquake Engineering and Structural Dynamics (Under Review).

[40] Melchers, R.E., 1987. Structural reliability. Horwood.

[41] Schotanus, M.I.J., Franchin, P., Lupoi, A., and Pinto, P.E., 2004. Seismic fragility analysis of 3D structures. Structural Safety, 26(4), 421-441.

[42] Dolsek, M., 2009. Incremental dynamic analysis with consideration of modeling uncertainties. Earthquake Engineering & Structural Dynamics, 38(6), 805-825.

[43] Vamvatsikos, D., and Fragiadakis, M., 2010. Incremental dynamic analysis for estimating seismic performance sensitivity and uncertainty. Earthquake Engineering and Structural Dynamics, 39(2), 141-163.

[44] Celarec, D., and Dolšek, M., 2013. The impact of modelling uncertainties on the seismic performance assessment of reinforced concrete frame buildings. Engineering Structures, 52, 340-354.

[45] Liel, A.B., Haselton, C.B., Deierlein, G.G., and Baker, J.W., 2009. Incorporating modeling uncertainties in the assessment of seismic collapse risk of buildings. Structural Safety, 31(2), 197-211.

[46] Jeong, S. H., Mwafy, A. M., and Elnashai, A. S., 2012. Probabilistic seismic performance assessment of code-compliant multi-story RC buildings, Engineering Structures, 34, 527-537.

[47] Zareian, F., Kaviani, P., and Taciroglu, E., 2015. Multiphase Performance Assessment of Structural Response to Seismic Excitations, Journal of Structural Engineering, 141(11), 04015041.

[48] Aslani, H., and Miranda, E., 2005. Probabilistic earthquake loss estimation and loss disaggregation in buildings, dissertation, Stanford University.

[49] Goulet, C.A., Haselton, C.B., Mitrani-Reiser, J., Beck, J.L., Deierlein, G.G., Porter, K.A., and Stewart, J.P., 2007. Evaluation of the seismic performance of a code-conforming reinforced-concrete frame building-from seismic hazard to collapse safety and economic losses. Earthquake Engineering & Structural Dynamics, 36(13), 1973-1997.

[50] Liel, A.B., and Deierlein, G.G., 2013. Cost-benefit evaluation of seismic risk mitigation alternatives for older concrete frame buildings, Earthquake Spectra, 29(4), 1391-1411.

[51] Miano A., Sezen H., Jalayer F., and Prota A. Performance based assessment methodology for retrofit of buildings. Earthq Spectra (Under Review).

[52] Setzler, E.J. and Sezen, H., 2008. Model for the lateral behavior of reinforced concrete columns including shear deformations. Earthq Spectra; 24(2): 493-511.

[53] Sezen, H., 2008. Shear deformation model for reinforced concrete columns. Struct Eng Mech; 28(1): 39-52.

[54] Krawinkler, H., 2005. Van Nuys hotel building testbed report: exercising seismic performance assessment, Technical Report PEER 2005/11, Berkeley, USA.

[55] Miano, A., Sezen, H., Jalayer, F., and Prota, A., 2017. Probability based comparison of retrofit methods for existing nonductile concrete frames. In: Proceedings of the 4th Thematic Conference on Smart Monitoring, Assessment and Rehabilitation of Civil Structures (SMAR 2017), Zurich, Switzerland, 13-15 September 2017.

[56] NISEE e-Library, 2016. The Earthquake Engineering Online Archive, https://nisee.berkeley.edu.

[57] Trifunac, M.D., Ivanovic, S.S., and Todorovska, M.I., 1999. Instrumented 7-storey reinforced concrete building in Van Nuys, California: description of the damage from the 1994 Northridge Earthquake and strong motion data. Report CE 99 2.

Chapter 2

MODELING DESCRIPTION

2.1 MODELING APPROACHES INTRODUCTION

Recent devastating earthquakes around the world have shown the vulnerability and deficiencies of existing structures including nonductile reinforced concrete (RC) frame buildings. These nonductile concrete frame structures are much more susceptible to collapse than modern code-conforming frames [1-2]. The amount and spacing of the transverse reinforcement in most columns do not meet the requirements of current seismic design code. Therefore, for this type of buildings, it is necessary to accurately model materials and column members and to choose the most suitable shear capacity model for assessment in order to capture the flexure, shear and flexure-shear failure modes in columns and the potential collapse of the building [3]. Based on these premises, this chapter focuses on modeling the behavior of reinforced concrete members subjected to lateral loads. The material and component models implemented in this work through OpenSees [4] can capture the column failures and potential collapse of the frame. This is crucial especially for columns with deficient seismic details such as those found in the hotel building case study, that are vulnerable to brittle shear or axial failure during earthquakes.

To capture the flexure-shear-axial interaction of structural members, analytical models and theories have been presented in the past. Modified compression field theory (MCFT, [5]) and the associated computer program called Response-2000 [6] can be used to model flexure-shear response of reinforced concrete elements. The application of the MCFT or sectional analysis

approach yields reliable flexure-shear response but requires complex computations, which are not simple for practical applications. Mostafaei and Kabeyasawa (2007, [7]) presented axial-shear-flexural interaction (ASFI) approach for the displacement-based analysis of reinforced concrete elements. ASFI is still computationally intensive and complicated due to coupling of the axial-flexure and axial-shear mechanisms and requires an iterative scheme at each loading step.

A suitable procedure is proposed in [8] to address critical modeling issues while predicting the response accurately and keeping overall computational process simple with easy implementation. This procedure has the goal to predict an envelope of the cyclic lateral response that includes the lateral displacement and corresponding strength predictions at the peak strength, onset of lateral strength degradation, and loss of axial-load-carrying capacity. The model also considers the rigid body rotation of the column due to slip of column longitudinal bars from the anchoring concrete. This rotation due to bar slip is not accounted for in flexural analysis, where the column ends are assumed to be fixed. Deformations due to flexure, reinforcement slip, and shear are modeled individually using existing models. In this research, as presented in details in [8], specific rules have been set in order to predict the flexure critical, shear critical and flexure-shear critical failure mechanisms of the members. In fact, based on the consideration that columns are often the most critical components of earthquake damage-prone structures, columns are classified into five categories based on a comparison of their predicted shear and flexural strengths, and rules for combining the three deformation components are established based on the expected behavior of columns in each category. Shear failure in columns initially dominated by flexural response is considered through the use of a shear capacity model. Based on the different categories, specific rules are set in order to sum the different deformational components. However, it's to note that the explicit modeling of the behavior of the masonry infills is neglected herein and it will be further studied.

2.2 MODELING DESCRIPTION FOR THE CASE STUDY

The Holiday Inn hotel building experienced multiple shear failures in the columns in the fourth story during the 1994 Northridge earthquake [9]. In the first three paragraphs, flexural, shear and slip models are singularly presented in details, while in the fourth paragraph the total lateral response of the member is presented in order to show how to combine the different deformational components [10-12].

2.2.1 FLEXURAL MODEL

Unidirectional axial behavior of concrete and steel materials are modeled to simulate the nonlinear response of beams and columns. Concrete material behavior is modeled using the Concrete01 material in OpenSees [4], based on the nominal mechanical properties of the concrete defined in Section 1.6.

Concrete 01 material includes zero tensile strength and a parabolic compressive stress-strain behavior up to the point of maximum strength with a linear deterioration beyond peak strength. This model is chosen as the best approximation combining the unconfined concrete material model by [13] in the post peak region and the confined concrete model by [14], where the uniaxial stress-strain relationship includes the effect of confinement provided by transverse reinforcement (as shown in Figure 2.1 (a) for f'_c=20.7 MPa). The transverse reinforcement both in beams and in columns is relatively low and poorly detailed, as explained in detail in [9]. Consequently, based on this consideration, for the existing analyzed frames, all concrete is modeled more close to the unconfined model with peak strength achieved at a strain of 0.002 and minimum post-peak strength achieved at a compressive strain of 0.006. The corresponding strength at ultimate strain is $0.05 \cdot f'_c$ for f'_c=34.5 MPa and f'_c=27.6 MPa and $0.2 \cdot f'_c$ for f'_c=20.7 MPa (as shown in Figure 2.1 a in Concrete01 model). Finally, it's to note that the confinement effect [14] will be considered for the retrofitted frames, presented in Chapter 6.

Longitudinal steel behavior is simulated using the Steel02 material in OpenSees [4]. This model includes a bilinear stress-strain envelope with a curvilinear unloading-reloading response under cyclic loading (as shown in

Figure 2.1 b). The previous research indicates that the observed yield strength of reinforcing steel exceeds the nominal strength [9, 14]. Following the recommendation of [15], instead than using the nominal values, yield strength of 345 MPa (50 ksi) and 496 MPa (72 ksi) are used in this research for Grade 40 and Grade 60 steel, respectively. Both Grade 40 and Grade 60 reinforcement are assumed to have a post-yielding modulus equal to 1% of the elastic modulus, which is assumed to be 200 GPa.

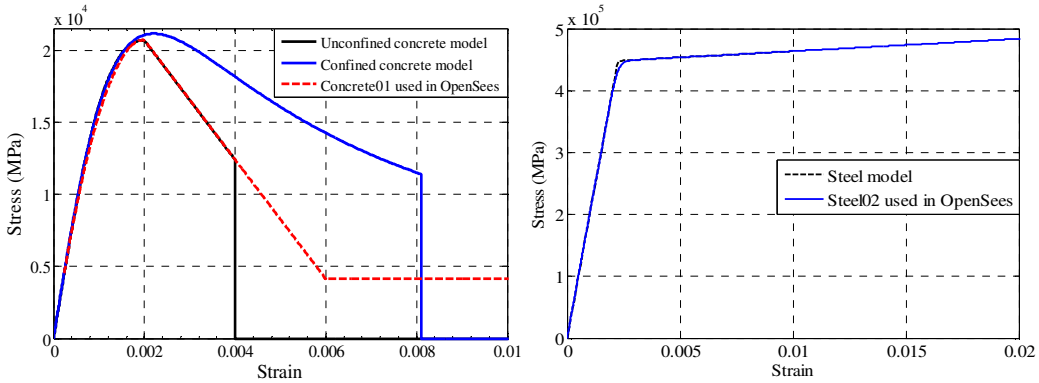

Figure 2.1: (a) Uniaxial stress-strain model relationship for concrete with f'_c=20.7 MPa and (b) longitudinal steel stress-strain model relationship for bars with f_y=495 MPa.

Flexural response of beams and columns is simulated using fiber cross sections representing the beam-column line elements. Uniaxial fibers within the gross cross section are assigned to have the property of either concrete (Concrete01 in Figure 2.1 (a)) or steel (Steel02 in Figure 2.1 (b)). A typical column cross section includes 30 layers of axial fibers in the longitudinal direction of the column. Effective slab width is included in beam cross section.

Figure 2.2 shows the moment-curvature relationship for a selected column (second column on the left in the second story and third column on the left in the third story in Figure 1.2 (a), obtained from a fiber cross section analysis. In Figure 2.2 four critical points in the moment-curvature relationship are shown. The first steel yielding occurred when the bottom tensile layer of steel reached the yield strain of 0.00248 (Figure 2.1 (b)). Concrete cover spalling occurred when the extreme compressive fiber reached the maximum unconfined concrete axial strain at 0.006 (Concrete01 in Figure 2.1 (a)). It is assumed that the ultimate flexural

deformation capacity is reached when the peak strength is reduced by 20% at a curvature of approximately 0.1 1/m. The failure of cross section is defined as the axial compressive failure of the last layer of concrete near neutral axis. Beyond the last concrete layer failure, where analysis stops, sectional strength is only contributed by longitudinal steel.

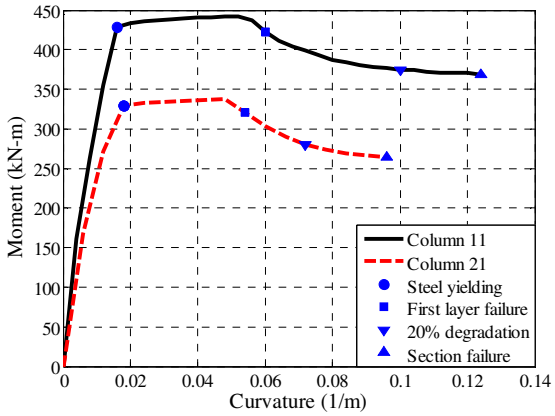

Figure 2.2: Moment-curvature relationship for a single column (second column on the left in the second story and third column on the left in the third story in Figure 1.2 (a).

In OpenSees [4], flexural beam-column members are modeled as force-based in which a specific moment distribution is assumed along the length of the member. An internal element solution is required to determine member deformations that satisfy the system compatibility.

In force-based column elements, distributed plasticity model is used in OpenSees [4] in order to allow for yielding and plastic deformations at any integration point along the flexural member length under increasing loads. In order to characterize the numerical integration options for the force-based column element and to accurately capture plastic deformations along the members, Newton-Cotes integration [16] is selected in this research. Newton-Cotes method distributes integration points uniformly along the length of the element, including one point at each end of the element (Figure 2.3 (a)).

Beam member force-deformation response is computed assuming that inelastic action occurs mainly at the member ends and that the middle of the member remains typically elastic, but this is not necessary. Plastic hinge

integration methods are used to confine nonlinear deformations in end regions of the element of specified length. The remainder of the element is assumed to stay linear elastic and it is assumed that the length of the plastic region is equal to the depth of the cross-section. The modified Gauss-Radau hinge integration method is used for numerical integration in OpenSees [4] to capture nonlinear deformations near the ends of the force-based beam elements [16]. The modified two-point Gauss-Radau integration within each hinge region is implemented at two integration points at the element ends and at 8/3 of the hinge length, $L_o=h$, from the end of the element (Figure 2.3 (b)), where h is the beam depth.

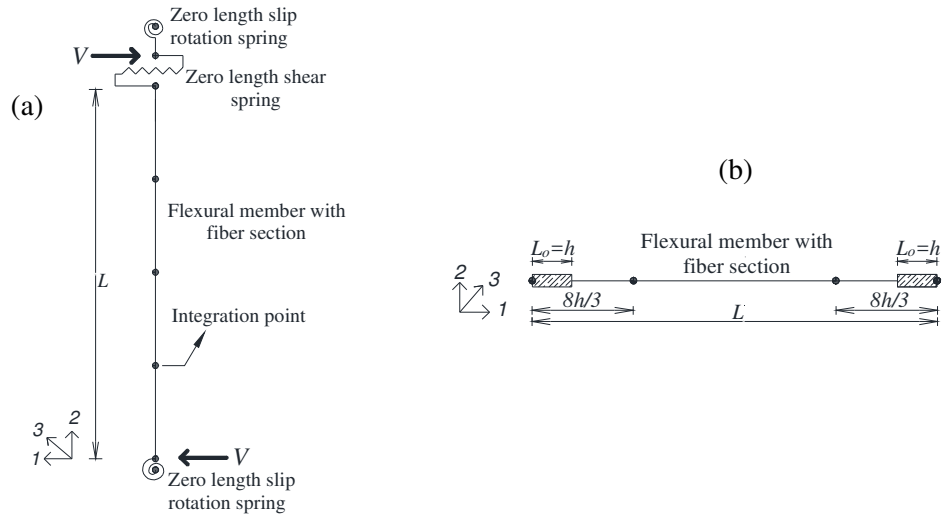

Figure 2.3: Spring model used for (a) column with fixed ends, and (b) beam with fixed ends.

2.2.2 SHEAR MODEL

As said in the precedent paragraphs, recent earthquakes have shown that columns in older RC buildings with poor seismic detailing, including the hotel building considered in this work, experience shear or flexure-shear failures. The shear model proposed by [8] can capture both the inelastic shear response and the shear failure.

The lateral force-shear displacement envelope includes three distinct points corresponding to: (a) maximum shear strength and corresponding shear

displacement; (b) onset of shear strength degradation and corresponding shear displacement; and (3) shear displacement at axial load failure.

Accordingly, the maximum shear strength, V_n, is predicted by the following expression [17]:

$$V_n = V_s + V_c = k\frac{A_v \cdot f_y \cdot d}{s} + k\left(\frac{0.5\sqrt{f_c'}}{a/d}\sqrt{1+\frac{P}{0.5\sqrt{f_c'}A_g}}\right)0.8\,\mathrm{A_g} \qquad (2.1)$$

where A_v is the transverse reinforcement area within a spacing, s, in the loading direction; f_y is the transverse reinforcement yield strength (MPa); d is the section depth; f'_c is the compressive strength of concrete; a is the shear span of the element; P is the axial load; A_g is the gross area of the section; and k is a factor to account for ductility-related strength degradation.

Shear displacements are calculated using a combination of two existing models, i.e., [8, 18]. The shear displacement corresponding to peak strength, $\Delta_{v,n}$, is calculated as:

$$\Delta_{v,n} = \left(\frac{f_y \rho_l}{5000 \cdot a/d \cdot \sqrt{P/A_g f_c'}} - 0.0004\right) \cdot L \qquad (2.2)$$

where ρ_l is the longitudinal steel ratio and L is the length of the column. As described in [8], the shear displacement at the onset of shear failure, Δ_u, can be adopted from [19]:

$$\Delta_u = \left(4 - 12\frac{v_n}{f_c'}\right) \cdot \Delta_{v,n} \qquad (2.3)$$

where v_n ($=V_n/(b \cdot d)$, b=width of cross section) is the shear stress at the peak strength and the shear displacement at the peak strength, $\Delta_{v,n}$, is calculated from Equation 2.2.

Shear displacement at axial failure, Δ_a, is obtained using the procedure given in [15], which requires the calculation of total lateral drift Δ_a/L. The latter is calculated using the equation proposed by [20]:

$$\frac{\Delta_a}{L} = \frac{4}{100} \cdot \frac{1+\tan^2\theta}{\tan\theta + P \cdot (\frac{s}{A_v \cdot f_y \cdot d_c \cdot \tan\theta})} \tag{2.4}$$

2.2.3 BAR SLIP MODEL

When a reinforcing bar embedded in concrete is subjected to tensile force, strain accumulates over the embedded length of the bar. This tensile strain causes the reinforcing bar to slip relative to the concrete in which it is embedded. Slip of column longitudinal bars at column ends (i.e., from the footing or beam-column joint) causes rigid body rotation of the column. This rotation is not accounted for in flexural analysis, where the column ends are assumed to be fixed.

The bar slip model, described in [8, 21], assumes a stepped function for bond stress between the concrete and reinforcing steel over the embedment length of the bar. Based on experimental observations [22], the bond stress is taken as $1 \cdot \sqrt{f'_c}$ MPa for elastic steel strains and as $0.5 \cdot \sqrt{f'_c}$ MPa for inelastic steel strains. The rotation due to slip, θ_s, is set equal to $slip/(d-c)$, where $slip$ is the extension of the outermost tension bar from the column end and d and c are the distances from the extreme compression fiber to the centroid of the tension steel and the neutral axis, respectively. Steel strains and neutral axis location, determined at each step during the moment curvature analysis, are used here to determine slip rotation under increasing moment or column lateral force. The column lateral displacement due to bar slip, Δ_{slip}, is equal to the product of the slip rotation and the column length ($\Delta_{slip} = \theta_s \cdot L$).

2.2.4 TOTAL LATERAL RESPONSE

The total lateral response of a RC column can be modeled using a set of springs in series in OpenSees [4]. The flexure, shear and bar slip deformation models discussed above are each modeled by a spring or element. Each spring is subjected to the same lateral force. Initially, the total displacement response is the sum of the responses of each spring. The combined column spring model is shown in Figure 2.3 (a).

A typical column element includes two zero-length bar slip springs at its ends, one zero-length shear spring and a flexural element with five integration points.

The shear behavior is modeled as a uniaxial hysteretic material defined for the spring in the shear direction (i.e., transverse direction of the column or direction 1 in Figure 2.3 (a)). The bar slip rotation is modeled with two rotational springs at the column ends using a uniaxial hysteretic material (i.e., direction 3 in Figure 2.3 (a)). Finally, same vertical displacement is maintained between nodes of zero length elements in the vertical direction (i.e., direction 2 in Figure 2.3 (a)), using the equalDOF option in OpenSees.

The three deformation components are simply added together to predict the total lateral response up to the peak strength of the column [8]. The rules are established for the post-peak behavior of the springs based on a comparison of the shear strength V_n, the yield strength V_y (the shear strength corresponding to moment capacity M_y at first longitudinal steel yielding, $V_y=2M_y/L$), and the flexural strength V_p ($V_p=2M_p/L$ for a fixed ended column with maximum flexural strength of M_p) required to reach the plastic moment capacity.

By comparing V_n, V_y, and V_p, the columns can be classified into five different categories, as described in details [8]:

- 1) Category I: $V_n<V_y$: the shear strength is less than the lateral load causing yielding in the tension steel.
  The column fails in shear while the flexural behavior remains elastic. After the peak of shear strength is reached, the shear behavior dominates the response. As the column strength decreases, shear deformations continue to increase according to the shear model, while the flexure and slip springs unload along their initial responses. The post-peak deformation at any lateral load level is the sum of the post-peak shear deformation and the pre-peak flexural and slip deformations corresponding to that load.

- 2) Category II: $V_y<V_n<0.95\cdot V_p$: the shear strength is greater than the yield strength, but slightly less than the flexural strength of the column.
  The column fails in shear, but inelastic flexural deformation occurring prior to shear failure affects the post-peak behaviour. As the column shear strength decreases, shear deformations continue to increase according to the shear model, but the flexure and slip springs are locked at their values at peak strength. The post-peak deformation at any lateral load level is the sum of the

flexural and slip deformations at peak strength and the post-peak shear deformation corresponding to that load.

- 3) Category III: $0.95 \cdot V_p < V_n < 1.05 \cdot V_p$: the shear and flexural strengths are very close.

  The peak strength is the smaller of the shear strength and the flexural strength. As the column strength decreases, all deformations continue to increase according to their individual models. The post-peak deformation at any lateral load level is the sum of the post-peak flexure, slip, and shear deformations corresponding to that load.

- 4) Category IV: $1.05 \cdot V_p < V_n < 1.4 \cdot V_p$: the shear strength is greater than the flexural strength of the column.

  The column experiences large flexural deformations potentially leading to a flexural failure. Inelastic shear deformations affect the post-peak behavior, and shear failure may occur as displacements increase. In particular, the peak strength of the column is the flexural strength, calculated in the flexure model. As the column strength decreases, flexural and slip deformations continue to increase according to their models, but the shear spring is locked at its value at peak strength. The post-peak deformation at any lateral load level is the sum of the post peak flexural and slip deformations corresponding to that load and the shear deformation at peak strength. However, it's to note that the column may experience a shear failure after being subjected to large deformations.

- 5) Category V: $V_p < 1.4 \cdot V_n$: the shear strength is much greater than the flexural strength of the column.

  The column fails in flexure while the shear behavior remains elastic. If the column flexural strength decreases, flexural and slip deformations continue to increase according to their models, while the shear spring unloads with an unloading stiffness equal to its initial stiffness. The post-peak deformation at any lateral load level is the sum of the postpeak flexural and slip deformations and the pre-peak shear deformation corresponding to that load.

Figure 2.4 shows as example the three different deformation components and the total lateral displacement for columns 11 and 29 of the longitudinal frame, presented in Figure 1.2 (a), belonging to two different categories described above (respectively Category I and Category IV).

This procedure of comparison and identification of failure mode are repeated for all of the columns of the frame. Table 1 compares V_n, V_y and V_p, for the columns in the first four stories, which typically affect the collapse mechanism due to characteristics of the frame.

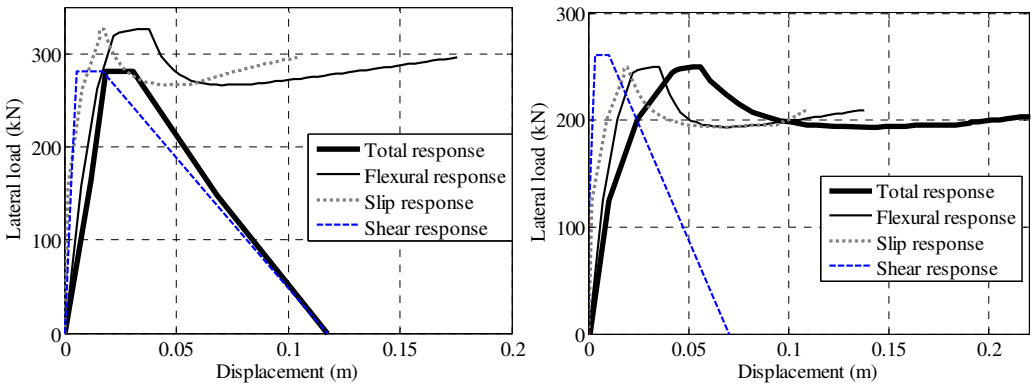

Figure 2.4 Three different deformation components and the total lateral displacement for columns 11 and 29 of the longitudinal frame, presented in Figure 1.2 (a). The columns belong respectively to Category I (left) and Category IV (right).

Table 2.1 Comparison of the shear strength V_n, the yield strength V_y and the flexural strength V_p and category classification for the columns in the longitudinal frame.

Column	Longitudinal bare frame					
	V_y (kN)	V_n (kN)	V_p (kN)	V_p/V_n	V_y/V_n	Category
1, 9	201	233	210	0.90	0.86	IV
2, 8	212	245	244	1.00	0.87	III
3 to 7	212	245	244	1.00	0.87	III
10, 18	158	189	176	0.93	0.84	IV
11, 17	295	279	325	1.16	1.06	I
12 to 16	248	281	266	0.95	0.88	IV
19, 27	143	171	162	0.95	0.84	IV
20, 26	268	260	309	1.19	1.03	I
21 to 25	224	260	249	0.96	0.86	IV
28, 36	138	164	154	0.94	0.84	IV
29, 35	163	175	168	0.96	0.93	III
30 to 34	163	176	168	0.96	0.93	III
37, 45	129	147	135	0.92	0.88	IV
38, 44	140	156	147	0.94	0.90	IV
39 to 43	140	156	147	0.94	0.90	IV
46, 54	121	140	127	0.91	0.86	IV
47, 53	129	147	135	0.92	0.88	IV
48 to 52	129	147	135	0.92	0.88	IV
55, 63	112	132	119	0.90	0.85	IV
56, 62	116	136	122	0.90	0.85	IV
57 to 61	116	136	122	0.90	0.85	IV

Table 2.2 Comparison of the shear strength V_n, the yield strength V_y and the flexural strength V_p and category classification for the columns in the transversal frame.

Column	Transversal bare frame					
	V_y (kN)	V_n (kN)	V_p (kN)	V_p/V_n	V_y/V_n	Category
1,4	223	226	243	1.07	0.99	II
2,3	288	337	305	0.91	0.85	IV
5,8	212	219	229	1.05	0.97	III
6,7	326	292	346	1.19	1.12	I
9,12	189	193	203	1.05	0.98	II
10,11	289	263	311	1.18	1.10	I
13,16	180	185	199	1.08	0.98	II
14,15	259	253	277	1.10	1.03	I
17,20	171	175	191	1.09	0.97	II
18,19	184	188	201	1.07	0.98	II
21,24	149	165	183	1.11	0.90	II
22,23	170	174	191	1.10	0.97	II
25,28	140	154	172	1.12	0.91	II
26,27	145	159	177	1.11	0.91	II

2.3 CONCLUSIONS

Recent devastating earthquakes around the world have confirmed the vulnerability and deficiencies of existing structures including nonductile reinforced concrete (RC) frame buildings. These nonductile concrete frame structures are much more susceptible to collapse than modern code-conforming frames. The amount and spacing of the transverse reinforcement in most columns do not meet the requirements of current seismic design code. Therefore, for this type of buildings, it is necessary to accurately model materials and column members and to choose the most suitable shear capacity model for assessment in order to capture the flexure, shear and flexure-shear failure modes in columns and the potential collapse of the building.

This chapter focuses on modeling the behavior of reinforced concrete members subjected to lateral loads. A suitable procedure is presented to address

critical modeling issues while predicting the response accurately and keeping overall computational process simple with easy implementation. This procedure has the goal to predict an envelope of the cyclic lateral response that includes the lateral displacement and corresponding strength predictions at the peak strength, onset of lateral strength degradation, and loss of axial-load-carrying capacity. The model also considers the rigid body rotation of the column due to slip of column longitudinal bars from the anchoring concrete. This rotation due to bar slip is not accounted for in flexural analysis, where the column ends are assumed to be fixed. Deformations due to flexure, reinforcement slip, and shear are modeled individually using existing and new models.

Specific rules have been set in order to predict the flexure critical, shear critical and flexure-shear critical failure mechanisms of the members. Columns, that are often the most critical components of earthquake damage-prone structures, are classified into five categories based on a comparison of their predicted shear and flexural strengths, and rules for combining the three deformation components are established based on the expected behavior of columns in each category. Shear failure in columns initially dominated by flexural response is considered through the use of a shear capacity model.

This model has the advantages to create a comprehensive and rigorous procedure in order to classify and analyze the structural members. Moreover, the model approach has been verified with the results of experimental tests for columns with a reasonably good match between the analytical model and the experimental results. In particular, the selected approach allows for explicit modeling of flexure-shear-axial load interaction based on simple sectional analysis. This is an accurate yet simple approach to model potential collapse and flexure-shear damage in nonductile columns.

2.4 REFERENCES

[1] Sezen, H., Whittaker, A., Elwood, K., and Mosalam, K, 2003. Performance of reinforced concrete buildings during the August 17, 1999 Kocaeli, Turkey earthquake, and seismic design and construction practise in Turkey, Engineering Structures, 25(1), 103-114.

[2] Liel, A. B., Haselton, C. B., Deierlein, G. G., and Baker, J. W., 2009. Incorporating modeling uncertainties in the assessment of seismic collapse risk of buildings, Structural Safety, 31(2), 197-211.

[3] De Luca, F. and Verderame G.M., 2013. A practice-oriented approach for the assessment of brittle failures in existing reinforced concrete elements. Engineering Structures, 48, 373-388.

[4] McKenna, F., 2011. OpenSees: a framework for earthquake engineering simulation, Computing in Science and Engineering, 13(4), 58-66.

[5] Vecchio, F.J., and Collins, M.P., 1986. The modified compression field theory for reinforced concrete elements subjected to shear, ACI Journal, Proceedings, 83(2), 219–231.

[6] Bentz, E. C., 2000. Sectional analysis of reinforced concrete members. Ph.D. Thesis, University of Toronto, Canada.

[7] Mostafaei, H., and Kabeyasawa, T., 2007. Axial-shear-flexure interaction approach for reinforced concrete columns, ACI Structural Journal, 104(2), 218.

[8] Setzler, E.J., and Sezen, H., 2008. Model for the lateral behavior of reinforced concrete columns including shear deformations, Earthquake Spectra, 24(2), 493-511.

[9] Krawinkler, H., 2005. Van Nuys hotel building testbed report: exercising seismic performance assessment, Pacific Earthquake Engineering Research Center, University of California, Berkeley.

[10] Miano, A., Sezen, H., Jalayer, F., and Prota, A. Performance based assessment methodology for retrofit of buildings. *Earthquake Spectra*, (Under Review).

[11] Miano, A., Sezen, H., Jalayer, F., and Prota, A., 2017. Performance based comparison of different retrofit methods for reinforced concrete structures. In: Proceedings of the 6th ECCOMAS Thematic Conference on Computational Methods in Structural Dynamics and Earthquake Engineering (COMPDYN 2017), Rhodes, Greece, 15-17 June 2017.

[12] Miano, A., Sezen, H., Jalayer, F., and Prota, A., 2017. Probability based comparison of retrofit methods for existing nonductile concrete frames. In: Proceedings of the 4th Thematic Conference on Smart Monitoring, Assessment and Rehabilitation of Civil Structures (SMAR 2017), Zurich, Switzerland, 13-15 September 2017.

[13] Roy, H.E., and Sozen, M.A., 1963. A model to simulate the response of concrete to multi-axial loading, University of Illinois Engineering Experiment Station.

[14] Mander, J.B., Priestley, M.J., and Park, R., 1988. Theoretical stress-strain model for confined concrete, Journal of structural engineering, 114(8), 1804-1826.

[15] Islam, M.S., 1996. Analysis of the Northridge earthquake response of a damaged non-ductile concrete frame building, The Structural Design of Tall Buildings, 5 (3): 151-182.

[16] Scott, M.H., and Fenves, G.L., 2006. Plastic hinge integration methods for force-based beam–column elements, Journal of Structural Engineering, 132 (2): 244-252.

[17] Sezen, H., and Moehle J.P., 2004. Shear strength model for lightly reinforced concrete columns, Journal of Structural Engineering, 130 (11): 1692-1703.

[18] Sezen, H., 2008. Shear deformation model for reinforced concrete columns, Structural Engineering and Mechanics, 28 (1): 39-52.

[19] Gerin, M., and Adebar, P., 2004. Accounting for shear in seismic analysis of concrete structures. In: Proceedings of the 13th World Conference on Earthquake Engineering, Vancouver, B.C., Canada, August 1-6.

[20] Elwood, K.J., and Moehle, J.P., 2005. Axial capacity model for shear-damaged columns. ACI Structural Journal, 102 (4): 578-587.

[21] Sezen, H., and Moehle, JP., 2003. Bond-slip behavior of reinforced concrete members. Fib Symposium on Concrete Structures in Seismic Regions, CEB-FIP, Athens, Greece.

[22] Sezen, H., 2004. Seismic behavior and modeling of reinforced concrete building columns, Ph.D. dissertation, Berkeley University, California.

Chapter 3

ANALYTICAL FRAGILITY ASSESSMENT USING UN-SCALED GROUND MOTION RECORDS

3.1 INTRODUCTION

This chapter proposes a journey through probabilistic performance based assessment and design based on linear dynamic analysis tools. In particular, Cloud Analysis is used to perform fragility assessment using un-scaled ground motion records and the results are compared with those obtained from the Incremental Dynamic Analysis (IDA) and Multiple Stripe Analysis (MSA) with conditional mean spectrum [1].

The definition of explicitly probabilistic performance objectives has found its way into design codes and guidelines as early as 1983 [2-5]. Today, there is wide-spread consensus for the utility and practicality of performance-based earthquake engineering (PBEE, [6], [7]) in quantifying the safety margin for newly designed buildings as well as existing ones located in seismic areas. The evolution of probabilistic PBEE has been closely intertwined with the galvanization of non-linear dynamic analysis procedures as the most suitable means of quantifying the structural response of multi-degree-of-freedom (MDOF) structures. This has been facilitated a great deal by the arrival of general purpose computer programs such as DRAIN-2D [8], Ruaumoko [9], and Opensees (http://opensees.berkeley.edu), just to name a few.

In the past fifteen years, many research efforts have been dedicated to an in-depth study of the implementation, the nuances and the potential complications of non-linear dynamic analysis procedures. Early versions of procedures later

coined as IDA [10], MSA [11-12], and Cloud Analysis [13] could be seen in works such as Bertero ([14], IDA), Singhal and Kiremidjian ([15], MSA), Bazzurro et al. ([16], MSA, Cloud), Shome et al. ([17], Cloud), and Luco and Cornell ([18], Cloud).

Both MSA and IDA involve the prediction of structural performance (often measured in terms of maximum inter-story drift) over the height of structure, over the entire time-history for a suite of ground motions, and based on increasing linear scaling of ground motion records in amplitude. The two methods are practically the same, if the suite of records remains invariant during the scaling. However, the MSA has the potential of using different suites of ground motion at different intensity levels. The IDA has been widely used by researchers to capture the record-to-record variability in structural response to ground motion. IDA is based on a fixed suite of records scaled successively to higher intensity levels. Nevertheless, in recent years a substantial debate has been raised regarding the potential bias in the IDA results due to (excessive) scaling (e.g., [19], and Adaptive IDA as in [20]). It has been argued that a careful selection of ground motion records can be avoided if the ground motion intensity measure (IM) adopted was sufficient [15, 21]. On the other hand, if the adopted IM was not sufficient (see [21-23] for alternative definitions/interpretations of sufficiency), the selected records at any given ground motion intensity level should ideally reflect the expected dominant ground motion characteristics. Among the various ground motion characteristics, epsilon or the number of logarithmic standard deviations that separate the ground motion intensity from the corresponding ground motion mean prediction in the log-scale, has been found to significantly influence the distance between structural response and its mean value at a given ground motion intensity level. In fact, epsilon has been often coined as a proxy for spectral shape considerations [24-25]. It has been argued [25] that a sufficient IM needs to take into the effect of spectral shape in one way (to consider the effect of higher modes) or another (in the case of significant non-linearity).

The Conditional Mean Spectrum (CMS) [15, 26] “anchors” the acceleration response spectra to the first-mode spectral acceleration value. The CMS provides a useful instrument for careful record selection based on mean spectral shape considerations adopting the first-mode spectral acceleration as the IM. Baker and Cornell [15] have selected, using CMS, different suites of ground motion records

for various intensity levels and have implemented them to perform MSA. They have shown that coupling careful record selection using the CMS with MSA leads to results analogous to those obtained based on record selection considering the expected distribution of epsilon at various intensity levels. The Conditional Spectrum (CS, [27], see also [26, 28]) is obtained by estimating both the logarithmic mean and standard deviation of the spectral shape spectrum conditioned on a given spectral acceleration value. This provides very useful means for selecting ground motion records whose conditional spectra respect the mean value and are constrained within a certain range (an offset with respect to the mean defined in terms of a desired factor of standard deviation).

The non-linear dynamic analysis procedure known as Cloud Analysis is based on fitting a linear regression model in the logarithmic scale to the pairs of structural response parameter (e.g., maximum inter-story drift) and IM (e.g., first-mode spectral acceleration) for a suite of as-recorded ground motions. This method is well-known both for the simplicity of its underlying formulation and for the relatively small number of structural analyses required. It has had a relatively wide use among researchers, e.g., [29-32]. However, the Cloud Analysis is also notorious for being based on a few simplifying assumptions (fixed standard error of regression, mean response varying linearly as a function of IM in the logarithmic scale, and structural response given IM being modeled as a Lognormal distribution), and for being very much sensitive to the selected suite of records [29]. Several researchers have proposed variations to the Cloud Analysis by relaxing some of the above-mentioned assumptions (e.g., [33-36]).

In this chapter a functional variation to the original Cloud Analysis is presented in order to take into account the cases leading to structural collapse (and/or dynamic instability due to large deformations). The proposed method, apart from resolving the frequently-encountered problem of the “collapse cases”, leads to a more realistic mathematical model for the structural response given IM; i.e., all of the above-mentioned simplifying assumptions (constant standard error of regression, the linear mean response versus IM in the logarithmic scale, and the lognormality of the response given IM) are relaxed. Finally, to reduce record-selection-dependence of the results, a Bayesian version of the Cloud Analysis considering the “collapse-cases” is presented in which the uncertainty in the structural fragility model parameters is considered. This leads to a Robust

Fragility estimate and a desired confidence interval defined around it. The term Robust Fragility was coined by Jalayer et al. [29] to effectively consider the parameter uncertainty in a prescribed fragility model (e.g., Lognormal). Robust Fragility as a concept is not a new one; similar issues under different names can be spotted as early as in probabilistic risk assessment of nuclear power plants ([3], average fragility curves), and later in the works such as but not limited to [37] (predictive fragilities), and [38-39].

In order to demonstrate the application of the proposed procedure in structural fragility assessment for the Near-Collapse limit state [40], three different types of moment resisting frames of the Van Nuys Hotel building in Northridge, presented in Chapter 1.6, are employed herein using the modelling approach presented in Chapter 2: (a) shear-critical transverse moment resisting frame; (b) shear/flexure-critical longitudinal frame; (c) flexure-dominated longitudinal frame retrofitted using reinforced concrete jacketing, presented in details in Chapter 5.2.

The Robust Fragility and its two-standard deviation confidence interval based on a suite of un-scaled records are obtained for all the three above-mentioned frames. The results are compared to both the classic IDA and MSA obtained by careful record-selection based on CS.

3.2 METHODOLOGY

3.2.1 THE INTENSITY MEASURE AND THE STRUCTURAL PERFORMANCE VARIABLE

The first-mode spectral acceleration denoted by $S_a(T_1)$ or simply S_a is adopted herein as the intensity measure (IM). This IM has been proved to be a relatively sufficient intensity measure for moment-resisting frames with first-mode periods lying within the moderate range (e.g., [17, 22-23]). Recently, many researchers have focused on IMs that are more suitable even with respect to S_a for predicting the structural performance such as the spectral acceleration averaged over a period range (e.g., [41-42]) or vector-valued IMs (e.g., [24-25, 43]). However, this work does not focus on selecting the most suitable IM.

The structural performance variable herein is taken to be the critical *Demand to Capacity Ratio* (*DCR*, [44] and see also [29]) for a desired limit state (*LS*),

denoted as DCR_{LS}. It is defined as the demand to capacity ratio for the component or mechanism that brings the system closer to the onset of a limit state *LS* (herein, the Near-Collapse limit state). The formulation is based on the cut-set concept [45], which is suitable for cases where various potential failure mechanisms (both ductile and brittle) can be defined a priori. DCR_{LS}, which is always equal to unity at the onset of limit state, is defined as:

$$DCR_{LS} = \max_{l}^{N_{mech}} \min_{j}^{N_l} \frac{D_{jl}}{C_{jl}(LS)} \tag{3.1}$$

where N_{mech} is the number of considered potential failure mechanisms; N_l is the number of components taking part in the lth mechanism; D_{jl} is the demand evaluated for the jth structural component of the lth mechanism; $C_{jl}(LS)$ is the limit state capacity for the jth component of the lth mechanism. The capacity values refer to the Near-Collapse limit state in this work, but the procedure can be used for any other prescribed limit state.

Near-Collapse Limit State: in the context of this work, the limit state of *Near-Collapse* is considered (according to [40]) and *D* is the demand expressed in terms of maximum chord rotation for the component, denoted as $\theta_{D,\max}$, and computed from nonlinear dynamic analysis. *C* is the component chord rotation capacity, denoted as $\theta_{C,\text{ultimate}}$, and identified as the point on the softening branch of the force-deformation curve of the member (considering the nonlinear deformations associated with flexure, shear and bar-slip), where a 20% reduction in the maximum strength takes place.

Collapse Limit State: when predicting non-linear response of structures, it is necessary to account for the possibility that some records may cause global "Collapse"; i.e., very high global displacement-based demands or non-convergence problems in the analysis software. It is obvious that $DCR_{LS}>1$ for the limit state of Near-Collapse does not necessarily imply the exceedance of collapse limit state. Since, the evaluation of the critical demand to capacity ratio for a collapsed structure might not be quite meaningful, it is important to identify the collapse-inducing records within the Cloud Analysis response. Herein, the criteria established by Galanis and Moehle [46] for defining global structural collapse is adopted, i.e., the structural collapse occurs when one of the two following conditions has reached: (a) 50%+1 of the columns in only one story reach the chord rotation θ_{axial}, where θ_{axial} corresponds to the point associated with the

complete loss of vertical-load carrying capacity of the component (to account for the loss of load bearing capacity); (b) the maximum inter-story drift exceeds 10% (to account for global dynamic instability).

3.2.2 A REGRESSION-BASED PROBABILISTIC MODEL FOR PREDICTING DCR_{LS} GIVEN S_A (CLOUD ANALYSIS)

Herein, a regression-based probability model is employed to describe the DCR_{LS} for a given IM=$S_a(T_1)$ level. Let $DCR_{LS}=\{DCR_{LS,i},\ i=1{:}N\}$ be the set of critical demand to capacity ratio for limit state *LS*, calculated through non-linear time-history analyses performed for a suite of *N* recorded ground motions, and $S_a=\{S_{a,i},\ i=1{:}N\}$ be the set of corresponding spectral acceleration values (where $DCR_{LS,i}$ and $S_{a,i}$ are calculated for the *i*th ground motion record). The *Cloud data* or simply *data* hereafter refer to the set $\mathbf{D}=\{(S_{a,i}, DCR_{LS,i}),\ i=1{:}N\}$.

The regression probabilistic model can be described as follows:

$$\mathbb{E}[\ln DCR_{LS} \mid S_a] = \ln \eta_{DCR_{LS}|S_a} = \ln a + b \ln S_a,\ \sigma_{\ln DCR_{LS}|S_a} = \sqrt{\sum_{i=1}^{N} \left(\ln DCR_{LS,i} - \ln \eta_{DCR_{LS}|S_{a,i}}\right)^2 \Big/ (N-2)} \quad (3.2)$$

where $\mathbf{E}[\ln DCR_{LS}|S_a]$ is the expected value for the natural logarithm of DCR_{LS} given S_a; $\eta_{DCRLS|Sa}$ is the median for DCR_{LS} given S_a; $\sigma_{\ln DCRLS|Sa}$ is the logarithmic standard deviation for DCR_{LS} given S_a. This non-linear dynamic analysis procedure, also known as the Cloud Analysis (e.g., [16-18, 21-23, 31, 33, 44, 47-49]), graphically invokes the idea of the scatter plot of data pairs of structural performance variable and the intensity measure for a given ground motion record. The Cloud Analysis is particularly useful when one deals with un-scaled ground motion records. The structural fragility obtained based on the Cloud Analysis can be expressed as the probability that DCR_{LS} exceeds unity given S_a:

$$P(DCR_{LS} > 1 \mid S_a, \boldsymbol{\chi}] = P(\ln DCR_{LS} > 0 \mid S_a, \boldsymbol{\chi}) = 1 - \Phi\left(\frac{-\ln \eta_{DCR_{LS}|S_a}}{\sigma_{\ln DCR_{LS}|S_a}}\right) = \Phi\left(\frac{\ln \eta_{DCR_{LS}|S_a}}{\beta_{DCR_{LS}|S_a}}\right) \quad (3.3)$$

where $\Phi(\cdot)$ is the standardized Gaussian Cumulative Distribution Function (CDF), $\boldsymbol{\chi}=[\ln a,\ b,\ \beta_{DCRLS|Sa}]$ denotes the model parameters and $\beta_{DCRLS|Sa} \triangleq \sigma_{\ln DCRLS|Sa}$. Note that Equation 3.3 is a three-parameter fragility model which can be determined as a function of known vector $\boldsymbol{\chi}$.

3.2.3 RECORD SELECTION FOR CLOUD ANALYSIS

As mentioned above, the Cloud Analysis is ideal for working with un-scaled records. Inevitably, the record selection for Cloud Analysis is particularly important and decisive. Here are few points to consider when selecting records for Cloud Analysis:

1. The records should be selected in a way that they cover a vast range of spectral acceleration values. In other words, the larger is the dispersion in S_a values, the smaller is the standard error in the estimation of the regression slope in the logarithmic scale. This increases the chances of having a non-zero regression slope with a high confidence.
2. The records should be selected in such a way that a significant proportion (say more than 30%) of records have DCR_{LS} greater than unity. The recommendation aims at avoiding extrapolation in regression and its implementation may involve some adjustments to the original suite of records.
3. Avoid selecting both horizontal components of the same recording unless the structural model is three-dimensional. Moreover, it is recommended to avoid selecting too many records (say more than 10% of total number of records) from the same seismic event (note that a limit of six records is generally recommended in [53]).

3.2.4 CLOUD ANALYSIS CONSIDERING COLLAPSE AND/OR GLOBAL DYNAMIC INSTABILITY

Correct implementation of the above recommendations for the selection of records for the Near-Collapse limit state (especially point 2) quite often leads to selection of a number of records that take the structure to verge upon "Collapse" (see [54] for a comprehensive review of the currently available methods to assess the collapse capacity of building structures) by: (a) loss of vertical load bearing capacity, and/or (b) global dynamic instability [55] (signaled herein by occurrence of very large *DCR* values, or non-convergence in the analyzing software). This section illustrates that, with some modifications, the Cloud Analysis can still be carried on in such cases. Let the Cloud data be partitioned into two parts: (a) *NoC* data which correspond to that portion of the suite of records for which the structure does not experience "Collapse", (b) *C* corresponding to the "Collapse"-

inducing records. The structural fragility for a prescribed limit state *LS*, expressed in Equation 3.3, can be expanded with respect to *NoC* and *C* sets using Total Probability Theorem (see also [56-57, 12]):

$$P\left(DCR_{LS}>1\middle|S_a\right)=P\left(DCR_{LS}>1\middle|S_a,NoC\right)\cdot\left(1-P(C\middle|S_a)\right)+P\left(DCR_{LS}>1\middle|S_a,C\right)\cdot P\left(C\middle|S_a\right) \quad (3.4)$$

where $P(DCR_{LS}>1|S_a,NoC)$ is the conditional probability that DCR_{LS} is greater than unity given that "Collapse" has not taken place (*NoC*) and can be described by a Lognormal distribution (a widely used assumption that has been usually verified for cases where the regression residuals represent unimodal behavior, e.g., [12, 17]):

$$P\left(DCR_{LS}>1\middle|S_a,NoC\right)=\Phi\left(\frac{\ln\eta_{DCR_{LS}|S_a,NoC}}{\beta_{DCR_{LS}|S_a,NoC}}\right) \quad (3.5)$$

where $\eta_{DCRLS|Sa,NoC}$ and $\beta_{DCRLS|Sa,NoC}$ are conditional median and standard deviation (dispersion) of the natural logarithm of DCR_{LS} for *NoC* portion of the data. $P(DCR_{LS}>1|S_a,NoC)$ is calculated in exactly the same manner as the standard Cloud Analysis discussed in Section 2.2 (see Equation 3.3). The term $P(DCR_{LS}>1|S_a,C)$ is the conditional probability of that DCR_{LS} is greater than unity given "Collapse". This term is equal to unity, i.e., in the cases of "Collapse", the limit state *LS* (herein, Near-Collapse) is certainly exceeded. Finally, $P(C|S_a)$ in Equation 3.4 is probability of collapse, which can be predicted by a logistic regression model (a.k.a., logit) as a function of S_a (see also [58]), and expressed as follows:

$$P\left(C\middle|S_a\right)=\frac{1}{1+e^{-\left(\alpha_0+\alpha_1\cdot\ln(S_a)\right)}} \quad (3.6)$$

where α_0 and α_1 are the parameters of the logistic regression. It is to note that the logistic regression model belongs to the family of generalized regression models and is particularly useful for cases in which the regression dependent variable is binary (i.e., can have only two values 1 and 0, *yes* or *no*, which is the case of *C* and *NoC* herein). Note also that the logistic regression model described above is applied to all records; they are going to be distinguished by 1 or 0 depending on whether they lead to collapse or not. Finally, the analytic fragility model in the case where the data includes "collapse-cases" can be obtained by substituting the terms $P(DCR_{LS}>1|S_a,NoC)$ and $P(C|S_a)$ from Equations 3.5 and 3.6 into Equation 3.4:

$$P\left(DCR_{LS}>1\middle|S_a,\boldsymbol{\chi}\right)=\Phi\left(\frac{\ln\eta_{DCR_{LS}|S_a,NoC}}{\beta_{DCR_{LS}|S_a,NoC}}\right)\cdot\frac{e^{-\left(\alpha_0+\alpha_1\ln(S_a)\right)}}{1+e^{-\left(\alpha_0+\alpha_1\ln(S_a)\right)}}+\frac{1}{1+e^{-\left(\alpha_0+\alpha_1\ln(S_a)\right)}} \quad (3.7)$$

Equation 3.7 illustrates a five-parameter fragility model whose model parameters can be denoted as $\boldsymbol{\chi}$=[ln$a$, b, $\beta_{DCRLS|NoC,Sa}$, α_0, α_1]. Given $\boldsymbol{\chi}$, the fragility can be perfectly determined (for simplicity, $\beta_{DCRLS|NoC,Sa}$ is replaced with β hereafter). The CDF of $DCR_{LS}|S_a$ for a given demand to capacity ratio dcr can be derived as follows based on Total Probability Theorem:

$$\begin{aligned}P\left(DCR_{LS}\le dcr\middle|S_a\right)&=P\left(DCR_{LS}\le dcr\middle|S_a,NoC\right)P\left(NoC\middle|S_a\right)+P\left(DCR_{LS}\le dcr\middle|S_a,C\right)P\left(C\middle|S_a\right)\\&=\Phi\left(\frac{\ln dcr-\ln\eta_{DCR_{LS}|S_a,NoC}}{\beta_{DCR_{LS}|S_a,NoC}}\right)P\left(NoC\middle|S_a\right)\end{aligned} \quad (3.8)$$

where it has been assumed that P($DCR_{LS} \le dcr$ $|C,S_a$)=0 assuming that DCR_{LS} is going to be un-boundedly large for the collapse cases. Equation 3.8 can be used in order to calculate the value $dcr=DCR^p$ corresponding to the percentile p by setting the left side of the Equation 3.8 equal to p and solving it for DCR^p:

$$DCR^p=\eta_{DCR_{LS}|S_a,NoC}\cdot\exp\left(\beta_{DCR_{LS}|S_a,NoC}\cdot\Phi^{-1}\left[p/P(NoC\,|\,S_a)\right]\right) \quad (3.9)$$

where Φ^{-1} is the inverse function of standardized normal distribution.

3.2.5 ROBUST FRAGILITY ASSESSMENT

Inspired from the concept of updated robust reliability [59-61], the *Robust Fragility* is defined as the expected value for a prescribed fragility model taking into account the joint probability distribution for the (fragility) model parameters $\boldsymbol{\chi}$ ([33, 62-63]). The Robust Fragility, by using Total Probability Theorem, can be written as:

$$P\left(DCR_{LS}>1\middle|S_a,\mathbf{D}\right)=\int_{\Omega_\chi}P\left(DCR_{LS}>1\middle|S_a,\boldsymbol{\chi}\right)f(\boldsymbol{\chi}|\mathbf{D})\,\mathrm{d}\boldsymbol{\chi}=\mathbb{E}_\chi\left[P\left(DCR_{LS}>1\middle|S_a,\mathbf{D},\boldsymbol{\chi}\right)\right] \quad (3.10)$$

where $\boldsymbol{\chi}$ is the vector of fragility model parameters and $\boldsymbol{\Omega_\chi}$ is its domain; $f(\boldsymbol{\chi}|\mathbf{D})$ is the joint probability distribution for fragility model parameters given the vector of Cloud data **D** (see Section 2.2). The term $P(DCR_{LS}>1|S_a,\boldsymbol{\chi})$ is the fragility model given that the vector $\boldsymbol{\chi}$ is known (see Equation 3.3 or Equation 3.7). Note that it has been assumed that the vector $\boldsymbol{\chi}$ is sufficient to describe the data **D** (that

is why **D** has been dropped from the right-hand side of the conditioning sign |). $\mathbf{E}_{\boldsymbol{\chi}}(\cdot)$ is the expected value over the vector of fragility parameters $\boldsymbol{\chi}$. The variance σ^2 in fragility estimation can be calculated as:

$$\sigma_{\boldsymbol{\chi}}^2\left[P\left(DCR_{LS}>1\middle|S_a,\mathbf{D},\boldsymbol{\chi}\right)\right]=\int_{\Omega_{\boldsymbol{\chi}}}P\left(DCR_{LS}>1\middle|S_a,\boldsymbol{\chi}\right)^2 f(\boldsymbol{\chi}|\mathbf{D})\,\mathrm{d}\boldsymbol{\chi}-\mathbb{E}_{\boldsymbol{\chi}}^2\left[P\left(DCR_{LS}>1\middle|S_a,\mathbf{D},\boldsymbol{\chi}\right)\right] \quad (3.11)$$

Note that calculating the variance over the vector of fragility parameters $\boldsymbol{\chi}$ from Equation 3.11, i.e. $\sigma^2\boldsymbol{\chi}(\cdot)$, provides the possibility of estimating a confidence interval of for the fragility considering the uncertainty in the estimation of the fragility model parameters.

3.2.6 CALCULATION OF ROBUST FRAGILITY USING SIMULATION

The integrals in Equation 3.10 and Equation 3.11 in general do not have analytic solutions and should be solved numerically. Simulation schemes provide very efficient means for numerical resolution of an integral. The Robust Fragility curve and its standard deviation can be calculated efficiently using Monte Carlo Simulation (see also [63]) by approximating Equation 3.10 and Equation 3.11 in the following manner:

$$P\left(DCR_{LS}>1\middle|S_a,\mathbf{D}\right)\approx\tilde{R}_F=1/n_{sim}\sum_{i=1}^{n_{sim}}P\left(DCR_{LS}>1\middle|S_a,\boldsymbol{\chi}_i\right) \quad (3.12)$$

$$\sigma_{\boldsymbol{\chi}}^2\left[P\left(DCR_{LS}>1\middle|S_a,\mathbf{D},\boldsymbol{\chi}\right)\right]\approx 1/n_{sim}\sum_{j=1}^{n_{sim}}P\left(DCR_{LS}>1\middle|S_a,\boldsymbol{\chi}_i\right)^2-P\left(DCR_{LS}>1\middle|S_a,\mathbf{D}\right)^2 \quad (3.13)$$

where $\tilde{R}_F$ is the estimator for the Robust Fragility curve, n_{sim} is the number of simulations, $\boldsymbol{\chi}_i$ is the ith realization of the vector of fragility parameters $\boldsymbol{\chi}$. The vector $\boldsymbol{\chi}_i$ is simulated based on its probability density function $f(\boldsymbol{\chi}|\mathbf{D})$. Herein, an advanced simulation scheme known as Markov Chain Monte Carlo (MCMC) Simulation is employed in order to directly sample from the posterior joint PDF $f(\boldsymbol{\chi}|\mathbf{D})$. An example of MCMC applied for calculating Robust Fragility can be seen in [64]). A straightforward alternative would be to calculate the 5-parameter fragility by estimating the coefficients [ln$a$, b, β] and [α_0, α_1] through simple linear regression and logistic regression, respectively, which can easily be determined using MATLAB toolboxes [65]. If the Robust Fragility calculated as the (posterior) expected value of the proposed fragility (see Equation 3.10) is

equal (or very close) to the (posterior) median of the sampled fragility curves, it (the Robust Fragility) is also going to be equal (or very close) to the fragility calculated based on the posterior median of χ. Therefore, if the optimized estimates provided by the MATLAB toolbox do not deviate too much from the posterior median of the model parameters χ, the resulting fragility curve (obtained by using the MATLAB toolbox) would be presumably close to the Robust Fragility curve calculated through Equations 3.10 and 3.12. This is due to the invariance of median (as an ordered statistics) to monotonic mapping (the fragility function in this case). Nevertheless, the real benefit gained by calculating the Robust Fragility lies in the estimation of $\sigma^2_{\chi}(\cdot)$ (see Equation 3.11 and 3.13) which is essential for creating intervals of confidence for the estimated fragility.

3.3 CASE STUDY RESULTS

Three different reinforced concrete (RC) moment-resisting frames are considered herein: the north longitudinal perimeter frame and the east as-built transverse perimeter frame of the seven-story Holiday Inn hotel building in Van Nuys, California (presented in Chapter 1.6) and the same longitudinal frame, retrofitted with RC jacketing method (presented in details in Chapter 6.2). All the details about the modelling issues have been presented in details in Chapter 2.

3.3.1 RECORD SELECTION FOR NON LINEAR DYNAMIC ANALYSES

In this section, the record selection criteria for each non-linear dynamic analysis procedure adopted is described in details.

3.3.1.1 RECORD-SELECTION FOR CLOUD ANALYSIS

A set of 70 strong ground-motion records are selected from the NGA-West2 database [66], and listed in Table 3.1. This suite of records covers a wide range of magnitudes between 5.5 and 7.9, and closest distance-to-ruptured area (denoted as RRUP) up to around 40 km, as illustrated by the scatter diagram in Figure 3.1 (a). The associated spectral shapes are shown in Figure 3.1 (b). The soil average shear wave velocity in upper 30 m of soil, Vs30, at the Holiday Inn hotel's site is around 218 m/sec. Accordingly, all selected records are chosen from NEHRP site classes C-D. As mentioned in Section 3.2.3, a limit of maximum six recordings

from a single seismic event has been considered (except for Loma Prieta event). Moreover, only one of the two horizontal components of each recording, the one with larger spectral acceleration at 1.0 sec is selected. The lowest useable frequency is set at 0.25 Hz, ensuring that the low-frequency content is not removed by the ground motion filtering process. There is no specific consideration on the type of faulting; nevertheless, all selected records are from strike-slip or reverse faults (consistent with California faulting). The records are selected to be free field or on the ground level. Finally, there are no specific considerations being taken into account for spectral shape, epsilon, ε, and no distinction is made between the wave-forms in terms of ordinary and pulse-like ground motions. The average values for magnitude and distance of the selected records (see Figure 3.1 (a)) are consistent with the deaggregation-based mean values (M=6.9 and $15 \leq R_{RUP} \leq 20$ for 10% to 2% exceedance of Sa(T=1.0sec) in 50 years) furnished by USGS National Seismic Hazard Mapping Project website (http://earthquake.usgs.gov/hazards, last accessed July 2016), which is a part of the 2008 Interactive Deaggregation web tool (http://geohazards.usgs.gov/deaggint/2008/, last accessed July 2016).

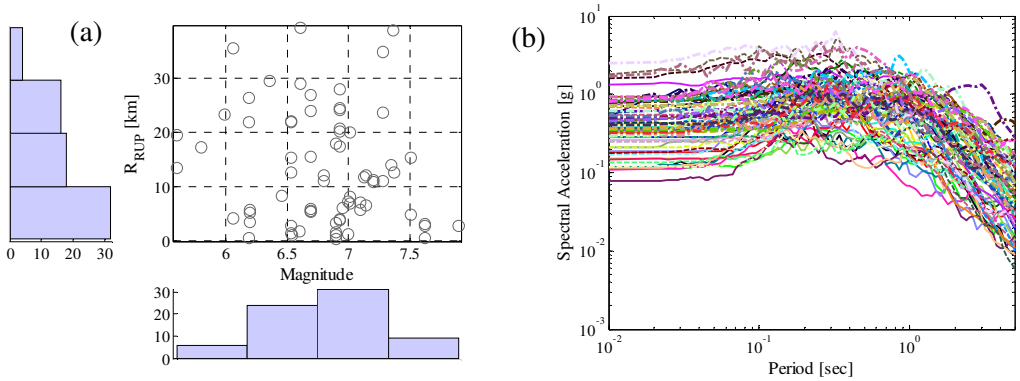

Figure 3.1: (a) Scatter diagram, and (b) spectral shape, for the suite of ground-motion records (Table 3.1).

Table 3.1: The suite of strong ground-motion records for Cloud Analysis (the highlighted records show the reduced record set).

Record Number	NGA Record Number	Earthquake Name	Station Name	Direction*
1	6	Imperial Valley-02	El Centro Array #9	1
2	15	Kern County	Taft Lincoln School	2
3	26	Hollister-01	Hollister City Hall	2
4	78	San Fernando	Palmdale Fire Station	1
5	93	San Fernando	Whittier Narrows Dam	2
6	139	Tabas, Iran	Dayhook	2
7	160	Imperial Valley-06	Bonds Corner	2
8	167	Imperial Valley-06	Compuertas	1
9	169	Imperial Valley-06	Delta	2
10	174	Imperial Valley-06	El Centro Array #11	1
11	176	Imperial Valley-06	El Centro Array #13	1
12	181	Imperial Valley-06	El Centro Array #6	1
13	214	Livermore-01	San Ramon-Eastman Kodak	1
14	338	Coalinga-01	Parkfield-Fault Zone 14	1
15	451	Morgan Hill	Coyote Lake Dam-SW Abut.	2
16	464	Morgan Hill	Hollister Diff. Array #3	1
17	502	Mt. Lewis	Halls Valley	2
18	522	N. Palm Springs	Indio	2
19	529	N. Palm Springs	North Palm Springs	1
20	548	Chalfant Valley-02	Benton	1
21	611	Whittier Narrows-01	Compton-Castlegate St	1
22	723	Superstition Hills-02	Parachute Test Site	1
23	737	Loma Prieta	Agnews State Hospital	1
24	739	Loma Prieta	Anderson Dam (Downst)	1
25	753	Loma Prieta	Corralitos	2
26	754	Loma Prieta	Coyote Lake Dam (Downst)	2
27	776	Loma Prieta	Hollister-South & Pine	1
28	779	Loma Prieta	LGPC	1
29	806	Loma Prieta	Sunnyvale-Colton Ave.	2
30	811	Loma Prieta	WAHO	2
31	825	Cape Mendocino	Cape Mendocino	1
32	827	Cape Mendocino	Fortuna-Fortuna Blvd	1
33	828	Cape Mendocino	Petrolia	2
34	838	Landers	Barstow	2
35	864	Landers	Joshua Tree	2
36	900	Landers	Yermo Fire Station	1
37	901	Big Bear-01	Big Bear Lake-Civic Cent.	1
38	982	Northridge-01	Administrative Building	2
39	995	Northridge-01	LA - Hollywood Stor FF	2
40	1003	Northridge-01	LA - Saturn St	2
41	1013	Northridge-01	LA Dam	1
42	1084	Northridge-01	Sylmar-Converter Sta	2

Record Number	NGA Record Number	Earthquake Name	Station Name	Direction*
44	1106	Kobe, Japan	KJMA	1
45	1114	Kobe, Japan	Port Island (0 m)	1
46	1119	Kobe, Japan	Takarazuka	1
47	1120	Kobe, Japan	Takatori	1
48	1158	Kocaeli, Turkey	Duzce	2
49	1176	Kocaeli, Turkey	Yarimca	2
50	1197	Chi-Chi, Taiwan	CHY028	2
51	1231	Chi-Chi, Taiwan	CHY080	1
52	1503	Chi-Chi, Taiwan	TCU065	1
53	1602	Duzce, Turkey	Bolu	2
54	1605	Duzce, Turkey	Duzce	2
55	1633	Manjil, Iran	Abbar	2
56	1787	Hector Mine	Hector	2
57	2114	Denali, Alaska	TAPS Pump Station #10	1
58	4040	Bam, Iran	Bam	1
59	4451	Montenegro, Yugo.	Bar-Skupstina Opstine	2
60	4458	Montenegro, Yugo.	Ulcinj-Hotel Olimpic	1
61	4875	Chuetsu-oki	Kariwa	1
62	4894	Chuetsu-oki	Kashiwazaki NPP, Unit 1	2
63	5482	Iwate	AKTH04	2
64	5825	El Mayor-Cucapah	Cerro Prieto Geothermal	2
65	6906	Darfield, NZ	GDLC	1
66	6911	Darfield, NZ	HORC	1
67	8123	Christchurch, NZ	Christchurch Resthaven	2
68	8130	Christchurch, NZ	Shirley Library	1
69	8157	Christchurch, NZ	Heathcote Valley	1
70	8161	El Mayor-Cucapah	El Centro Array #12	2

* "Direction" denotes one of the two horizontal components of each recording, and is assigned by "1" or "2" based on its appearance in the NGA-West2 data set.

3.3.1.2 RECORD-SELECTION FOR IDA

A subset of 34 ground-motion records are extracted from the 70 records of the original set defined in Section 3.2.3 (see also Table 3.1). The only criterion for this selection of records in order to implement Incremental Dynamic Analysis (IDA) was to limit the number of records from a single seismic event to one.

This criterion aims to eliminate eventual intra-event correlations between different registrations of the same earthquake. The records of this subset are highlighted with grey stripes in Table 3.1.

3.3.1.3 RECORD-SELECTION FOR MSA

Multiple-Stripe Analysis (MSA) consists of a set of single-stripe analyses (i.e., the results of nonlinear dynamic analyses of a suite of records scaled to a common IM value), performed at multiple levels of the IM to provide statistical information about the demand parameter over a wide range of IM values. Note that MSA (if the same suite of records is used for all IM levels) is simply a re-compilation of the results of IDA. The IDA curve connects the resulting demand parameters associated with each ground motion record scaled to multiple IM levels. Alternatively, the MSA can be performed so that the response spectra for the suite of records at each IM level match a target response spectrum mean and/or variance [19]; hence, different suite of records are selected at different IM levels. Herein, MSA is performed at each IM level by selecting recorded ground motions whose spectrum match the Conditional Spectrum (CS) mean and variance [27-28].

At each IM level, the target CS is constructed based on Method 1 described in [27], which is the most basic method for computing an approximate CS, based on a single earthquake scenario and single GMPE. The ground motions are selected to match the target CS mean and variance using ground-motion selection algorithm proposed in [67] (see http://web.stanford.edu/~bakerjw/gm_selection.html for the related MATLAB code, last accessed July 2016). The code uses the Campbell and Bozorgnia 2008 (CB08, [68]) ground-motion model for constructing the approximate CS and adopts disaggregation-based mean values for magnitude and distance furnished by the USGS Interactive Deaggregation web tool (see Section 3.3.1.1 for more details).

Three key issues are addressed at this point: (1) calculation of exact CS [27-28] is not done herein as it is not feasible for practical applications; however, following the recommendations in [69], the standard deviation values (obtained from approximate CS) are inflated by 10% in order to better match the exact CS; (2) the selected records' amplitude should not be magnified more than 4 times the original value; (3) the aforementioned MATLAB code for CS-based record selection uses NGA as the reference database. Therefore, some adjustments were made herein to identify the same records in the NGA-WEST2 database (the reference database in this work). For the three case-study frames with different fundamental periods, the CS are constructed at various IM levels. For each stripe, a set of 38 records that provide the best fit to the prescribed CS are selected. This is a reasonable number of records in order to perform the time-consuming MSA, that is also somewhat consistent with the number of records for IDA.

Figure 3.2 shows the response spectra of 38 ground motions (scaled to Sa(T1)) selected to match the CS for a given level of $Sa(T_1)$, where T_1 is close to the first-mode period of the case-study frames. The desired levels of $Sa(T_1)$ correspond to specific probabilities of exceedance (reported in the figure) in 50 years according to the site-specific mean hazard of the site.

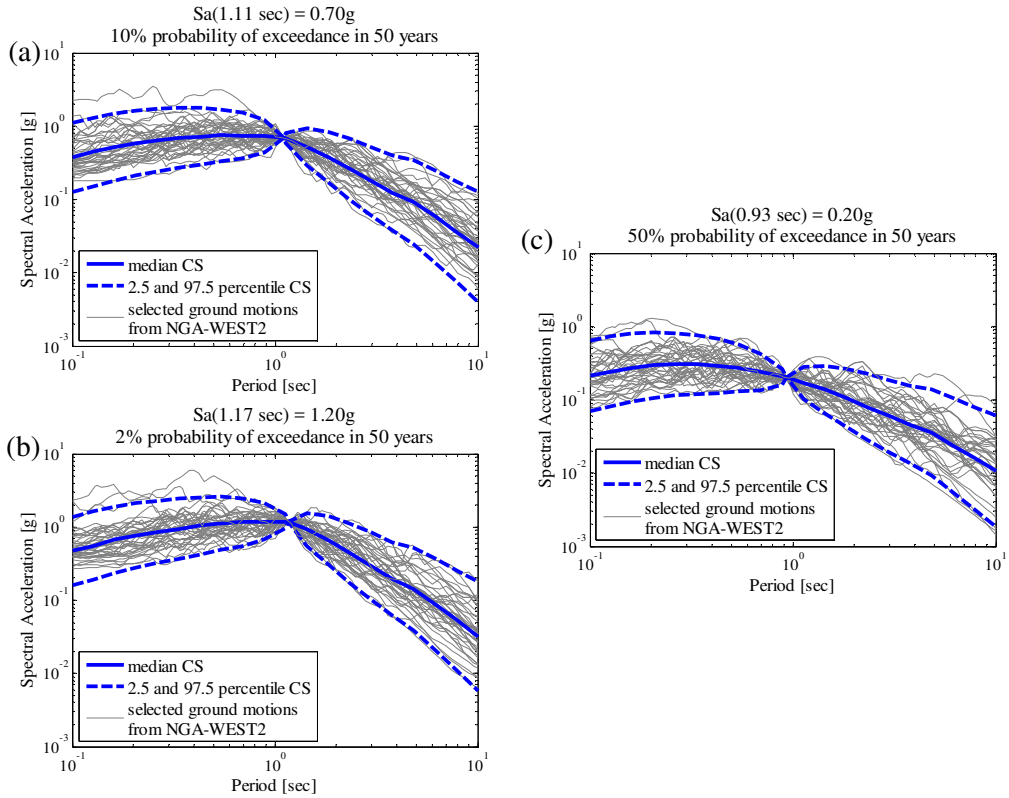

Figure 3.2 Response spectra of 38 ground motions selected to match the CS for a given level of Sa(T_1) for (a) transverse frame, (b) longitudinal frame, (c) retrofitted longitudinal frame.

3.3.2 CLOUD ANALYSIS

Figures 3.3 (a, b, c) show the scatter plots for Cloud data **D**={($S_{a,i}$, $DCR_{LS,i}$), i=1:70} for the three case-study frames and for the set of records outlined in Table 3.1. For each data point (colored squares), the corresponding record number is shown. The cyan-colored squares represent the *NoC* data, while the red-colored squares indicate the *C* data or "collapse-cases" (see Section 3.2.4). In order to have a better representation of *NoC* data, an upper-bound limit of 10 is assigned to the horizontal DCR_{LS}-axis. The figures illustrate the Cloud Analysis regression prediction model (i.e., regression line and the estimated parameters, see Equation 3.2) fitted to the *NoC* data. The Lognormal distribution displayed in Figure 3.3 (a, b, c) denotes the distribution of DCR_{LS} given $S_a(T_1)$=0.20g. Moreover, the line DCR_{LS}=1 corresponding to the onset of limit state (herein, Near-Collapse) is

shown with red-dashed line. It can be noted that, consistently with the Section 3.2.3 recommendations, the Cloud data not only covers a vast range of spectral acceleration values, but it also provides numerous data points in the range of DCR_{LS}>1. However, in case of retrofitted longitudinal frame, it was more difficult to find un-scaled records that could push the (strengthened) structure to pass the onset of Near-Collapse limit state. It can also be noted that the *b*-value (the logarithmic slope of the regression line) is similar for both longitudinal and transverse frames (~0.90); whereas, the *b*-value for the retrofitted frame (=1.20) is larger compared to the original frame indicating that the retrofitted structure is more ductile. The conditional dispersion β for the transverse frame (~0.2) is smaller that of the longitudinal frame (~0.3).

Furthermore, Figures 3.3 (a,b,c) illustrate the histograms of the regression residuals in the logarithmic scale for the non-collapse portion of the Cloud data. It can be observed that histograms reveal substantially uni-modal and symmetric shapes which justify the use of a Lognormal (Normal in the Logarithmic scale) fragility model. However, the histogram relative to the longitudinal frame represents a slightly heavy tail to the right. This can be attributed to the presence of numerous data points in the range of DCR_{LS} around 1 (see Figure 3.3 (b)), where some moderate deviations from the regression prediction can be observed. It should be noted that in these cases (i.e., DCR_{LS} around 1), the critical column reaches the softening branch of its corresponding backbone curve. Nevertheless, even for this frame, the distribution of the residuals does not seem to deviate too much from an uni-modal symmetric behavior to justify the use of distributions other than Lognormal.

Figures 3.3 (d, e, f) illustrate the fragility curves obtained by Equation 3.7 considering the collapse-cases explicitly (thick black lines). The figures also illustrate (in dashed red lines) the conditional probability of having *NoC*, $P(NoC|S_a)=1-P(C|S_a)$ (see Equation 3.6). According to Equation 3.4, the term $P(NoC|S_a)$ is multiplied by fragility curve of *NoC* data and summed with the $P(C|S_a)$ to obtain the fragility curve from Equation 3.7. These fragility curves considering collapse cases (thick black lines) are compared with those calculated from Equation 3.5 considering only *NoC* data (dotted gray lines). As a result, the explicit consideration of collapse-cases, based on the procedure described in Section 3.2.4, leads to the fragility curve that shifts slightly to the left (i.e., more

vulnerable structure). The shift in fragility to the left is more apparent in case of retrofitted longitudinal frame. This can be attributed to the fact that, for this frame, almost all the records that lead to DCR_{LS} >1 are identified as collapse-inducing (Figure 3.3 (c)). In other words, the NoC data represent the linear behavior more-or-less and the softening is considered almost entirely by consideration of collapse cases through Equation 3.7. It is important to highlight that, as it was expected, the number of collapse cases related to the existing frames (to the longitudinal one that is the most vulnerable, but also to the transversal one) is sensibly higher with respect to the number of collapse cases related to the retrofitted frame. In particular, the main condition that brings the existing frames to the collapse is related to the achievement of the maximum axial capacity of half plus one of the columns in one floor. With reference to the logistic regression model parameters (α_0 and α_1), they can be predicted in two alternative ways: (a) using a generalized linear regression with Logit link function in MATLAB [65] on the entire Cloud data; and (b) through Bayesian inference. Bayesian estimation of logistic model parameters is more suitable as it provides the joint posterior distribution of both linear (a, b and β) and logistic (α_0 and α_1) regression model parameters based on Cloud data. Hence, for the rest of the paper, the fragility curves considering collapse-cases are drawn with logit model parameters estimated by Bayesian inference.

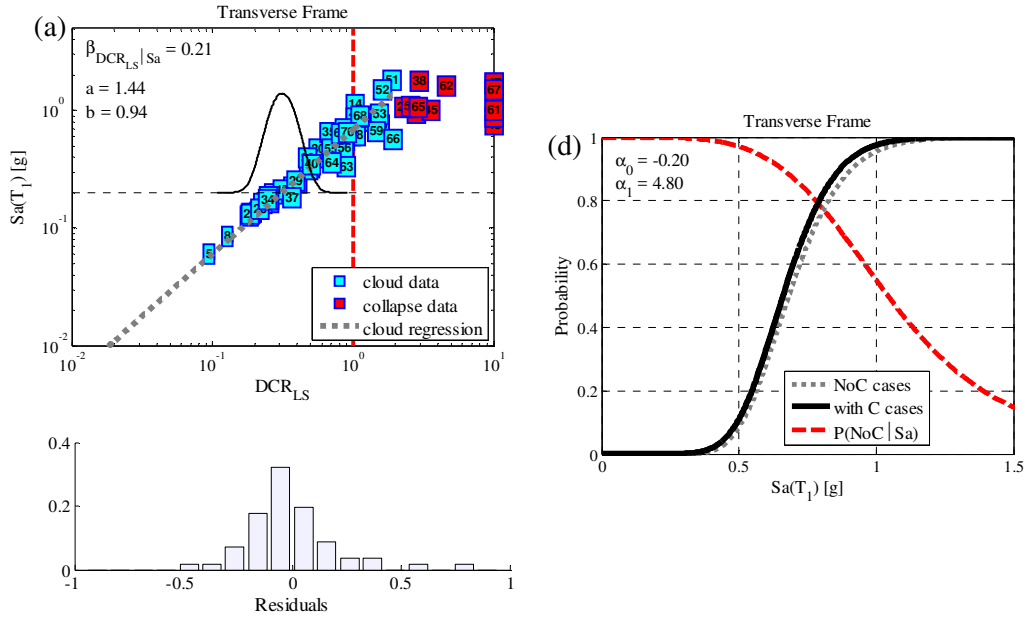

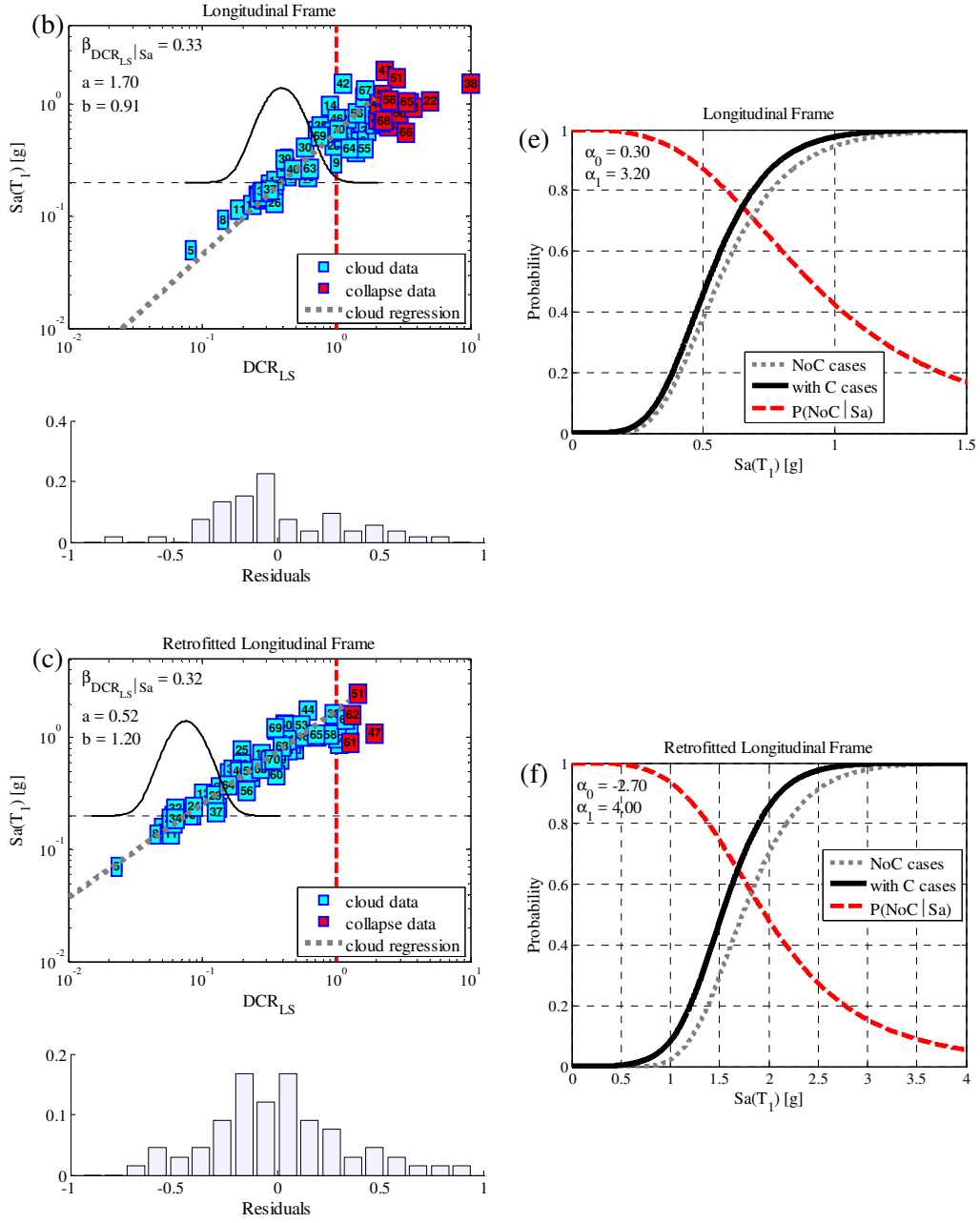

Figure 3.3 Cloud data and regressions, fragility curves, and probability of observing NoC for (a, d) transverse frame, (b, e) longitudinal frame, and (c, f) retrofitted longitudinal frame, considering the entire set of records in Table 3.1.

The Cloud Analysis is also performed for the reduced set of records (the subset of 34 ground motions highlighted in Table 3.1 as mentioned in Section 3.3.1.1). Comparing Figures 3.4 (a, b, c) with their counterparts in Figure 3.3 (a, b, c), it is evident that the regression parameters do not alter for transverse and retrofitted longitudinal frames. However, the regression coefficients (i.e., ln$a$, b) for the longitudinal frame are slightly larger when the reduced set of records is used. This is to be expected since, according to Figures 6(b) and 5(b), the reduced set of ground motion records does not adequately populate the DCR_{LS}>1 zone.

The fragility curves for both complete and reduced set of records together with their associated $P(NoC|S_a)$ are compared in Figure 3.4 (d, e, f). The fragility curve obtained from the reduced records set is different from that obtained based on the entire set for both longitudinal frames. This can be explained by the difference in the regression parameters and the significantly smaller number of collapse-cases (only one C data is available) when the reduced set is employed.

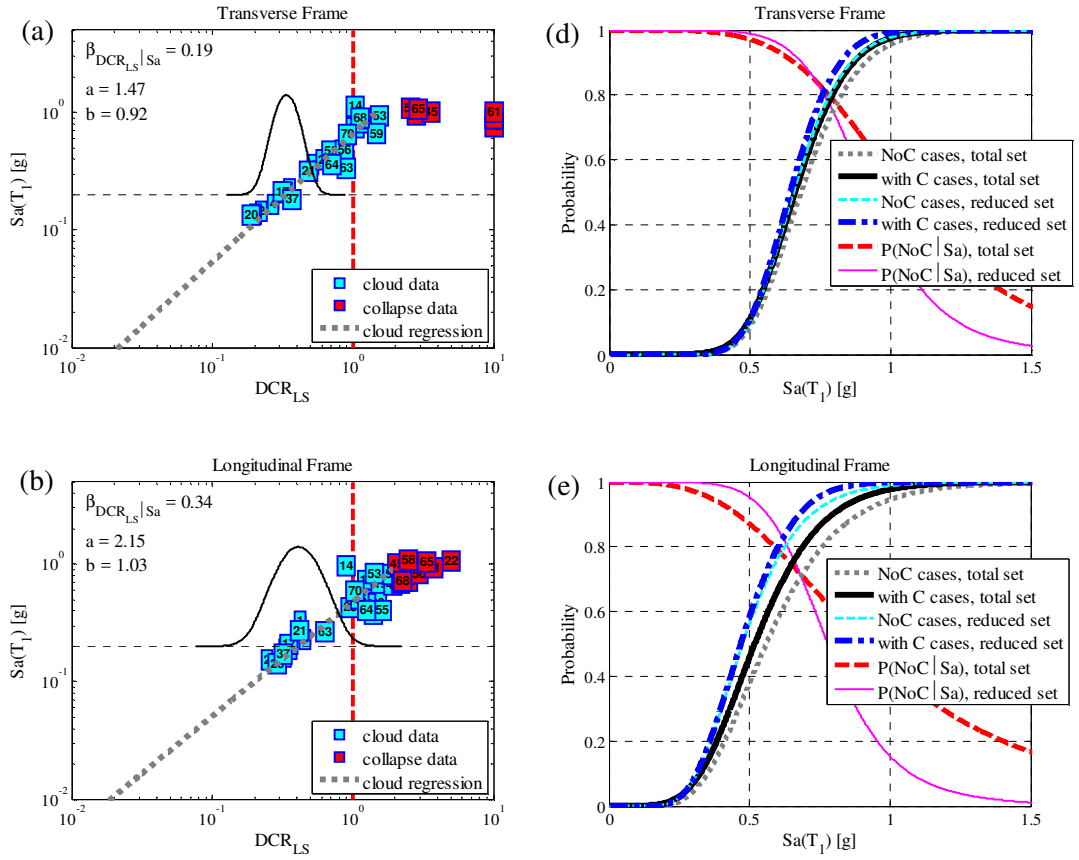

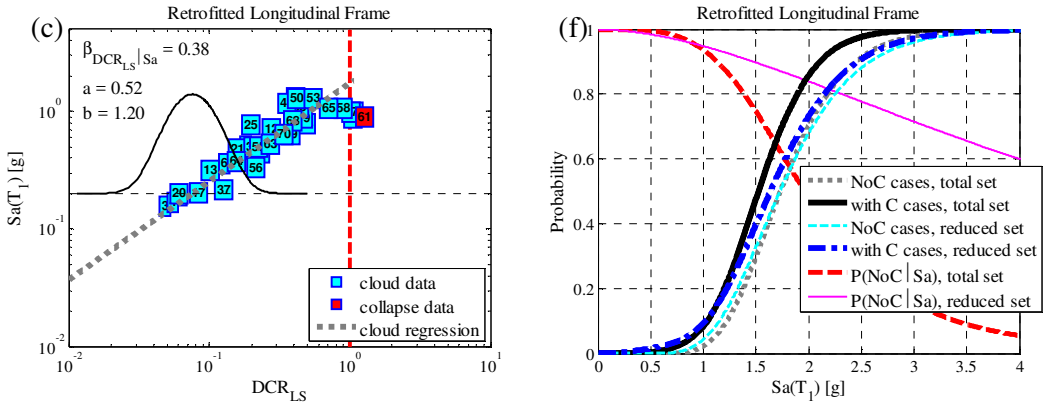

Figure 3.4 Cloud data and regressions for the reduced set in Table 3.1, and comparison of the fragility curves based on both set of records (entire and reduced) for (a, d) transverse, (b, e) longitudinal, and (c, f) retrofitted longitudinal frames.

3.3.3 INCREMENTAL DYNAMIC ANALYSIS (IDA)

This section is dedicated to benchmarking the Cloud results with respect to IDA results obtained for the suite of 34 ground-motion records described earlier in Section 3.3.1.2.

Figures 3.5 (a, b, c) illustrate the IDA curves (in thin gray lines). Each IDA curve traces the variation in DCR_{LS} for a given ground motion record as a function of $S_a(T_1)$ as the record's amplitude is linearly scaled-up. The gray dot at the end of each IDA curve marks the ultimate meaningful $S_a(T_1)$ level before the structure collapses.

The spectral acceleration values at DCR_{LS}=1, denoted as $S_a^{DCR=1}$ and obtained by cutting through the IDA curves by the vertical dashed red line plotted at DCR_{LS}=1, are marked on the plot as red stars. The figures also show (in blue dashed line) the (Lognormal) probability density function (PDF) fitted to the $S_a^{DCR=1}$ values. This PDF is later converted to a CDF in order to obtain the IDA-based fragilities [47] (referred to hereafter as the "Jalayer et al. 2007" method). The median of $S_a^{DCR=1}$ values (denoted as $\eta_{Sa}^{DCR=1}$, equal to the median of the IDA-based fragility curve) is illustrated in the figures as horizontal blue-dashed line.

In order to facilitate the comparison with Cloud Analysis results, the following information are plotted in Figures 3.5 (a, b, c): the Cloud data (cyan squares representing *NoC* data, red squares defining *C* data for the entire set of records in Table 3.1, see also Figure 3.3); the *NoC* regression prediction ($\eta_{DCRLS|Sa,NoC}$, see Equation 3.5, in black dotted line); and finally the Cloud prediction considering the collapse cases (i.e., 50th percentile DCR_{LS} denoted as DCR^{50th} and calculated from Equation 3.9) in black solid line. Note that two predictions (i.e., only *NoC* and considering also the *C* data) are very close up to DCR_{LS}=1; they start to diverge for large demand values DCR_{LS}>1.

It is seen that calculation of percentiles by using Equation 3.9 considering the *C* data has the advantage of "catching" the softening of percentile curves associated with the occurrence of global dynamic instability at high demand values. Accordingly, the spectral acceleration value at DCR^{50th}=1 (denoted as $S_a^{DCR50th=1}=(1/a)^{1/b}$) is illustrated as a horizontal dashed-dot black line. $S_a^{DCR50th=1}$ represents the median of Cloud-based fragility curve for the Near-Collapse limit state. It is interesting to note that the distance between the horizontal black dashed-dot ($S_a^{DCR50th=1}$) and blue dashed ($\eta_{Sa}^{DCR=1}$) lines marks the shift between the medians of the Cloud- and IDA-based fragility curves. It can be observed that this shift is more pronounced in the case of retrofitted longitudinal frame and less so for the other two frames.

Figure 3.5 (d, e, f) show the resulting IDA-based (Lognormal, blue-dashed lines) and Cloud-based (thick black lines) fragilities. It can be observed that the two fragility curves are quite close for the three frames with different trends. The difference between the median of the two curves is more pronounced for the transverse frame; this difference is less marked for the other two frames.

For the longitudinal frame, the dispersion in the IDA-based fragility is smaller than that of the Cloud-based fragility, while for the longitudinal retrofitted frame, the trend in the dispersions is reversed (see also Table 3.2 for comparing the median η and the logarithmic standard deviation β associated with the Cloud-, and IDA-based fragility curves). Figures 3.5 (d, e, f) show also alternative IDA-based fragility curves (in dash-dotted red line) obtained by following the fragility fitting method proposed in [70] (the method is called herein as "Baker 2015" and was originally proposed for MSA with different ground motions in each stripe).

It can be observed that “Jalayer et al. 2007” and “Baker 2015” lead to almost identical IDA-based fragility curves.

The two sets of IDA-based (light thick grey lines) and Cloud-based (Equation 3.9, black thick lines) 16th, 50th and 84th percentiles of performance variable DCR_{LS} given S_a are shown in Figures 3.5 (g, h, i).

It is observed that consideration of collapse information in Cloud Analysis manages to capture the softening trend in the (deformation-based) performance variable for large DCR_{LS} values (i.e., DCR_{LS}>1).

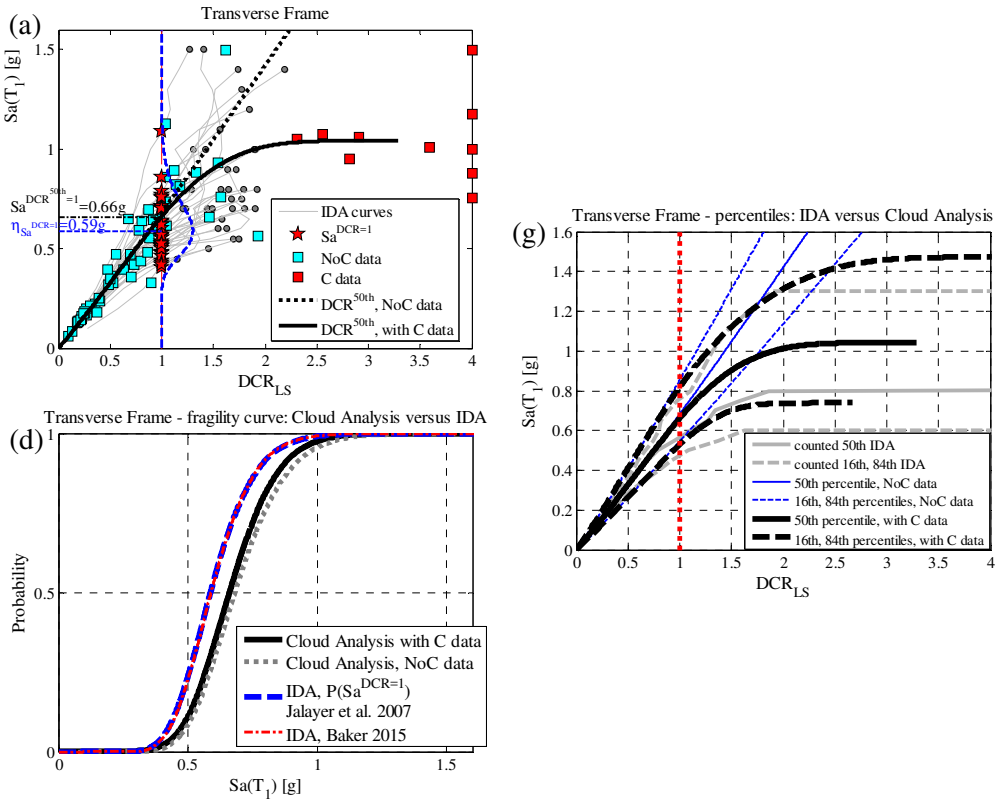

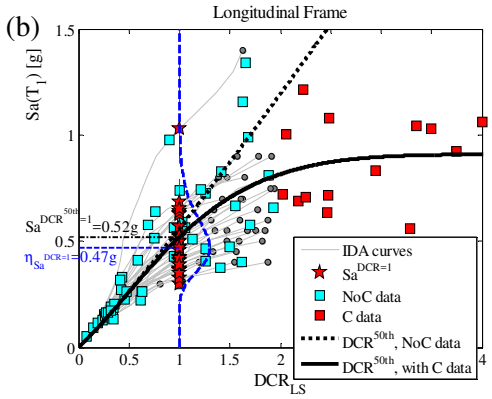
(b)
Longitudinal Frame
Sa(T1) [g]
DCRLS
IDA curves
Sa DCR=1
NoC data
C data
DCR 50th, NoC data
DCR 50th, with C data

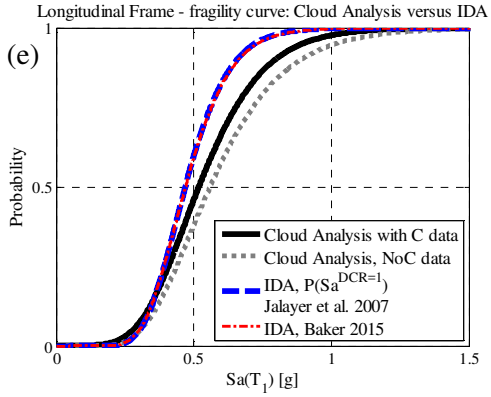
(e)
Longitudinal Frame - fragility curve: Cloud Analysis versus IDA
Probability
Sa(T1) [g]
Cloud Analysis with C data
Cloud Analysis, NoC data
IDA, P(Sa DCR=1)
Jalayer et al. 2007
IDA, Baker 2015

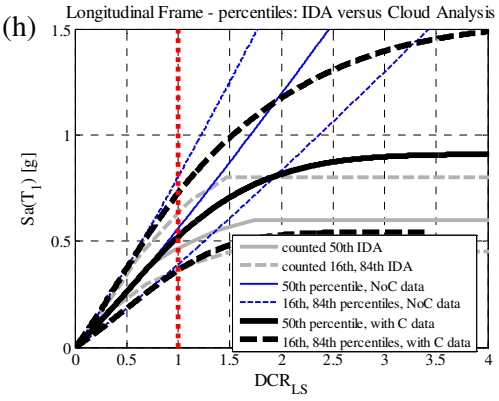
(h)
Longitudinal Frame - percentiles: IDA versus Cloud Analysis
Sa(T1) [g]
DCRLS
counted 50th IDA
counted 16th, 84th IDA
50th percentile, NoC data
16th, 84th percentiles, NoC data
50th percentile, with C data
16th, 84th percentiles, with C data

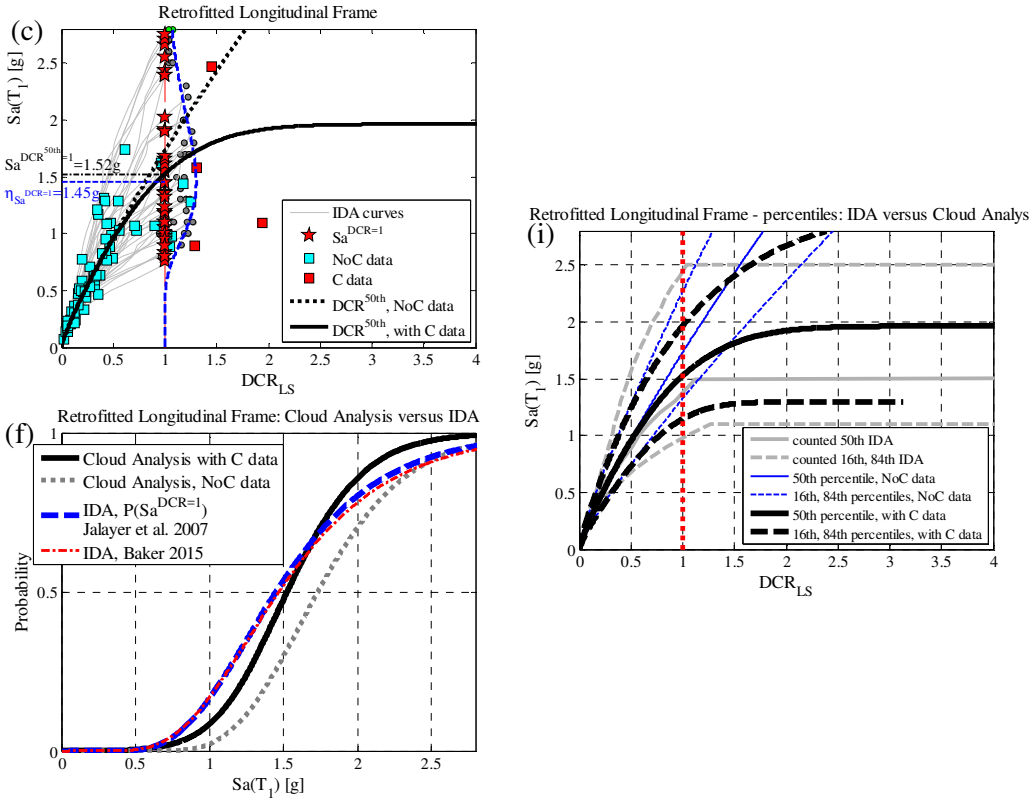

Figure 3.5 IDA curves, Cloud data and the regression predictions, and fragility curves for (a, d, g) transverse frame, (b, e, h) longitudinal frame, and (c, f, i) retrofitted longitudinal frame.

3.3.4 MULTIPLE STRIPE ANALYSIS (MSA)

In this section, MSA with different ground motions (selected compatible with the CS as in Section 3.3.1.3) at each IM level is used as a benchmark for comparing Cloud Analysis and IDA results. Figures 3.6 (a, b, c) shows MSA raw data (*Sa-DCR$_{LS}$*) for which the analyses are performed up to *IM* amplitudes where all ground motions cause collapse. Figures 3.6 (d, e, f) illustrate the MSA-based fragility curves (in red dash-dotted line) obtained by method of "Baker 2015" [70] compared with IDA- (in blue dashed line) and Cloud- (black solid line) based fragility curves. Moreover, Figures 3.6 (d, e, f) illustrate the empirical MSA-based fragility estimates (in red dots) obtained for each stripe as the ratio of the number of records with *DCR$_{LS}$*>1 to the total number of records in the stripe. It can be observed that, in the case of as-built longitudinal and transverse frames, the MSA-

based fragilities are in close agreement with Cloud-based fragilities (in comparison to the IDA-based curves).

In the case of the retrofitted frame with flexure-dominated behavior in the range of high non-linearity, the MSA- and Cloud-based fragilities start to diverge for spectral acceleration values larger than about 1.25g. This is to be expected because it is more difficult to populate the zone of $DCR_{LS}>1$ with Cloud data points (see Figure 3.3 (c) compared to Figures 3.3 (a) and 3.3 (b)). This covers the range of significant probability content for the fragility and hazard convolution integral (i.e., risk), as it is also evident from the hazard curve in Figure 3.6 (f). Furthermore, it is interesting to note that the MSA-based empirical fragility estimates per stripe are almost identical to the Cloud-based fragility curve for the retrofitted frame up to spectral acceleration values about 1.50g (equal to the median spectral acceleration value for the onset of Near-Collapse limit state, $DCR_{LS}\approx 1$, see Figure 3.5 (c)). The Cloud-based fragility indicates global Collapse with unit probability at S_a around 2.50g; this is while the MSA-based fragility indicates the global collapse at S_a around 4.0g. It should however be kept in mind that the records selected at very high spectral acceleration values have a CS-dictated spectral shape but they may not (they are not) records that have physically happened. This is also implied by the CS itself; the spectral shape pattern and its distribution is conditioned on the fact that an earthquake with a very large S_a value takes place (it is clearly very low-probability at S_a around 2.50g). Recall that the record selection in Table 3.1 used for Cloud Analysis has a maximum $S_a(T_1)$ around 2.50g. This is reflected also through the site-specific hazard (at T=1 sec, from USGS National Seismic Hazard Mapping Project website (http://earthquake.usgs.gov/hazards, last accessed July 2016) shown in Figures 3.6 (a, b, c) in cyan color where the difference between the Cloud Analysis- and MSA-based fragilities are more accentuated for the retrofit frame in the zone of very small hazard values.

Table 3.2 reports the Lognormal-equivalent statistics (median, η, and logarithmic standard deviation, β) associated with the Cloud-, MSA, and IDA-based fragility curves shown in Figures 3.6 (a, b, c). It can be observed that the dispersion associated with the MSA-based fragility for the retrofitted frame (0.44) is more than 1.5 times the dispersion associated with Cloud-based fragility.

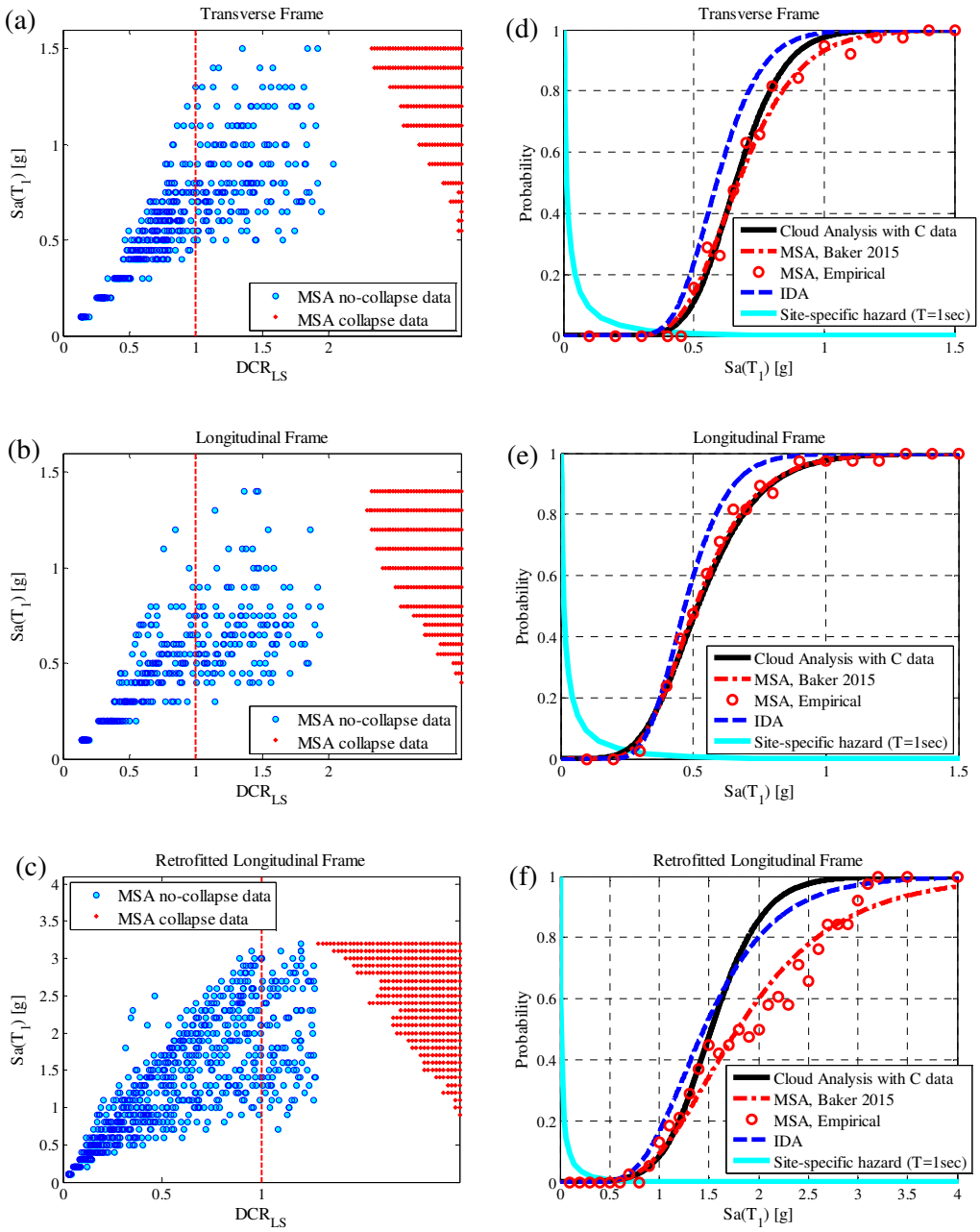

Figure 3.6 MSA results, and Cloud Analysis, MSA, and IDA fragility curves for (a, d) transverse frame, (b, e) longitudinal frame, and (c, f) retrofitted longitudinal frame.

Table 3.2: The median and logarithmic standard deviation (dispersion) for fragility curves.

Frame	Cloud Analysis		MSA		IDA	
	η [g]	β	η [g]	β	η [g]	β
transverse	0.66	0.22	0.67	0.27	0.59	0.23
longitudinal	0.52	0.35	0.51	0.34	0.47	0.26
longitudinal retrofitted	1.52	0.27	1.79	0.44	1.45	0.38

3.3.5 ROBUST CLOUD ANALYSIS CALCULATION

Figure 3.7 illustrates the Cloud-based Robust Fragility curves (thick black line) and their plus/minus two standard deviation confidence intervals (gray-colored area). The Robust Fragility curves and their confidence intervals are obtained following the procedure described in Section 3.2.6. Note that the Robust Fragility, denoted as $\tilde{R}_F$ (Equation 3.12), is very close to the fragility curve from Cloud Analysis considering *C* data (in cyan color, based on the MATLAB toolbox estimates). This is in agreement with the discussion in Section 3.2.6 (please also see the posterior statistics reported in Table 3.4 and the related discussion). The estimated standard deviation of the fragility model, denoted as σ_χ, (Equation 3.13) is also shown in Figure 3.7.

To have a comparison, the fragility curves obtained based on Cloud Analysis considering *NoC* data (gray dotted line), MSA (red dash-dotted line), and IDA (blue dashed line) are potted. The Cloud Analysis-based fragility considering only *NoC* data is within the confidence band for all frames. It can be observed that the confidence band calculated based on Cloud Analysis properly captures the IDA-based and MSA-based fragility curves associated with the transverse and longitudinal frames.

In case of the retrofitted frame, plus/minus two standard deviation confidence interval captures the trend of fragility curves from IDA and MSA (up to median). It is noted that in case of MSA, selected records do not reflect the real recordings taken place in any registered database. From another point of view, the lack of registered recordings can lead to more conservative Robust Fragility estimates based on Cloud Analysis. In case of IDA, it can be presumed that amplitude scaling of the selected set of records cause overestimation of Near-Collapse limit state probability compared to MSA-based fragility.

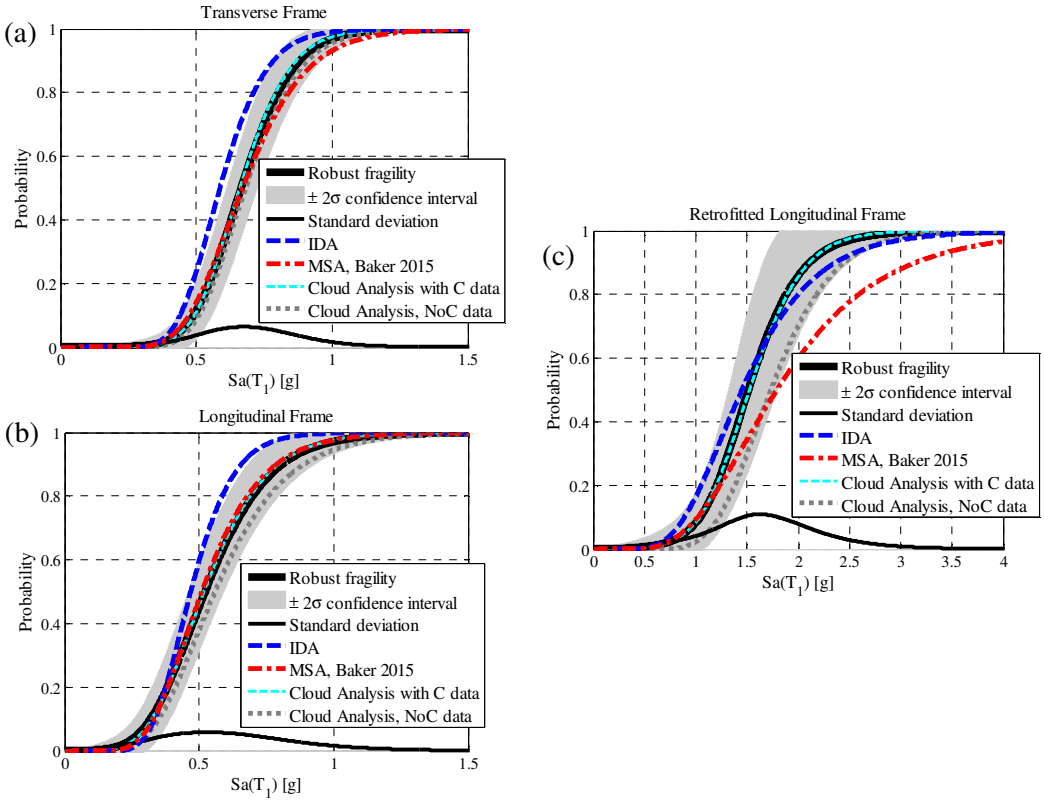

Figure 3.7 Comparison of the Robust fragility estimates and other fragility curves for (a) transverse, (b) longitudinal, and (c) retrofitted longitudinal frames.

Table 3.3 illustrates the mean annual frequencies of exceeding the Near-Collapse limit state (i.e., risk obtained by integrating the fragility and site-specific hazard curve) denoted by λ_{LS} corresponding to the Robust Fragility and its confidence interval. $\tilde{R}_F$ denotes the Robust Fragility and $\tilde{R}_F \pm 2\sigma_{\chi}$ defines the Robust Fragility plus/minus its two standard deviation confidence intervals. In addition, Table 3.3 shows λ_{LS} corresponding to IDA and MSA by integrating their fragilities over the hazard curve which lie within the confidence interval of λ_{LS} associated with Robust Fragility estimation. Contrary to the expectations, the IDA-based risk estimate for the retrofitted longitudinal frame is lower than the Cloud-based one. In fact, looking at the two curves at very low spectral acceleration values (corresponding to the highest hazard values and affecting the risk significantly), it can be noted that the IDA-based curve indicates lower fragility (this trend is reversed for moderate intensity levels).

Table 3.3: Mean annual frequency of exceeding the limit state.

Frame	λ_{LS} using the Robust fragility			λ_{LS} using the IDA fragility	λ_{LS} using the MSA fragility
	$\tilde{R}_F$-2σ_{χ}	$\tilde{R}_F$	$\tilde{R}_F$+2σ_{χ}		
transverse	1.2×10^{-3}	2.4×10^{-3}	3.5×10^{-3}	3.0×10^{-3}	2.3×10^{-3}
longitudinal	1.8×10^{-3}	5.1×10^{-3}	8.4×10^{-3}	5.2×10^{-3}	4.7×10^{-3}
longitudinal retrofitted	0.1×10^{-3}	0.6×10^{-3}	0.0165	0.35×10^{-3}	0.2×10^{-3}

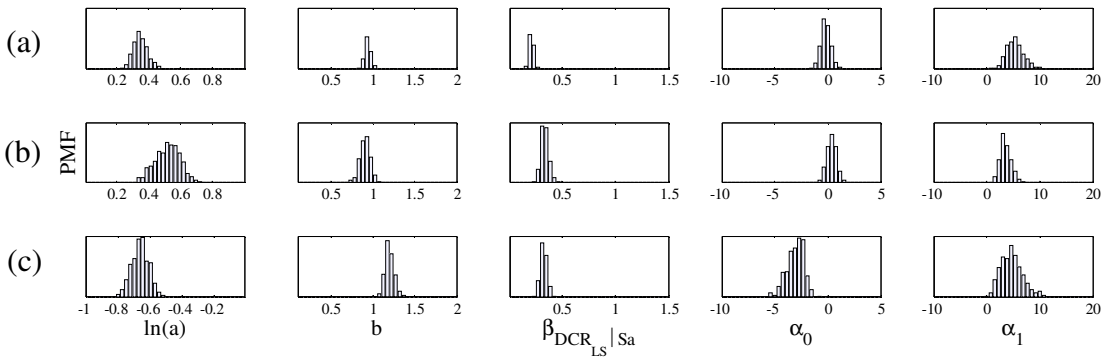

Figure 3.8: The marginal PMF's corresponding to the five model parameters for (a) transverse, (b) longitudinal, and (c) retrofitted longitudinal frames.

Figure 3.8 shows the marginal probability mass functions (PMF) corresponding to the five model parameters denoted in Section 3.2.4 as $\boldsymbol{\chi}$=[ln$a$, b, $\beta_{DCRLS|Sa}$, α_0, α_1]. By employing MCMC simulation algorithm, samples are generated as a Markov Chain sequence directly from the posterior (target) probability distribution $f(\boldsymbol{\chi}|\boldsymbol{D})$. The MCMC procedure is carried out by generating 5000 samples herein. The posterior MCMC-based mean, median and standard deviation and the optimized MATLAB-based estimates (also shown in Figure 3.3) for the fragility parameters are reported in Table 3.4.

It can be observed that the (posterior) means and medians of the first three parameters [ln$a$, b, $\beta_{DCRLS|Sa}$] have a very good agreement with their counterparts based on the MATLAB toolbox, while the mean and median for logistic model parameters α_0 and α_1 are slightly different from the MATLAB-based estimates (see the discussion at the end of Section 3.2.6). This indicates that logistic model parameters could have some correlation with the linear regression model parameters. It is also interesting to note that among the model parameters, parameters b and $\beta_{DCRLS|Sa}$ have the lowest variation.

Table 3.4: Statistics of model parameters χ.

Frame	ln$a$			b			$\beta_{DCRLS\|Sa}$		
	mean/med*	std†	M‡	mean/med	std	M	mean/med	std	M
transverse	0.35/0.35	0.04	0.36	0.94/0.94	0.03	0.94	0.22/0.22	0.02	0.21
longitudinal	0.52/0.52	0.07	0.53	0.90/0.91	0.06	0.91	0.34/0.34	0.03	0.33
retrofitted	-0.66/-0.66	0.05	-0.65	1.20/1.19	0.05	1.20	0.33/0.33	0.03	0.32

Frame	α_0			α_1		
	mean/med	std	M	mean/med	std	M
transverse	-0.19/-0.21	0.45	-0.20	5.34/5.24	1.51	4.80
longitudinal	0.37/0.38	0.44	0.30	3.55/3.43	1.00	3.20
retrofitted	-3.04/-2.94	0.79	-2.70	4.69/4.58	1.98	4.00

* median, † standard deviation, ‡ MATLAB estimate

3.4 CONCLUSIONS

This chapter is focused on the implementation of Cloud Analysis as non-linear dynamic analysis procedure based on a set of unscaled ground motion records and simple linear regression in the logarithmic scale. It can lead to very good fragility estimates on two conditions: (1) the ground motion records are chosen carefully; and (2) a scalar demand to capacity ratio that is always equal to one at the onset of the limit state is adopted as the performance variable. Two simple rules are defined for records selection: (1) make sure that a significant portion of the records leads to demand to capacity ratios greater than one; and (2) make sure that the suite of records covers a wide range of seismic intensity levels. Satisfying the above-mentioned rules almost always entails the presence of records that lead the structure into collapse. Therefore, the original simple logarithmic regression fragility model is extended into a five-parameter fragility model, which is created analytically as a mix of linear logarithmic regression and logistic regression. These parameters are estimated through Bayesian inference adopting a Markov Chain Monte Carlo simulation procedure which leads to a "Robust" Fragility and its plus/minus k standard deviation confidence band (e.g., k=2) that consider the uncertainties in fragility parameters. Two different benchmarks are set: fragility obtained based on the IDA (the records are scaled) and fragility obtained based on MSA with variable conditional spectrum-compatible records per intensity levels (again scaling is tolerated within a certain limit). The methods are

demonstrated using three frames representing shear-critical, shear-critical/flexure-dominated and flexure-dominated behaviour.

It is observed that the difference with IDA-based and MSA-based fragilities are almost always contained within the plus/minus two standard deviation confidence intervals. For the shear-critical and shear-critical/flexure-dominated frames, the Robust Fragility obtained from Cloud Analysis-based fragility is very close to that obtained based on MSA while IDA-based fragility seems somehow more distant. The MSA results picture the flexure-dominated frame as an almost invincible structure; a result that is obtained based on ground motion records that have not physically occurred. In this case, the Cloud Analysis results lie somewhere in between the MSA and IDA results (that remain particularly conservative). Moreover, comparison of two sets of records containing 34 and 70 records further emphasizes the importance of populating adequately all intensity levels with data points. It is also worth mentioning that the Bayesian parameter estimation procedure based on Markov Chain Monte Carlo is particularly useful for providing the confidence intervals for the Robust Fragility curve and for capturing the correlation between various fragility parameters. One can also obtain the fragility estimate (without the confidence band) by using simple MATLAB toolboxes of regression and generalized regression (without obtaining the joint distribution of the fragility parameters). This work is done for the limit state of Near-Collapse but can be performed for any other limit state. It should be underlined that the current work considers the uncertainty due to record-to-record variability in the ground motion and the uncertainty in the fragility parameters. Nevertheless, in Chapter 5 an application is presented to show how to extend this work in order to consider also the structural modeling uncertainties.

3.5 REFERENCES

[1] Jalayer, F., Ebrahimian, H., Miano, A., Manfredi, G., and Sezen, H., 2017. Analytical fragility assessment using un-scaled ground motion records. Earthquake Engineering and Structural Dynamics; https://doi.org/10.1002/eqe.2922.

[2] Hickman, J.W., 1983. PRA procedures guide: a guide to the performance of probabilistic risk assessments for nuclear power plants. NUREG/CR-2300, U.S. Nuclear Regulatory Commission, Washington, DC.

[3] Kennedy, R.P., Short, A.S., McDonald, R.R., McCann, Jr M.W., Murray, R.C., Hill, J.R., and Gopinath, V., 1994. Natural phenomena hazards design and evaluation criteria for department of energy facilities. DOE-STD-1020–94, U.S. Department of Energy, Washington, DC.

[4] FEMA-350 Recommended Seismic Design Criteria for New Steel Moment-Frame Buildings. Federal Emergency Management Agency: Washington, DC, 2000.

[5] FEMA P-58-1 Seismic Performance Assessment of Buildings Volume 1-Methodology. Federal Emergency Management Agency: Washington, DC, 2012.

[6] Krawinkler, H., 1999. Challenges and progress in performance-based earthquake engineering. International Seminar on Seismic Engineering for Tomorrow-In Honor of Professor Hiroshi Akiyama, Tokyo, Japan, November 26, 1999.

[7] Cornell, C.A., Krawinkler, H., 2000. Progress and challenges in seismic performance assessment. PEER Center News; 3 (2): 1-3.

[8] Kannan, A.E., and Powell, G.H., 1973. Drain-2D: a general-purpose computer program for dynamic analysis of inelastic plane structures. Earthquake Engineering Research Center (EERC) 73-6, University of California, Berkeley, CA.

[9] Carr A.J., 2001. Ruaumoko. Computer Program Library, Department of Civil Engineering, University of Canterbury: New Zealand.

[10] Vamvatsikos, D., and Cornell, C.A., 2002. Incremental dynamic analysis. Earthquake Engineering and Structural Dynamics; 31 (3): 491-514.

[11] Jalayer, F., and Cornell, C.A., 2003. A Technical Framework for Probability-Based Demand and Capacity Factor Design (DCFD) Seismic Formats. Pacific Earthquake Engineering Center (PEER) 2003/08.

[12] Jalayer, F., and Cornell, C.A., 2009. Alternative non-linear demand estimation methods for probability-based seismic assessments. Earthquake Engineering and Structural Dynamics; 38 (8): 951-972.

[13] Cornell, C.A., Jalayer, F., Hamburger, R.O., and Foutch, D.A., 2002. Probabilistic basis for 2000 SAC federal emergency management agency steel moment frame guidelines. Journal of Structural Engineering (ASCE); 128 (4): 526-533.

[14] Bertero, V.V., 1980. Strength and deformation capacities of buildings under extreme environments. In Structural engineering and structural mechanics,

A Volume Honoring Edgar P. Popov, Pister K (ed.). Prentice-Hall: Englewood Cliffs, N.J.; 188-237.

[15] Singhal, A., and Kiremidjian, A.S., 1996. Method for probabilistic evaluation of seismic structural damage. Journal of Structural Engineering; 122 (12): 1459-1467.

[16] Bazzurro, P., Cornell, C.A., Shome, N., and Carballo, J.E., 1998. Three proposals for characterizing MDOF nonlinear seismic response. Journal of Structural Engineering (ASCE); 124 (11): 1281-1289.

[17] Shome, N., Cornell, C.A., Bazzurro, P., and Carballo, J.E., 1998. Earthquakes, records, and nonlinear responses. Earthquake Spectra; 14 (3): 469-500.

[18] Luco, N., and Cornell, C.A., 1998. Seismic drift demands for two SMRF structures with brittle connections. Structural Engineering World Wide; Elsevier Science Ltd., Oxford, England, Paper T158-3.

[19] Baker, J.W., and Cornell, C.A., 2006. Spectral shape, epsilon and record selection. Earthquake Engineering and Structural Dynamics; 35 (9): 1077-1095.

[20] Lin, T., and Baker, J.W., 2013. Introducing Adaptive Incremental Dynamic Analysis: A new tool for linking ground motion selection and structural response assessment. In: Proceedings of the 11th International Conference on Structural Safety and Reliability (ICOSSAR 2013), Deodatis G, Ellingwood B, Frangopol D. (eds.). The International Association for Structural Safety and Reliability: New York, NY, 2013.

[21] Luco, N., and Cornell, C.A., 2007. Structure-specific scalar intensity measures for near-source and ordinary earthquake ground motions. Earthquake Spectra; 23 (2): 357-392.

[22] Jalayer, F., Beck, J., and Zareian, F., 2012. Analyzing the sufficiency of alternative scalar and vector intensity measures of ground shaking based on information theory. Journal of Engineering Mechanics; 138 (3): 307-316.

[23] Ebrahimian, H., Jalayer, F., Lucchini, A, Mollaioli, F., and Manfredi, G., 2015. Preliminary ranking of alternative scalar and vector intensity measures of ground shaking. Bulletin of Earthquake Engineering; 13 (10): 2805-2840.

[24] Baker, J.W., and Cornell, C.A., 2005. A vector - valued ground motion intensity measure consisting of spectral acceleration and epsilon. Earthquake Engineering and Structural Dynamics; 34 (10): 1193-1217.

[25] Baker, J.W., and Cornell, C.A., 2008. Vector-valued intensity measures incorporating spectral shape for prediction of structural response. Journal of Earthquake Engineering; 12 (4): 534-554.

[26] Baker, J.W., 2011. Conditional Mean Spectrum: Tool for ground motion selection. Journal of Structural Engineering (ASCE); 137 (3): 322–331

[27] Lin, T., Harmsen, S.C., Baker, J.W., and Luco N., 2013. Conditional Spectrum computation incorporating multiple causal earthquakes and ground motion prediction models. Bulletin of the Seismological Society of America; 103 (2A): 1103–1116.

[28] Ebrahimian, H., Azarbakht, A.R., Tabandeh, A., and Golafshani, AA., 2012. The exact and approximate conditional spectra in the multi-seismic-sources regions. Journal of Soil Dynamics and Earthquake Engineering; 39 (1): 61-77.

[29] Ellingwood, B.R, Celik, O.C., and Kinali, K., 2007. Fragility assessment of building structural systems in Mid - America. Earthquake Engineering and Structural Dynamics; 36 (13): 1935-1952.

[30] Celik, O.C., and Ellingwood, B.R., 2010. Seismic fragilities for non-ductile reinforced concrete frames–Role of aleatoric and epistemic uncertainties. Structural Safety; 32 (1): 1-12.

[31] Elefante, L., Jalayer, F., Iervolino, I., and Manfredi. G., 2010. Disaggregation-based response weighting scheme for seismic risk assessment of structures. Soil Dynamics and Earthquake Engineering; 30 (2): 1513-1527.

[32] Jeong, S.H., Mwafy, A.M., and Elnashai, A.S., 2012. Probabilistic seismic performance assessment of code-compliant multi-story RC buildings. Engineering Structures; 34: 527-537.

[33] Jalayer, F., De Risi, R., and Manfredi, G., 2015. Bayesian Cloud Analysis: efficient structural fragility assessment using linear regression. Bulletin of Earthquake Engineering; 13 (4): 1183-1203.

[34] Romão, X., Delgado, R., and Costa, A., 2013. Alternative closed - form solutions for the mean rate of exceedance of structural limit states. Earthquake Engineering and Structural Dynamics; 42 (12): 1827-1845.

[35] Modica, A., and Stafford, P.J., 2014. Vector fragility surfaces for reinforced concrete frames in Europe. Bulletin of Earthquake Engineering; 12 (4): 1725-1753.

[36] Zareian, F., and Kaviani, P., 2015. Taciroglu E. Multiphase Performance Assessment of Structural Response to Seismic Excitations. Journal of Structural Engineering (ASCE); 141 (11): 04015041.

[37] Sasani, M., Kiureghian, A.D., 2001. Seismic fragility of RC structural walls: displacement approach. Journal of Structural Engineering (ASCE); 127 (2): 219-228.

[38] Shinozuka, M., Feng, M.Q., Lee, J., Naganuma, T., 2000. Statistical analysis of fragility curves. Journal of engineering mechanics (ASCE); 126 (12): 1224-1231.

[39] Radu, A.C., and Grigoriu, M., 2015. Bayesian statistics: applications to earthquake engineering. Encyclopedia of Earthquake Engineering edited by Beer M, Patelli E, Kougioumtzoglou I, and Au S-K, pp 225-235.

[40] CEN. Eurocode 8: design of structures for earthquake resistance. Part 1: General rules, seismic actions and rules for buildings. EN 1998-1 CEN Brussels: April 2004.

[41] Bianchini, M., Diotallevi, P.P., and Baker J.W., 2009. Prediction of inelastic structural response using an average of spectral accelerations. 10th International Conference on Structural Safety and Reliability (ICOSSAR09), Osaka, Japan, 2009.

[42] Eads, L., Miranda, E., and Lignos, D.G., 2015. Average spectral acceleration as an intensity measure for collapse risk assessment. Earthquake Engineering and Structural Dynamics; 44 (12): 2057-2073.

[43] Kohrangi, M., Bazzurro, P., and Vamvatsikos, D., 2016. Vector and scalar IMs in structural response estimation, Part I: Hazard analysis. Earthquake Spectra; 32 (3): 1507-1524.

[44] Jalayer, F., Franchin, P., and Pinto, P.E., 2007. A scalar damage measure for seismic reliability analysis of RC frames. Earthquake Engineering and Structural Dynamics; 36 (13): 2059–2079.

[45] Ditlevsen, O., Madsen, H.O., 1996. Structural reliability methods. Wiley: New York.

[46] Galanis, P.H., and Moehle, J.P., 2015. Development of collapse indicators for risk assessment of older-type reinforced concrete buildings. Earthquake Spectra; 31 (4): 1991-2006.

[47] Jalayer, F., Asprone, D., Prota, A., and Manfredi G., 2011. Multi-hazard upgrade decision making for critical infrastructure based on life-cycle cost criteria. Earthquake Engineering and Structural Dynamics; 40 (10): 1163-1179.

[48] Jalayer, F., Asprone, D., Prota, A., and Manfredi, G., 2009. A decision support system for post-earthquake reliability assessment of structures subjected to aftershocks: an application to L'Aquila earthquake. Bulletin of Earthquake Engineering 2011; 9 (4): 997-1014.

[49] Ebrahimian, H., Jalayer, F., Asprone, D., Lombardi, A.M., Marzocchi, W., Prota, A., and Manfredi, G., 2014. A performance-based framework for adaptive seismic aftershock risk assessment. Earthquake Engineering and Structural Dynamics; 43 (14): 2179-2197.

[50] Haselton, C.B, and Deierlein, G.G., 2007. Assessing seismic collapse safety of modern reinforced concrete moment-frame buildings. Pacific Earthquake Engineering Center (PEER) 2007/08.

[51] Villaverde, R., 2007. Methods to assess the seismic collapse capacity of building structures: State of the art. Journal of Structural Engineering; 133 (1): 57-66.

[52] Zareian, F., and Krawinkler, H., 2007. Assessment of probability of collapse and design for collapse safety. Earthquake Engineering and Structural Dynamics; 36 (13): 1901-1914.

[53] Shome, N., and Cornell, C.A., 1999. Probabilistic seismic demand analysis of nonlinear structures. Report No. RMS35, Stanford University, CA, 1999: 320 pp.

[54] Stoica, M., Medina, R.A., McCuen, R.H., 2007. Improved Probabilistic Quantification of Drift Demands for Seismic Evaluation. Structural Safety; 29 (2): 132-45.

[55] Jalayer, F., and Ebrahimian, H., 2016. Seismic risk assessment considering cumulative damage due to aftershocks. Earthquake Engineering and Structural Dynamics; 46: 369-389, DOI: 10.1002/eqe.2792.

[56] Papadimitriou, C., Beck, J.L., and Katafygiotis, L.S., 2001. Updating robust reliability using structural test data. Probabilistic Engineering Mechanics; 16 (2): 103-113.

[57] Beck, J.L., and Au S.K., 2002. Bayesian updating of structural models and reliability using Markov Chain Monte Carlo simulation. Journal of Engineering Mechanics (ASCE); 128 (4): 380-391.

[58] Jalayer, F., Iervolino, I., and Manfredi, G., 2010. Structural modeling uncertainties and their influence on seismic assessment of existing RC structures. Structural Safety; 32 (3): 220-228.

[59] Jalayer, F., Elefante, L., Iervolino, I., and Manfredi, G., 2011. Knowledge-based performance assessment of existing RC buildings. Journal of Earthquake Engineering; 15 (3): 362-389.

[60] Jalayer, F., Carozza, S., De Risi, R., Manfredi, G., and Mbuya, E., 2016. Performance-based flood safety-checking for non-engineered masonry structures. Engineering Structures; 106: 109-123.

[61] Straub, D., and Der Kiureghian, A., 2008. Improved seismic fragility modeling from empirical data. Structural Safety; 30 (4): 320-336.

[62] The Mathworks 2016, MATLAB 2016b Release. http://softwaresso.unina.it/matlab/ [accessed on 15 September 2016].

[63] Metropolis, N., Rosenbluth, A.W., Rosenbluth, M.N., Teller, A.H., and Teller, E., 1953. Equations of state calculations by fast computing machines. Journal of Chemical Physics; 21 (6): 1087-1092.

[64] Hastings, W.K., 1970. Monte-Carlo sampling methods using Markov chains and their applications. Biometrika; 57 (1): 97-109.

[65] ACI 318-14. Building Code Requirements for Structural Concrete. ACI Committee 318, American Concrete Institute, 2014.

[66] Ancheta, T.D., 2014. et al. NGA-West2 Database. Earthquake Spectra; 30(3), 989-1005.

[67] Jayaram, N., Lin, T., and Baker, J.W., 2011. A computationally efficient ground-motion selection algorithm for matching a target response spectrum mean and variance. Earthquake Spectra; 27 (3): 797-815.

[68] Campbell, K.W., and Bozorgnia, Y., 2008. NGA ground motion model for the geometric mean horizontal component of PGA, PGV, PGD and 5% damped linear elastic response spectra for periods ranging from 0.01 to 10 s. Earthquake Spectra; 24 (1): 139-171.

[69] NEHRP NIST GCR 11-917-15. Selecting and scaling earthquake ground motions for performing response-history analyses. National Institute of Standards and Technology, Engineering Laboratory: Gaithersburg, Maryland, 2011.

[70] Baker, J.W., 2015. Efficient analytical fragility function fitting using dynamic structural analysis. Earthquake Spectra; 31 (1): 579-599.

Chapter 4

CLOUD TO IDA: EFFICIENT FRAGILITY ASSESSMENT WITH LIMITED SCALING

4.1 INTRODUCTION

Chapter 4 proposes a new procedure that fuses together Cloud Analysis and IDA [1]. In fact, the goal of this chapter is to extend the work presented in Chapter 3 in order to find an efficient solution for performing IDA, based on the consideration that the intensity levels to scale should be chosen strategically to scaling in a strictly necessary manner the records. Certainly, this chapter, as the previous one, deals mainly with the accurate identification of the level of performance in order to facilitate efficient seismic assessment and classification of old nonductile buildings [2, 3]. In this context, analytic structural fragility assessment is one of the fundamental steps in the modern performance-based engineering [4]. In general, as previously presented, methods for assessing the structural fragility for a given limit state can range from the simplest methods based on the response of an equivalent single-degree-of-freedom (SDOF) model, to complex nonlinear dynamic analysis procedures performed for a structural model subjected to a set of ground-motion records [5].

With reference to the latter, there are alternative procedures available in the literature for characterizing the relationship between Engineering Demand Parameters (*EDP*s) and Intensity Measures (*IM*s) and performing fragility calculations based on recorded ground motions, such as, the Incremental Dynamic Analysis (IDA, [6, 7]), the Multiple-Stripe Analysis (MSA, see [8, 9]) and the Cloud Analysis [10-16]. The IDA is arguably the most frequently used non-linear dynamic analysis procedure. However, the application of IDA can be quite computationally demanding as the non-linear dynamic analyses are going to be

repeated by scaling the ground motions to increasing levels of *IM*. It can be particularly useful to reduce both the computational effort within the IDA procedure while keeping almost the same level of accuracy. In such context, different approximate methods have emerged. These methods usually encompass schemes to perform nonlinear dynamic analyses of an equivalent simple SDOF model [17-19]. In addition, Vamvatsikos and Cornell [6-7] have proposed the *hunt & fill* algorithm, that ensures the record scaling levels to be appropriately selected to minimize the number of required runs: analyses are performed at rapidly increasing levels of *IM* until numerical non convergence is encountered, while additional analyses are run at intermediate *IM* levels to capture the onset of collapse and to increase the accuracy at lower *IM*s. A progressive IDA procedure, involving a precedence list of ground-motion records, has been proposed for optimal selection of records from an ensemble of ground-motions in order to predict the median IDA curve [20, 21]. Dhakal et al. [22] strived to identify in advance those ground motion records that are the best representatives for the prediction of a median seismic response. On the other hand, [23, 24] suggest that excessive scaling of records within the IDA procedure may lead to ground motion wave-forms whose frequency content might not represent the corresponding intensity level. This might manifest itself in terms of a bias in the IDA-based fragility curve with respect to fragility curves obtained based on no scaling [14] or spectral-shape-compatible scaling [25-27].

Adopting an *IM* (intensity measure)-based fragility definition facilitates the implementation of the IDA analysis, which is usually carried out by adopting the maximum inter-story drift ratio as the structural response parameter. That is, the structural fragility can be also interpreted as the Cumulative Distribution Function (CDF) for the intensity values corresponding to the onset of the prescribed limit state. The main advantage of adopting this definition, in the context of IDA, is that one can stop the upward scaling of a record after the first excursion of the limit state. On the other hand, estimating the maximum inter-story drift ratio corresponding to the onset of the limit state is by no means a trivial task. Several guidelines [28-30] recommend assigning the minimum between the maximum inter-story drift corresponding to a given reduction in the original slope of the IDA curve (say 80-84%) and a fixed sentinel value (e.g., 10%) as the onset of collapse prevention [31, 32] (roughly close to the European code's near-collapse

limit state [33]). Such definitions are somewhat qualitative and subjected to potential inaccuracies at high intensity levels. For instance, Baker [34] proposes the truncated IDA method for the collapse limit state, to avoid scaling up the records to very high intensity levels.

Liberally inspired from the code-based definition of demand to capacity ratios evaluated at the local level [31] for safety-checking purposes, the critical demand to capacity ratio, denoted as DCR_{LS}, that takes the structure closest to the onset of a prescribed limit state *LS* is adopted as the performance variable herein. This performance variable has been proposed as an effective and rigorous way of mapping the local structural behavior to the global level [35]. It has been shown [14-15, 35-39] that adopting DCR_{LS} as structural damage measure/performance variable facilitates the determination of the onset of a given limit state. DCR_{LS} is --by definition-- equal to unity at the onset of the limit state. Thus, adopting DCR_{LS} as the performance variable and plotting the IDA curves in terms of such variable facilitates the identification of intensity values corresponding to the onset of limit state as the intensity values corresponding to a DCR_{LS} equal to unity through the IDA curves.

The almost universal adoption of the maximum inter-story drift ratio as the global structural response parameter is implicitly based on the fact that, for moment resisting frames, the maximum inter-story drift ratio is an effective global representation of local joint rotations (due to rotations in the columns, the beams and the panel joint itself). To this end, it is noteworthy that DCR_{LS} can be defined in entirely deformation-based terms so that it represents the critical joint rotation throughout the structure (e.g., [14-15]).

Adopting DCR_{LS} as the performance variable, an IDA curve can be obtained with only two data points consisting of pairs of intensity versus critical DCR_{LS}. It is most desirable that the interval of values covered by the two points includes the demand to capacity ratio equal to one --to avoid extrapolation for estimating the intensity level corresponding to the onset of the limit state. Based on such a premise, an efficient solution for performing IDA is presented herein in which the intensity levels to scale to are chosen strategically to perform the minimum number of analyses and minimum amount of scaling strictly necessary. To this end, one can exploit the simple linear (logarithmic) regression predictions made based on the results of the structural analysis to the un-scaled registered records

(a.k.a., the simple Cloud Analysis) to identify the range of intensity values near DCR_{LS} equal to unity. This procedure, which is coined herein as "*Cloud to IDA*", delivers *IM*-based fragility curves by exploiting IDA curves constructed with minimum amount of scaling and minimum number of analyses strictly necessary. These fragility curves are shown later to be remarkably close to those obtained based on the IDA procedure.

This chapter uses as numerical example the transverse frame of the seven-story existing RC building in Van Nuys, CA, presented in Chapter 1.6. The frame is modeled in Opensees [40] by considering the flexural-shear-axial interactions in the columns, using the modeling approach presented in details in Chapter 2. In particular, being an older reinforced concrete frame, the column members are potentially sensible to shear failure during earthquakes. Hence, the non-linear model, presented in Chapter 2.2, is used to predict the envelope of the cyclic shear response [41-42]. This envelope includes the shear displacements and the displacements related to fixed-end rotations due to bar slip in the estimation of the total lateral displacement of the members. Finally, the 5% damped first-mode spectral acceleration denoted as $S_a(T_1)$ is adopted as the intensity measure in this chapter as in previous Chapter 3.

4.2 METHODOLOGY

4.2.1 THE INTENSITY MEASURE AND THE STRUCTURAL PERFORMANCE VARIABLE

The original framework for performance-based earthquake engineering (PBEE, [4]) propagates the various sources of uncertainty in the structural performance assessment through adopting a series of generic variables representing the seismic intensity (intensity measure, *IM*), the structural response (engineering demand parameter, EDP), the structural damage (damage measure, *DM*), and the structural performance (decision variable, *DV*). Herein, the critical demand to capacity ratio for a prescribed limit state [14-15, 35] and denoted as DCR_{LS}, has been adopted as a proxy for the structural performance variable (*DV*). This *DV* is going to be convoluted directly with the intensity measure (IM) to estimate the seismic risk in the performance-based earthquake engineering

framework. DCR_{LS} is defined as the demand to capacity ratio for the component or mechanism that brings the system closer to the onset of limit state *LS* (herein, the *near-collapse* limit state). The formulation refers to Equation 3.1 and is based on the cut-set concept [43], which is suitable for cases where various potential failure mechanisms (both ductile and brittle) can be identified a priori. DCR_{LS}, which is always equal to unity at the onset of limit state. In this chapter, as presented in Chapter 3.2.1, the critical demand to capacity ratio is going to be evaluated for the near-collapse limit state of the European Code [33]. The component demand to capacity ratios are expressed in terms of the maximum component chord rotation. This leads to a deformation-based DCR_{LS}. For the near-collapse limit state, it is defined as the point on the softening branch of the backbone curve in term of force-deformation of the component, where a 20% reduction in the maximum strength takes place. In this study, the possible failure mechanisms associated with the near-collapse limit state correspond to ductile and/or brittle failure of the columns.

Finally, also herein as in Chapter 3.2.1, the global *Collapse* of the structure is identified explicitly by verifying the following two criteria: (1) accounting for the loss of load bearing capacity when 50% +1 of the columns of a story reach the chord rotation corresponding to the complete loss of vertical-load carrying capacity of the component [44]; (2) accounting for global dynamic instability when maximum inter-story drift exceeds 10%.

4.2.2 RECORD SELECTION CRITERIA

In this section, the record selection criteria adopted herein for each non-linear dynamic analysis procedure are presented.

4.2.2.1 RECORD SELECTION FOR CLOUD

As discussed in details in Chapter 3.2.3, Cloud Analysis is usually employed for working with un-scaled records. There are a few relatively simple criteria to consider for selecting records for Cloud Analysis when adopting DCR_{LS} as the performance variable (see [15] and [45] for more details). In the first place, the selected records should cover a vast range of intensity values. This helps in reducing the error in the estimation of the regression slope. It is also quite important to make sure that a significant portion of the records (there is no specific

rule, say more than 30%) have DCR_{LS} values greater than unity. This recommendation aims at providing enough data points in the region of interest (i.e., vicinity of DCR_{LS} equal to unity). Finally, it is important to avoid selecting too many records (say more than 10% of total number of records) from the same earthquake. This final recommendation aims at reducing the potential correlations between DCR_{LS} values evaluated for different records.

4.2.2.2 RECORD SELECTION FOR IDA

As far as it regards the record-selection criteria for IDA procedure, as highlighted in [6], the number of records should be sufficient to capture the record-to-record variability in structural response. Previous studies [7] have assumed that for mid-rise buildings, 20 to 30 records are usually enough to provide sufficient accuracy in the estimation of seismic demands, assuming a relatively efficient *IM*, like S_a (T_1). Furthermore, a careful selection of ground motion records could be avoided if the adopted *IM* was sufficient (e.g., [23-24]). On the other hand, if the adopted IM was not sufficient (see [46-48] for alternative definitions/interpretations of sufficiency), the selected records at any given ground motion intensity level should ideally reflect the expected dominant ground motion characteristics. The record selection for IDA procedure can be done so that it represents a dominant earthquake scenario identified by a magnitude and distance bin (see e.g., [7, 9]).

It is to keep in mind that the accuracy of IDA procedure somehow depends on avoiding excessive scaling. Current literature [23-24] suggests making sure that the frequency content of the scaled records is still (roughly) representative of the intensity to which they are scaled. This criterion might not be satisfied for records selected based on criteria recommended for Cloud Analysis –as it is desirable that they cover a wide range of intensity levels (i.e., large scale factors might be required for scaling them all to the same intensity level). The *Cloud to IDA* procedure can benefit from the information provided by the Cloud Analysis to ensure that the records are not scaled excessively. As it is described later, the procedure can the avoid potential scaling bias sometimes attributed to IDA results.

4.2.2.3 RECORD SELECTION FOR MSA

The record selection for the MSA in this work is carried out by selecting different suits of conditional-spectrum (CS) compatible records per intensity level (see also [25-27, 49]). This ensures that the spectral shapes of the selected records are compatible with the expected spectral shape for a given intensity level. The details of the record selection procedure are outlined in Section 3.3.1.

4.2.3 STRUCTURAL FRAGILITY ASSESSMENT

Fragility estimation based on *Cloud to IDA* is compared with alternative non-linear dynamic analysis procedures such as Cloud Analysis considering the collapse cases, IDA, and Multiple-Stripe Analysis (MSA). This section describes briefly fragility assessment, discussed in details in Chapter 3.2, based on these alternative methods.

4.2.3.1 FRAGILITY ASSESSMENT BASED ON SIMPLE CLOUD ANALYSIS

Since the proposed *Cloud to IDA* procedure described later is based on the predictions of the simple Cloud Analysis, a very brief overview of this method is provided herein. As presented in details in Chapter 3.2.3, the Cloud data encompasses pairs of ground motion *IM*, herein first-mode spectral acceleration $S_a(T_1)$ (referred to as S_a for brevity), and its corresponding structural performance variable DCR_{LS} (see Equation 3.1) for a set of ground-motion records. To estimate the statistical properties of the Cloud data, conventional linear regression (using least squares) is applied to the data in the natural logarithmic scale, which is the standard basis for the underlying log-normal distribution model. This is equivalent to fitting a power-law curve to the Cloud data in the original (arithmetic) scale. As explained also in Chapter 3.2.2, it results in a curve that predicts the conditional median of DCR_{LS} for a given level of S_a denoted as $\eta_{DCR_{LS}|S_a}$ (read as median DCR_{LS} given S_a):

$$\ln \eta_{DCR_{LS}|S_a}(S_a) = \ln a + b \cdot \ln(S_a) \tag{4.1}$$

where ln a and b are parameters of linear regression. The (constant) conditional logarithmic standard deviation of DCR_{LS} given S_a, $\beta_{DCR_{LS}|S_a}$ (read as logarithmic standard deviation of DCR_{LS} given S_a), can be estimated as:

$$\beta_{DCR_{LS}|S_a} = \sqrt{\sum_{i=1}^{N}\left(\ln DCR_{LS,i} - \ln(a \cdot S_{a,i}{}^{b})\right)^2 \Big/ (N-2)} \tag{4.2}$$

where $DCR_{LS,i}$ and $S_{a,i}$ are the corresponding Cloud data for *i*th record in the set and N is the number of records.

In particular, the conditional median of DCR_{LS} for a given level of S_a, $\eta_{DCR_{LS}|S_a}$, is very important in this chapter because it will be the connection between Cloud Analysis and IDA procedures, as later explained.

4.2.3.2 FRAGILITY ASSESSMENT BASED ON CLOUD ANALYSIS CONSIDERING THE COLLAPSE CASES

For ultimate limit states, a portion of the selected records may induce structural collapse. Including these records and their corresponding DCR_{LS} in simple Cloud Analysis described right above is of questionable validity (e.g., very large DCR_{LS} values or non-available DCR_{LS} values due to convergence problems). This section describes very briefly fragility assessment based on the Cloud analysis explicitly considering the collapse cases (see Chapter 3.2.4 and [15] for a complete description of how to handle such cases in Cloud Analysis). Let the Cloud data be partitioned into two parts: (a) *NoC* data which correspond to that portion of the suite of records for which the structure does not experience "Collapse", (b) *C* corresponding to the "Collapse"-inducing records. The structural fragility for a prescribed limit state *LS* can be expanded with respect to *NoC* and *C* sets using Total Probability Theorem (see also [8, 50-51]), following Equation 3.4, introduced in Chapter 3.2.4, together with the explanation of all the different terms of Equation 3.4.

4.2.3.3 FRAGILITY ASSESSMENT BASED ON IDA

As mentioned before in the introduction, the structural fragility can also be expressed, in an *IM*-based manner, as the cumulative distribution function for the *IM* values that mark the limit state threshold. Taking advantage of the *IM*-based fragility definition and assuming that the critical spectral acceleration values at the onset of the limit state denoted by $S_a{}^{DCR=1}$ are Lognormally distributed, the structural fragility based on IDA analysis can be calculated as:

$$P\left(DCR_{LS} > 1 \mid Sa\right) = P\left(S_a{}^{DCR=1} < S_a\right) = \Phi\left(\frac{\ln S_a - \ln \eta_{S_a{}^{DCR=1}}}{\beta_{S_a{}^{DCR=1}}}\right) \tag{4.3}$$

where $\eta_{S_a{}^{DCR=1}}$ and $\beta_{S_a{}^{DCR=1}}$ are the median and standard deviation of the spectral acceleration values $S_a{}^{DCR=1}$ marking the onset of limit state.

4.2.3.4 FRAGILITY ASSESSMENT BASED ON MSA

In Multiple-stripe analysis (MSA, [8-9]), a suite of ground motion records (or different suits of ground motion records) are scaled to increasing intensity levels. At each level, the statistics of the structural response such as median, logarithmic standard deviation and probability of collapse can be estimated. MSA could lead to the same results as IDA if the same suite of records is employed throughout different intensity levels. However, compared to IDA, the MSA provides the possibility of using different suites of records per intensity level. Herein, the MSA implemented with different suites of conditional-spectrum-compatible records [25-27, 52] (see also [15] for more details on MSA-related record selection) is used as the "best-estimate" in order to benchmark the *Cloud to IDA* results. The MSA-based fragility herein is estimated by following the procedure in [34] in which a bi-parametric logarithmic fragility model is fitted through a maximum likelihood method to the fragility function.

4.2.4 ROBUST FRAGILITY ASSESSMENT

To compare the fragility curves obtained based on alternative non-linear analysis procedures and suites of ground motion records of different sizes, it is desirable to find a way for quantifying the uncertainty in the evaluation of structural fragility. This is done herein by employing the concept of *Robust Fragility* to define a prescribed confidence interval for the estimated fragility curve. The Robust Fragility [3, 14-15, 53] is defined as the expected value for a prescribed fragility model considering the joint probability distribution for the (fragility) model parameters χ. The Robust Fragility is written by using Total Probability Theorem, as presented in Equation 3.10. Moreover, it is also possible the variance σ^2 in fragility estimation, based on Equation 3.11. It's important to highlight that $\sigma^2(\cdot)$, provides the possibility of estimating a confidence interval of for the fragility considering the uncertainty in the estimation of the fragility model parameters χ. However, Robust Fragility assessment for Cloud Analysis considering the global dynamic instability and IDA are described in details in Chapter 3.2.5 and in [15] and [53], respectively.

4.2.5 CLOUD TO IDA PROCEDURE

The *Cloud to IDA* procedure aims at deriving IDA-based fragility curves by obtaining the spectral acceleration values corresponding to unity denoted as $S_a^{DCR=1}$. This is done with extreme efficiency by obtaining IDA curves with very few data points for each. This section provides an overview of the method, and how and why it works.

There is a natural link between Cloud and IDA procedures. The Cloud data can also be viewed as the first point on the various IDA curves; where the threshold DCR_{LS}=1 divides the data into two zones: those points with DCR_{LS} less than one and those with DCR_{LS} greater than one (see Figure 4.1). In fact, the regression prediction fitted to the portion of the Cloud data that does not include the collapse cases (NoC), denoted as $\eta_{DCR_{LS}|S_a}$ (median DCR_{LS} given *Sa*, see Sections 4.2.3 and 4.2.4.1, note that the conditioning on NoC is dropped for simplicity of notation) and furnished based on the Cloud data as in Equation 4.1, provides a reasonable first estimate of the median IDA curve (Figure 4.1). Figure 4.1 also shows the spectral acceleration value, denoted as $S_{a,Cloud}^{DCR=1}$, at which the regression prediction $\eta_{DCR_{LS}|S_a}$ intersects the demand to capacity ratio equal to unity. This spectral acceleration represents a value that brings the records close to DCR_{LS}=1. This information provides useful indications for careful selection of records with the objective to avoid excessive scaling. Therefore, the original Cloud data points can be screened to find those records whose spectral accelerations are close to $S_{a,Cloud}^{DCR=1}$ and whose DCR_{LS}'s are not too distant from unity. These qualitative indications can be formalized a bit by defining two confidence bands --corresponding to prescribed probability contents-- centred around $S_{a,Cloud}^{DCR=1}$ and DCR_{LS}=1, respectively. The (logarithmic) standard deviation for DCR_{LS} at a given *Sa* value (say $S_{a,Cloud}^{DCR=1}$) can be estimated as equal to the standard error of regression $\beta_{DCR_{LS}|S_a}$. Moreover, the logarithmic standard deviation of $S_{a,Cloud}^{DCR=1}$ for a given DCR_{LS} value (say DCR_{LS}=1) can be estimated as $\beta_{DCR_{LS}|S_a}/b$ (a simple proof can be provided by inverting the relationship $DCR_{LS} = aS_a{}^b$ to derive S_a in terms of DCR_{LS}). These two standard deviation values can help in establishing a certain confidence interval around $S_{a,Cloud}^{DCR=1}$ and DCR_{LS}=1. Figure 4.1 shows the box-shape area that is created by the intersection

of plus/minus one and half standard deviation from $S_{a,Cloud}^{DCR=1}$ and plus/minus two standard deviations from DCR_{LS}=1 (in the logarithmic scale). The records used in the *Cloud to IDA* procedure can be selected as those that lie within this so-called box. It is worth mentioning that the choice of the width of the confidence bands is qualitative. The essential idea is to choose those records that are going to be potentially scaled up/down by a factor close to unity (say less than 1.5). It is important to find a balance between a reasonable number of records and the eventual amount of scaling involved. In other words, a smaller box certainly leads to a smaller number of records and probably involves less scaling.

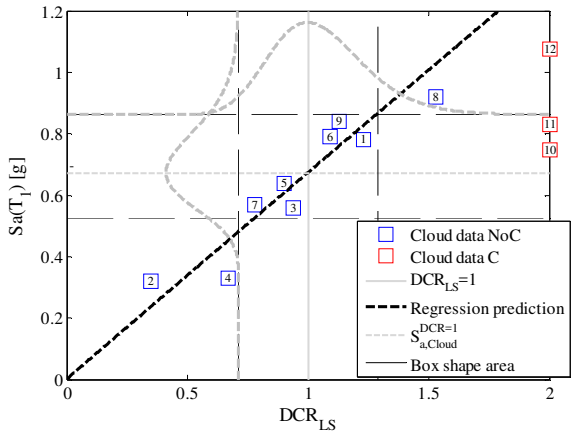

Figure 4.1: *Cloud to IDA* procedure: simple Cloud Analysis results, linear regression fitted to *NoC* data in the logarithmic scale, box shape area and the lognormal distributions associated to $S_{a,Cloud}^{DCR=1}$ and DCR_{LS}=1.

Figure 4.2 (a) shows the selected records for *Cloud to IDA* scaled to (a value slightly larger or smaller than the) the spectral acceleration value $S_{a,Cloud}^{DCR=1}$ corresponding to the intersection of the regression prediction curve and DCR_{LS}=1. For those records that are to the right with respect to the regression prediction curve, the spectral acceleration value to scale to is going to be slightly smaller than the value corresponding to the intersection of the regression prediction curve and DCR_{LS}=1 and vice versa (for the same spectral acceleration, the points to the right of the regression prediction have a larger DCR_{LS} and probably need less scaling for arriving to DCR_{LS}=1). Having two data points per

record now, one can connect them to obtain a first version of the IDA curves/lines (as shown in Figure 4. 2(b)).

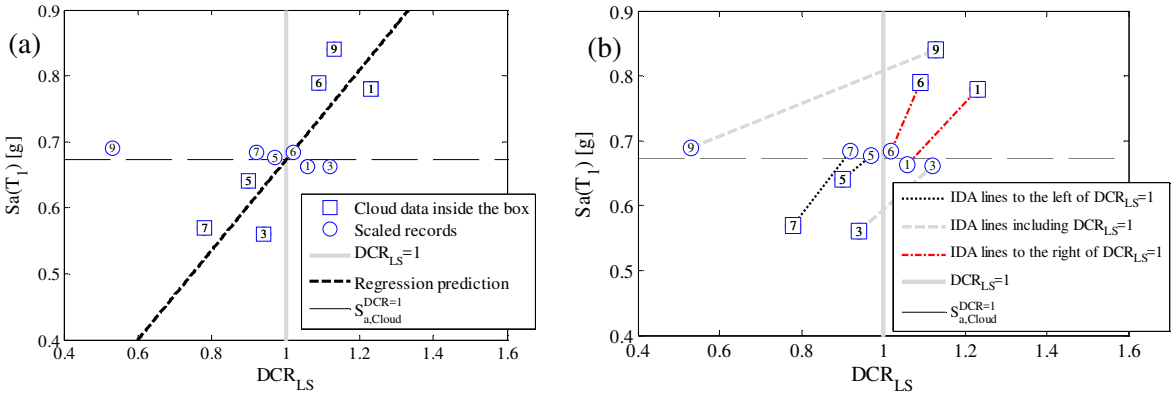

Figure 4.2: *Cloud to IDA* procedure: (a) scaled records; (b) IDA lines.

Given that the objective is to find the spectral acceleration values that correspond to DCR_{LS}=1, at this point a visual survey of whether the DCR_{LS}=1 falls within the IDA lines or outside can be performed. For those records in which the DCR_{LS}=1 falls within the IDA line (the gray dashed lines in Figure 4.2 (b)), the scaling operation may stop at this point (i.e., the $S_a^{DCR=1}$ value can be obtained through interpolation). However, it is desirable to continue the scaling also for these records to obtain more accurate estimates for $S_a^{DCR=1}$ values. The figure also shows the IDA lines completely to the left of DCR_{LS}=1 (the black dotted lines) and those completely to the right (the red dashed dot lines).

Figure 4.3 (a) shows the intersection of the IDA lines and the value DCR_{LS}=1 shown as the "projected" $S_a^{DCR=1}$ values. For a portion of the records, this entails extending the IDA line beyond the second point on the IDA curve (see black dotted lines); for another portion this entails extending the line beyond the first point on the IDA curve (see red dashed dot lines); for the rest of the records (those for which the $S_a^{DCR=1}$ values can be obtained in the previous step by interpolation), the intersection simply lies between the two points (see gray dashed lines). In the next step, the records can be scaled to (a value slightly larger or smaller than the) spectral acceleration value that corresponds to the intersection of the IDA lines with the value DCR_{LS}=1 (Figure 4.3 (b)). For those records whose IDA curves are

to the left of DCR_{LS}=1, the spectral acceleration value to scale to is going to be slightly larger than the value corresponding to DCR_{LS}=1 and vice versa.

Finally, for the rest of the records (those for which the $S_a^{DCR=1}$ values can be already obtained in the previous step by interpolation), the scaling value is the spectral acceleration value that corresponds to the intersection of the IDA lines with the value DCR_{LS}=1. The advantage of scaling the records to the projected intersection with unity is that it will lead to a third point on the IDA curve close to unity. At this point, most probably, it is going to be possible to obtain the $S_a^{DCR=1}$ values by interpolation for all the records. However, if there are still records which fall completely to left or to right of DCR_{LS}=1, the last step described above can be repeated.

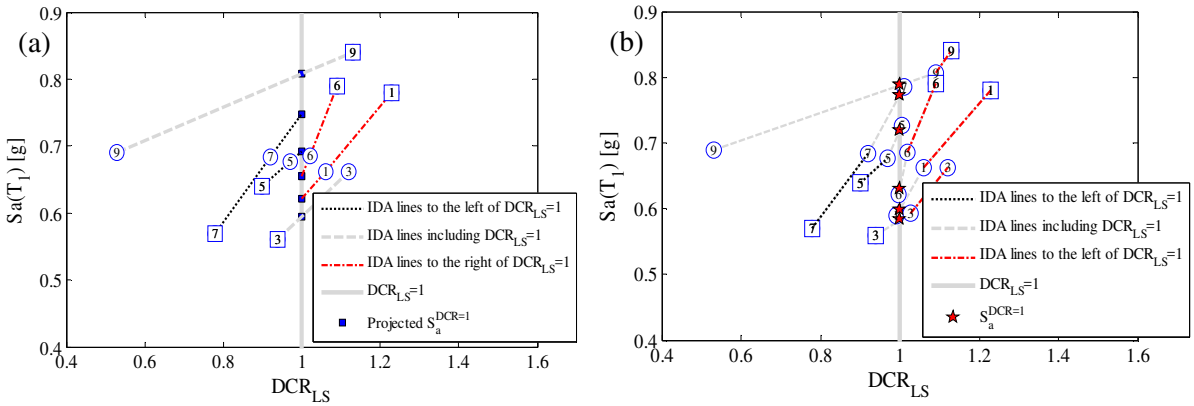

Figure 4.3: Cloud2IDA procedure: (a) intersection of the IDA lines and the "projected" SaDCR=1 values; (b) additional scaling of the records and the obtained SaDCR=1 values.

4.2.5.1 HOW TO TREAT THE COLLAPSE CASES

It was mentioned in the above paragraph that the regression line should be fitted to the non-collapse portion of the Cloud data. Nevertheless, the collapse-inducing records can be scaled down so that they can lead to reasonable DCR_{LS} values. The choice of the scaling value is somehow subjective; it is enough to make sure that after scaling all the collapse-inducing records can be treated as "normal" non-collapse-inducing data points. It should be kept in mind that the regression prediction to be used in the *Cloud to IDA* procedure is still the one fitted to the non-collapse portion of the Cloud data, i.e. $\eta_{DCR_{LS}|S_a}$. To this end, the

scaled collapse-inducing records can be treated as a part of NoC cloud data and the *Cloud to IDA* procedure can be followed as described in Section 4.2.6. In case one is keen on not scaling the Cloud Data, the simple regression prediction can be obtained based on the original un-scaled NoC data.

Figure 4.4 describes graphically the handling of collapse-inducing records within the *Cloud to IDA* procedure. Herein, the collapse-induced records have been scaled down by the ratio of the mean *Sa* of the collapse data (denoted here in as $\overline{S_{a,C}}$) divided by the value $S_{a,Cloud}^{DCR=1}$.

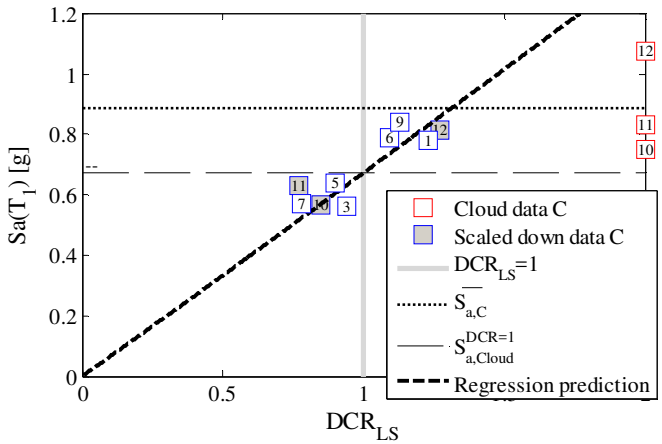

Figure 4.4: *Cloud to IDA* procedure: how to treat the collapse cases.

4.2.5.2 CLOUD TO IDA DESCRIBED IN A STEP-BY-STEP MANNER

Figure 4.5 demonstrates the flowchart of the *Cloud to IDA* procedure. The flowchart in Figure 4.5 provides a step-by-step guide to *Cloud to IDA*:

1- Establish an original record selection for Cloud Analysis. One might choose records based on criteria suggested specifically for Cloud Analysis as in [15]. Otherwise one can start from an established set of records such as the ones proposed by FEMA [29].

2- Perform structural analysis and obtain the Cloud data points. Identify the collapse-inducing records (*NoC* and *C* portions of the Cloud data).

3- (Optional) Scale down the collapse cases and merge them together with the non-collapse portion of the Cloud data. This step can be skipped if one is keen on avoiding excessive scaling.

4- Fit a linear regression in the logarithmic scale to the non-collapse portion of the Cloud data (that may include scaled down C data). Identify $S_{a,Cloud}^{DCR=1}$ as the spectral acceleration corresponding to DCR_{LS}=1 by the regression prediction.

5- Define prescribed confidence intervals around $S_{a,Cloud}^{DCR=1}$ and DCR_{LS} =1. This leads to the identification of box-shape area. The records that lie within this area can be selected as the records suitable for next steps of the *Cloud to IDA* procedure.

6- Scale all the records thus-obtained to (a value slightly larger or smaller than the) the spectral acceleration value $S_{a,Cloud}^{DCR=1}$. For those records, that are to the right of the regression prediction, the spectral acceleration value to scale to is going to be slightly smaller than $S_{a,Cloud}^{DCR=1}$ and vice versa (see Section 4.2.5 for more details). Execution of this step provides the second point of IDA curve for all the records.

7- Connect the two data points in order to obtain the IDA lines. Find the projected $S_a^{DCR=1}$ values as the intersection of the IDA lines (or their extension to the left or right) with DCR_{LS}=1.

8- Scale all the records to the projected $S_a^{DCR=1}$ values to obtain the third data point on the IDA curves.

9- Check if the value DCR_{LS}=1 falls within one of the IDA line segments and obtain the corresponding $S_a^{DCR=1}$ value through interpolation.

10- Repeat steps 8 and 9 for those records in which the value DCR_{LS}=1 falls completely to one side of the IDA line segments obtained so far.

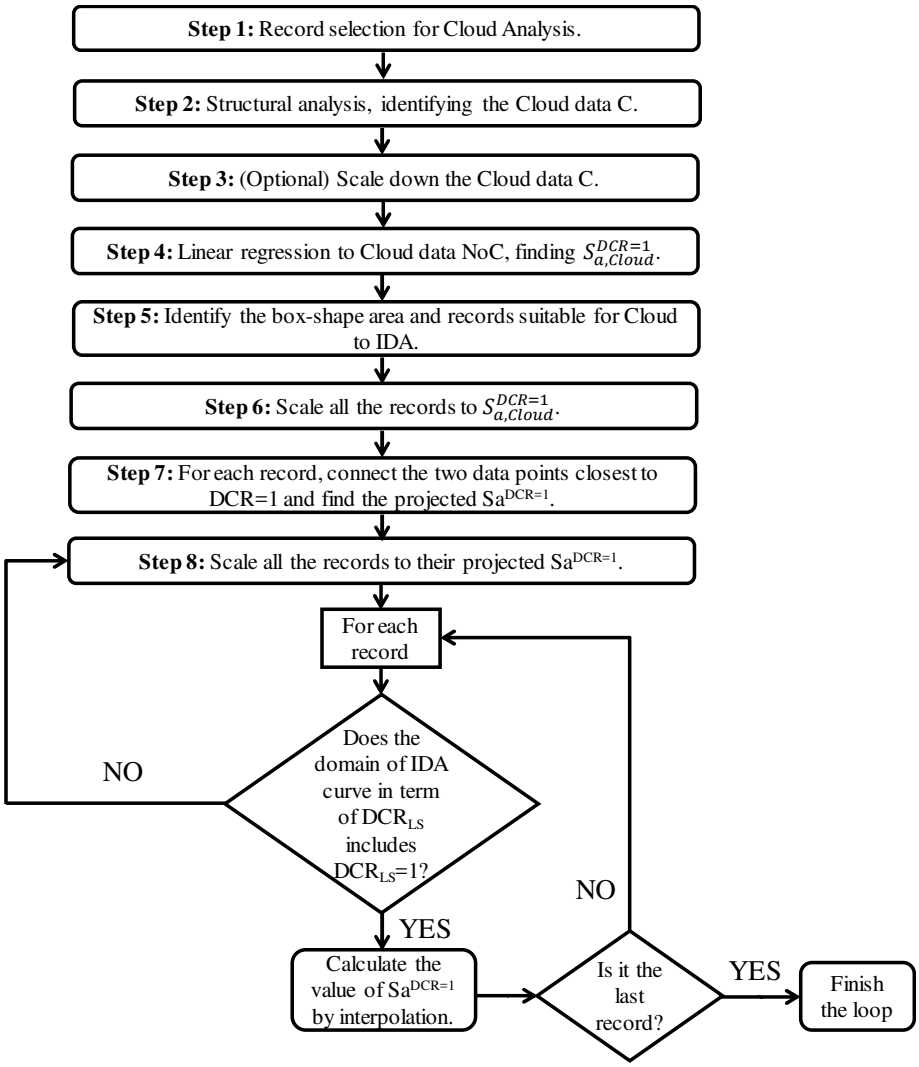

Figure 4.5: Flowchart for *Cloud to IDA* procedure.

4.3 CASE STUDY RESULTS

A reinforced concrete (RC) moment-resisting frame is considered herein as case study: the east as-built transverse perimeter frame of the seven-story Holiday Inn hotel building in Van Nuys, California (completely presented in Chapter 1.6). All the details about the modelling issues have been presented in Chapter 2.

4.3.1 RECORD SELECTION

As mentioned in the methodology, each non-linear dynamic analysis procedure has its own specific criteria for record selection. Comparing the proposed Cloud to IDA procedure to alternative non-linear dynamic procedures, this paper deals with various record sets. These record sets are described in this section.

4.3.1.1 THE FEMA RECORD SET FOR CLOUD ANALYSIS AND IDA

The set of records presented in FEMA P695 [29] is used for the Cloud and IDA Analyses. The FEMA set (listed in Table 4.1) includes twenty-two far-field records and twenty-eight near-field records. With reference to the twenty-eight near-field records, fourteen records are identified as “pulse-like”. Only one horizontal component of each record has been selected. The FEMA suite of records covers a range of magnitudes between 6.5 and 7.9, and closest distance-to-ruptured area (denoted as RRUP) up to around 30 km, as illustrated in the scatter diagram in Figure 4.6 (a). Figure 4.6 (b) shows the records' spectra and the associated median, 16th and 84th percentiles.

4.3.1.2 THE VARIABLE SET OF RECORDS FOR MSA

As mentioned before in Sections 2.2 and 2.3, MSA implemented with variable suites of conditional spectrum (CS)-compatible records [25-27] is used as the benchmark “best-estimate”. The details of record selection compatible with conditional spectrum for the case-study frame are described in Chapter 3.3.1.3 and in [15]. For each stripe, a set of 38 records that provide the best fit to the prescribed CS is selected. A. Figure 4.6 (c) shows the response spectra of 38 ground motions (scaled to $Sa(T_1)$) selected to match the CS for a given level of Sa, where T_1 is close to the first-mode period of the case-study frame.

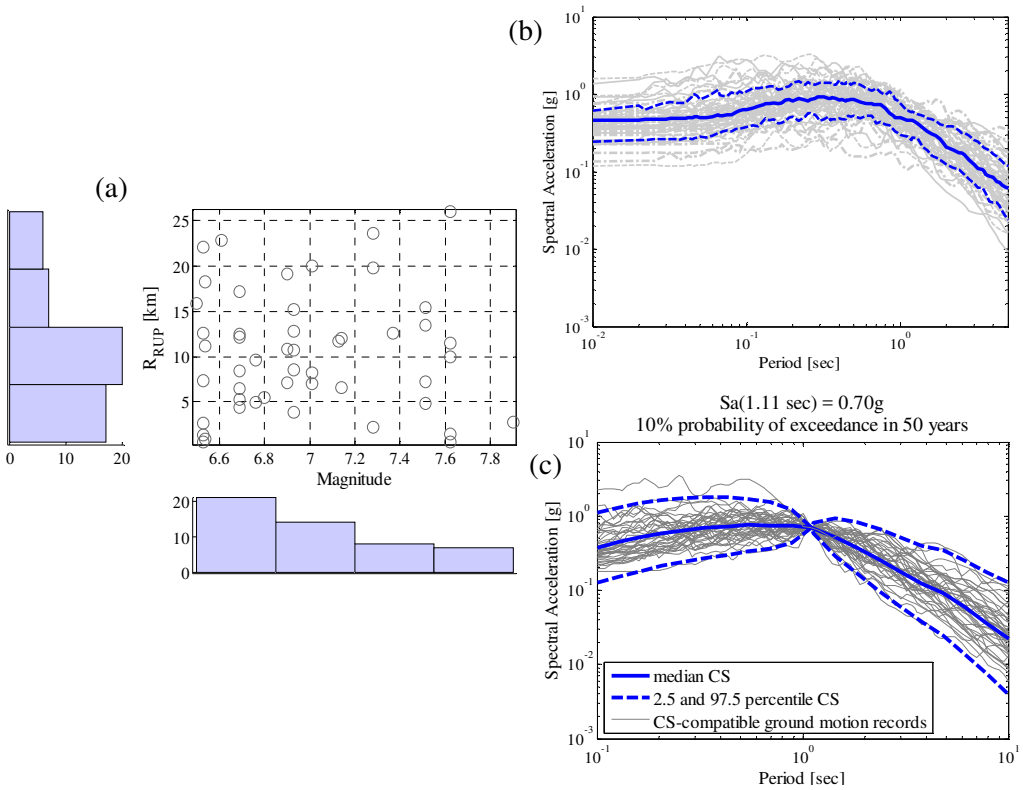

Figure 4.6: (a) The magnitude-RRUP scatter diagram of FEMA record set, (b) the elastic response spectra for FEMA set of records, (c) response spectra of 38 records scaled to a given level of $Sa(T_1)$ and the matching the CS.

Table 4.1: The suite of strong ground-motion records from FEMA P695.

Record Number	NGA Record Number	Earthquake Name	Station Name	Direction* / Type**
1	68	San Fernando	LA - Hollywood Stor FF	1 / FF
2	125	Friuli, Italy-01	Tolmezzo	2 / FF
3	126	Gazli, USSR	Karakyr	2 / NF
4	160	Imperial Valley-06	Bonds Corner	2 / NF
5	165	Imperial Valley-06	Chihuahua	2 / NF
6	169	Imperial Valley-06	Delta	2 / FF
7	174	Imperial Valley-06	El Centro Array #11	2 / FF
8	181	Imperial Valley-06	El Centro Array #6	1 / NFP
9	182	Imperial Valley-06	El Centro Array #7	2 / NFP
10	292	Irpinia, Italy-01	Sturno (STN)	1 / NFP
11	495	Nahanni, Canada	Site 1	2 / NF
12	496	Nahanni, Canada	Site 2	2 / NF
13	721	Superstition Hills-02	El Centro Imp. Co. Cent	1 / FF
14	723	Superstition Hills-02	Parachute Test Site	2 / NFP
15	725	Superstition Hills-02	Poe Road (temp)	1 / FF
16	741	Loma Prieta	BRAN	1 / NF
17	752	Loma Prieta	Capitola	1 / FF
18	753	Loma Prieta	Corralitos	2 / NF
19	767	Loma Prieta	Gilroy Array #3	2 / FF
20	802	Loma Prieta	Saratoga - Aloha Ave	1 / NFP
21	821	Erzican, Turkey	Erzincan	2 / NF
22	825	Cape Mendocino	Cape Mendocino	1 / NF
23	827	Cape Mendocino	Fortuna - Fortuna Blvd	1 / FF
24	828	Cape Mendocino	Petrolia	1 / NFP
25	848	Landers	Coolwater	2 / FF

Record Number	NGA Record Number	Earthquake Name	Station Name	Direction* / Type**
26	879	Landers	Lucerne	1 / NFP
27	900	Landers	Yermo Fire Station	1 / FF
28	953	Northridge-01	Beverly Hills-Mulhol	2 / FF
29	960	Northridge-01	C. Country-W Lost Cany	2 / FF
30	1004	Northridge-01	LA-Sepulveda VA Hospital	2 / NF
31	1048	Northridge-01	Northridge-17645 Saticoy St	2 / NF
32	1063	Northridge-01	Rinaldi Receiving Sta	2 / NFP
33	1086	Northridge-01	Sylmar-Olive View Med FF	1 / NFP
34	1111	Kobe, Japan	Nishi-Akashi	1 / FF
35	1116	Kobe, Japan	Shin-Osaka	1 / FF
36	1148	Kocaeli, Turkey	Arcelik	2 / FF
37	1158	Kocaeli, Turkey	Duzce	2 / FF
38	1165	Kocaeli, Turkey	Izmit	2 / NFP
39	1176	Kocaeli, Turkey	Yarimca	2 / NF
40	1244	Chi-Chi, Taiwan	CHY101	2 / FF
41	1485	Chi-Chi, Taiwan	TCU045	2 / FF
42	1503	Chi-Chi, Taiwan	TCU065	2 / NFP
43	1504	Chi-Chi, Taiwan	TCU067	2 / NF
44	1517	Chi-Chi, Taiwan	TCU084	2 / NF
45	1529	Chi-Chi, Taiwan	TCU102	2 / NFP
46	1602	Duzce, Turkey	Bolu	1 / FF
47	1605	Duzce, Turkey	Duzce	2 / NFP
48	1633	Manjil, Iran	Abbar	2 / FF
49	1787	Hector Mine	Hector	2 / FF
50	2114	Denali, Alaska	TAPS Pump Station #10	2 / NF

* "Direction" denotes one of the two horizontal components of each recording, and is assigned by "1" or "2" based on its appearance in the NGA data set.

** Record Type: FF = Far-Field record, NF = Near-Field record with no-Pulse, NFP = Near-Field record with Pulse.

4.3.2 CLOUD ANALYSIS CONSIDERING COLLAPSE OR GLOBAL DYNAMIC INSTABILITY

Figure 4.7 (a) shows the scatter plots for Cloud data based on the ground motion records listed in the FEMA record set (see Table 4.1) where for each data point (colored squares) the corresponding record number is shown. The cyan-colored squares represent the *NoC* data, while only one record out of fifty ground motions causes collapse or global dynamic instability (*C* data) as shown with a red-colored square. The Cloud Analysis regression model (i.e., regression prediction, the estimated regression parameters, and the standard error of regression as described in Section 4.2.3) fitted to the *NoC* data is shown on the figure. The black solid line represents the regression prediction $\eta_{DCR_{LS}|S_a}$ which can be interpreted as the 50th percentile (a.k.a., median) DCR_{LS} given spectral acceleration conditioned on *NoC*. The line DCR_{LS}=1 corresponding to the onset of limit state (herein, near-collapse) is shown with red-dashed line. It can be seen that the Cloud Analysis data not only covers a vast range of spectral acceleration values, but also provides numerous data points in the vicinity of DCR_{LS}=1. The horizontal black dash-dotted line indicates the spectral acceleration $S_{a,Cloud}^{DCR=1}$ =$(1/a)^{1/b}$ corresponding to DCR_{LS}=1 based on the regression prediction. Figure 4.7 (b) illustrates the histogram of the regression residuals in the logarithmic scale for the non-collapse portion of the Cloud data. This histogram shows a substantially unimodal and symmetric shape that seems to be fine for the use of a lognormal (normal in the logarithmic scale) fragility model. Figure 4.7 (c) shows the fragility curves based on Cloud Analysis considering the collapse cases (cyan dashed line) and the Robust Fragility with its two standard deviation confidence interval (plotted as black solid line and the shaded area, based on Cloud Analysis considering the collapse cases as described in Section 4.2.3). The figure also illustrates the conditional probability of collapse given intensity $P(C|S_a)$ as in Equation 3.6 and reports the logistic (α_0 and α_1) regression model parameters. Note that this $P(C|S_a)$ is the structural fragility for the collapse limit state.

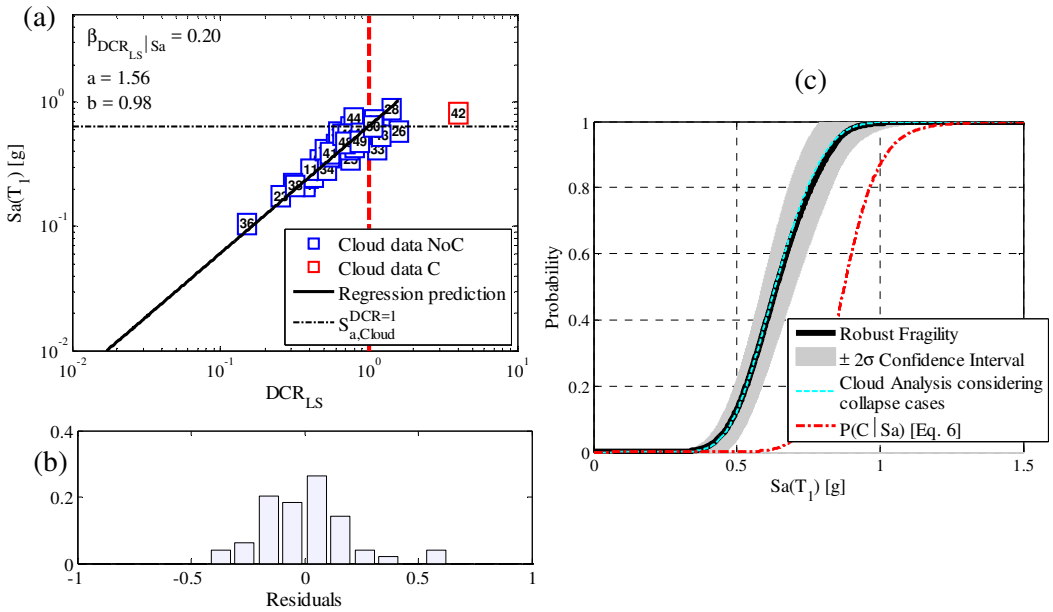

Figure 4.7: (a) Cloud data and regression, (b) regression residuals and (c) the fragility curves.

4.3.3 IDA Analysis

The IDA is performed for the suite of fifty FEMA ground-motion records described earlier in Section 4.3.2. The IDA curves are plotted in thin gray lines in Figure 4.8 (a). Each curve shows the variation in the performance variable DCR_{LS} for a given ground-motion record as a function of Sa while the record's amplitude is linearly scaled-up. The gray dot at the end of each IDA curve denotes the ultimate Sa level before numerical non-convergence or global collapse is encountered (based on the two criteria defined in Section 4.2.1). The Sa values on the IDA curves corresponding to DCR_{LS}=1 and denoted as $Sa^{DCRLS=1}$ (i.e., the intensity levels marking the onset of the limit state) are shown as red stars. The histogram of $Sa^{DCRLS=1}$ values together with the fitted (Lognormal) probability density function (PDF), plotted as a black solid line, are shown in Figure 4.8 (a). The horizontal thin black dash-dotted line represents the median of $Sa^{DCRLS=1}$, which is denoted as $\eta_{S_a\,DCR=1}$ and known as median spectral acceleration capacity (see Equation 4.3). Figure 4.8 (b) shows the comparison between the Robust Fragilities and their plus/minus two standard deviation confidence intervals based on Cloud Analysis considering the collapse cases (black solid line and the

corresponding shaded area) and IDA (blue dotted line and the small blue dotted lines for identifying the confidence interval), as described in Sections 4.2.3.2, 4.2.3.3, and 4.2.4. The difference between Cloud- and IDA-based fragilities is contained within a 2 standard deviation confidence band for both methods; with the IDA-based fragilities being on the more conservative side.

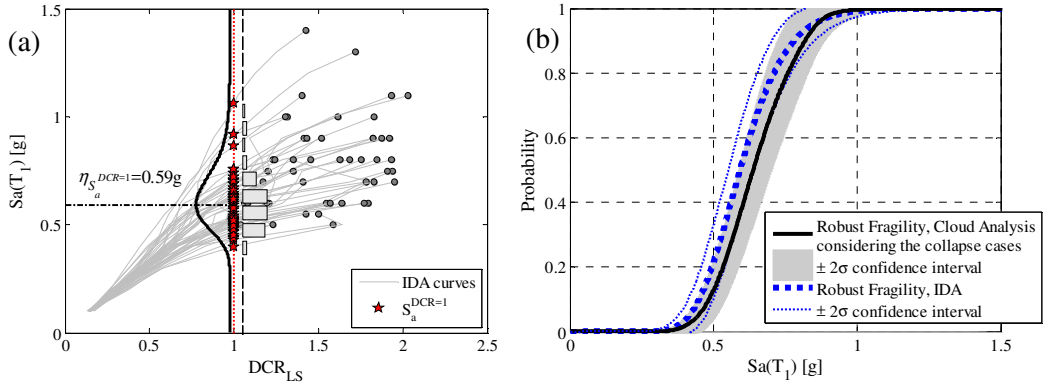

Figure 4.8: (a) The IDA curves and the spectral acceleration capacity values $S_a^{DCRLS=1}$; (b) comparison between the fragility curves based IDA and Cloud Analysis considering the collapse cases.

4.3.4 MULTIPLE-STRIPE ANALYSIS (MSA)

MSA is performed as described in [15] on the case-study frame. Figure 4.9 (a) shows MSA raw data (*Sa-DCR*$_{LS}$) for which the analyses are performed up to *IM* amplitudes where all ground motions cause collapse. Figure 4.9 (b) illustrates the MSA-based fragility curve (in gray dash-dotted line) obtained by method of "Baker 2015" [34] compared with IDA- (in blue dotted line) and Cloud- (black solid line) based fragility curves. Moreover, Figure 4.9 (b) illustrates the empirical MSA-based fragility estimates (in gray circles) obtained for each stripe as the ratio of the number of records with $DCR_{LS}>1$ to the total number of records in the stripe. It can be observed that the MSA-based fragilities are in close agreement with Cloud-based fragilities (in comparison to the IDA-based curves) up to a spectral acceleration of 0.70g (i.e., the range of high probability content for risk calculations [14]; it can be seen also through the site-specific hazard curve). A slight bias in IDA results due to scaling can be observed.

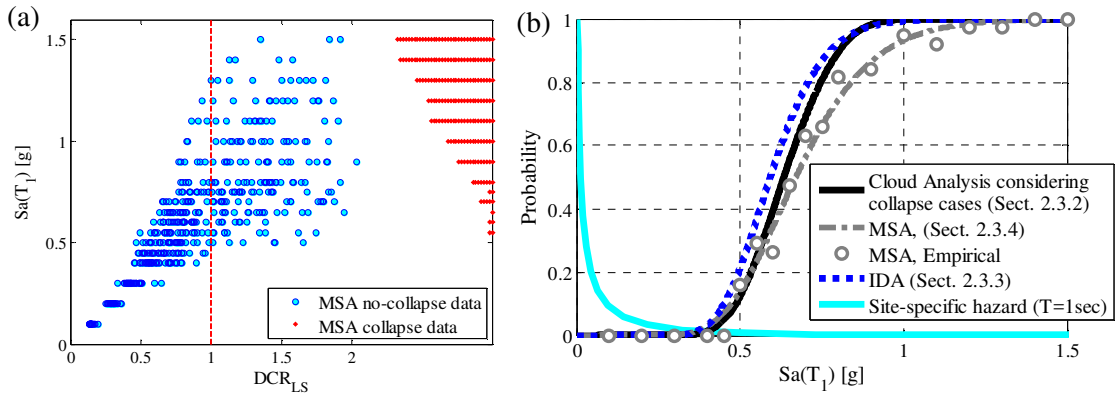

Figure 4.9: (a) MSA results, (b) the fragility curves based on Cloud considering the collapse cases, MSA, and IDA.

4.3.5 CLOUD TO IDA PROCEDURE

The step-by-step *Cloud to IDA* procedure as described in the methodology section (see the flowchart in Figure 4.5) is applied herein considering two reduced record sets obtained with the objective of limiting the scaling of ground motion records (*Reduced set 1* and *Reduced set 2* as described in the next paragraphs).

- As mentioned before, the first step of the procedure is accomplished by choosing the FEMA record set as the original record selection for Cloud Analysis.
- The second step is to perform structural analysis and to identify the collapse-inducing records (C and NoC data, only one case of collapse is identified).
- The step three of the procedure has been skipped because only one collapse case was identified.
- In the next step, a linear regression in the logarithmic scale is performed on the non-collapse portion of the Cloud data (Figure 4.7 (a)). At this point, the spectral acceleration at DCR_{LS}=1, i.e. $S_{a,Cloud}^{DCR=1}$, and the constant conditional logarithmic standard deviation of DCR_{LS} given S_a denoted as $\beta_{DCR_{LS}|S_a}$, as shown in Figure 4.7 (a) are calculated.
- The next step involves defining prescribed confidence intervals around $S_{a,Cloud}^{DCR=1}$and DCR_{LS}=1 with the purpose of selection of records that are going to be subjected to least amount of scaling (as predicted by the regression). It should be mentioned that the procedure can also be carried out with the

original set of records. In such case, there is no specific control in place against excessive scaling. Two suites of reduced record sets are selected from the pool of FEMA records (see Table 4.1 and Figure 4.6):

- *Reduced set* 1: *N*=10 records that lie within the box defined by the plus/minus one (logarithmic) standard deviation stripes away from $S_{a,Cloud}^{DCR=1}$ and DCR_{LS}=1 (see Figure 4.10 (a));
- *Reduced set* 2: *N*=19 records that lie within the box defined by the plus/minus one (logarithmic) standard deviations away from $S_{a,Cloud}^{DCR=1}$ and plus/minus 1.5 (logarithmic) standard deviations away from DCR_{LS}=1 (see Fig. Figure 4.10 (b)).

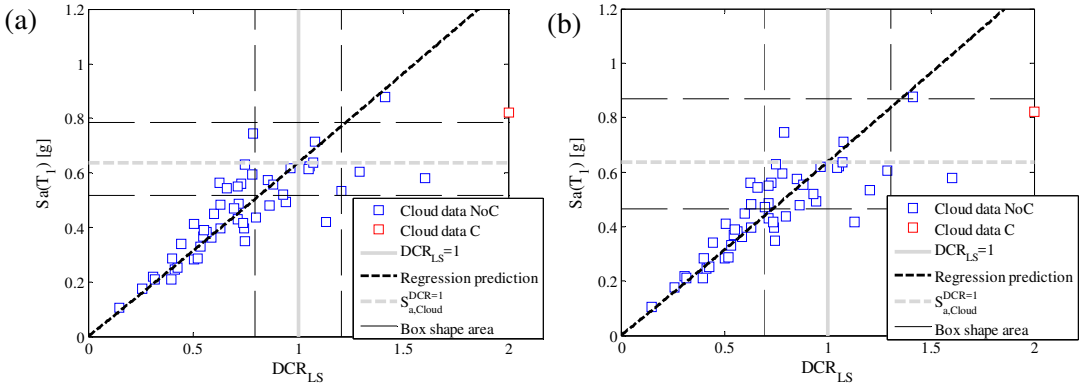

Figure 4.10: Box shape areas defining (a) reduced set 1, and (b) reduced set 2.

The rest of the *Cloud to IDA* procedure is described hereafter for the *Reduced set* 2 (*N*=19, the procedure is carried out for both record sets and the results are reported at the end of this section).

- In the next step, all the records within the rectangular area are scaled to (a value slightly larger or smaller than the) the spectral acceleration value $S_{a,Cloud}^{DCR=1}$. For those records, that are located to the right with respect to the regression prediction (which for the same intensity have a larger DCR_{LS} with respect to the regression prediction), the spectral acceleration value to scale to is going to be slightly smaller than $S_{a,Cloud}^{DCR=1}$ and vice versa. In case the scaled records become collapse-inducing, the spectral acceleration to scale to should be adjusted accordingly so that the scaled record does not lead to collapse (this

might require some iteration). At the end of this step, IDA line segments for all the records can be obtained by connecting the two points (Figure 4.11 (a)).

- Given that the objective is to find the spectral acceleration values that correspond to DCR_{LS} equal to unity, at this point a visual survey of whether the DCR_{LS}=1 falls within the IDA lines or outside can be performed. Figure 4.11 (b) shows the intersection/projection of the IDA lines and the value DCR_{LS}=1 denoted as "projected" $S_a^{DCR=1}$ for each record. For a portion of the records, this entails extending the IDA line beyond the second point on the IDA curve (see black dotted lines); for another portion this entails extending the line beyond the first point on the IDA curve (see red dashed dot lines); for the rest of the records (i.e., those for which the $S_a^{DCR=1}$ values can be obtained in the previous step by interpolation) the intersection simply lies between the two points (see gray dashed lines).
- The last step is to scale all the records to the "projected" $S_a^{DCR=1}$ in order to obtain the third data point on the IDA curves. Note that the records can be scaled to a value slightly larger or smaller than the "projected" $S_a^{DCR=1}$ (Figure 4.11 (c)). For example, for those records whose IDA curves are to the left of DCR_{LS}=1 (black dotted), the spectral acceleration value to scale to is going to be slightly larger than the "projected" $S_a^{DCR=1}$ and vice versa. Even for the rest of the records (the gray dashed IDA lines), it is desirable to carry out this last step in order to obtain more accurate estimates for $S_a^{DCR=1}$. The obvious advantage of scaling the records to the projected intersection with unity is that it will lead to a third point on the IDA curve close to a DCR_{LS}=1. At this point, most probably, as in the case study in Figure 4.11 (c), the $S_a^{DCR=1}$ values can be calculated by interpolation for all the records (i.e., for all of the records a gray dashed line segment can be found). Finally, the fragility curve can be obtained based on the statistics of $S_a^{DCR=1}$ values (as in Equation 4.3). In case there are still records for which the DCR_{LS}=1 falls totally to the left or the right of the three points obtained so far, the previous step can be repeated until an IDA line segment including DCR_{LS}=1 can be identified. In the case study, the $S_a^{DCR=1}$ values are obtained for all the records based on only three IDA points.

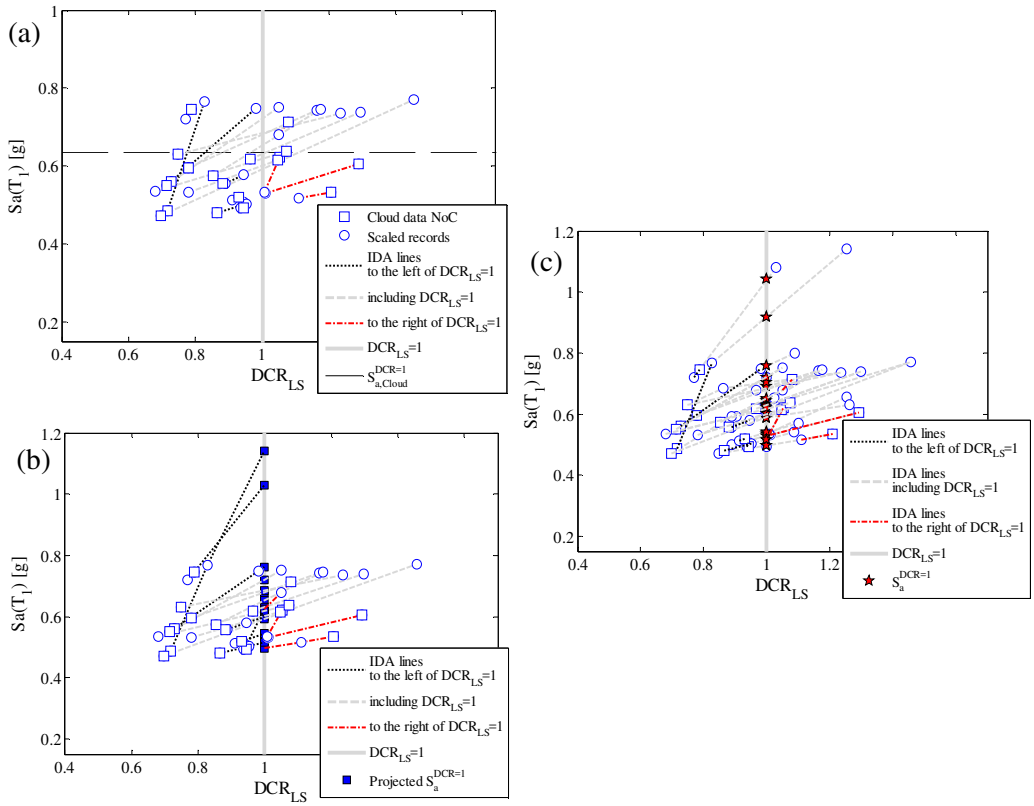

Figure 4.11: *Cloud to IDA* procedure: (a) the first scaling and the resulting IDA line segments; (b) the "projected" $S_a^{DCR=1}$ values; (c) the resulting $S_a^{DCR=1}$ values used to develop the *Cloud to IDA* fragility curve.

4.3.6 RESULTS AND DISCUSSIONS

Figure 4.12 reported below shows the Robust Fragility curves and their plus/minus one standard deviation interval obtained by employing the *Cloud to IDA* procedure (as described above) for Reduced set 1 and Reduced set 2, in red dashed lines of different thickness (thicker for Reduced set 2 which is larger set) and the corresponding confidence intervals are marked by thin red dashed lines of the different color shades (darker for Reduced set 2 which is larger set). Note that the Robust Fragility calculation for *Cloud to IDA* is the same as IDA as described in detail in [53]. The confidence band is clearly wider for the smaller record set (with only N=10 records). Moreover, it can be seen that the Robust Fragility curves obtained based on the two sets of records are in close agreement (contained within the plus/minus one standard deviation interval of each other).

Figure 4.13 demonstrates the Robust Fragility curve and its plus/minus one standard deviations confidence interval based on the Cloud Analysis considering the collapse cases (the procedure for Robust Fragility assessment in this case is described in detail in Chapter 3.2.5 and in [15]) in solid black line and a gray shaded area together with the Robust Fragility curves obtained through the *Cloud to IDA* procedure based on *Reduced set* 1 and *Reduced set* 2 (red dashed lines of different thickness to reflect the size of the set). These two fragility curves are entirely contained inside the plus/minus one standard deviation of the Robust Fragility curve based on the Cloud Analysis considering the collapse cases. It is worth noting that, for all the methods for which the Robust Fragility is calculated herein, the fragility and its "Robust" version are almost identical. A comprehensive and detailed discussion about the reasons for which this happens is presented in [15].

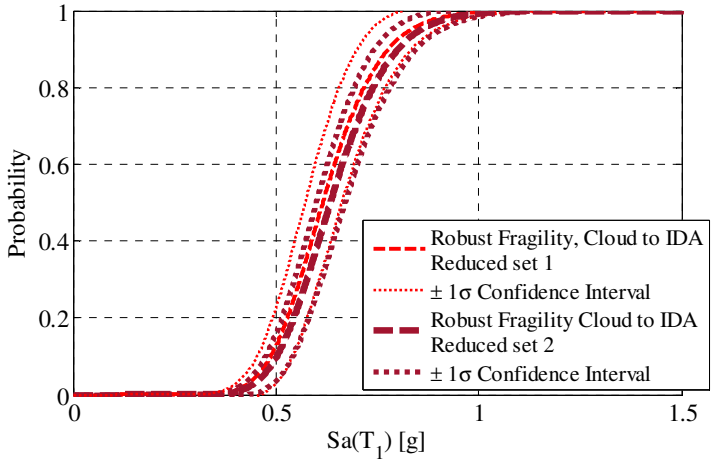

Figure 4.12: Robust Fragility curves and their plus/minus one standard deviation intervals for *Reduced set 1* and *Reduced set 2*.

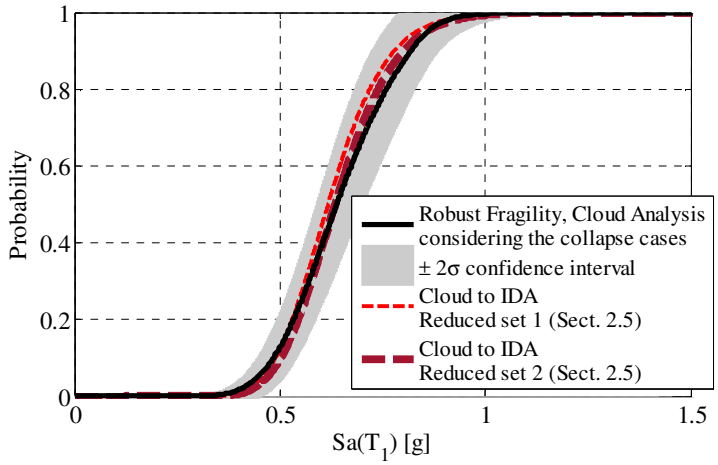

Figure 4.13: Cloud Analysis considering the collapse cases and its plus/minus two standard deviations confidence interval and the Robust Fragility curves for the *Cloud to IDA* procedure and based on the two sets *Reduced set 1* and *Reduced set 2*.

Figure 4.14 illustrates a comparison between *Cloud to IDA* based on *Reduced set* 1 (*N*=10) in red dashed line, IDA in blue dotted line and MSA with CS-compatible records in gray dashed dot line.

Figure 4.15 illustrates a similar comparison between *Cloud to IDA* based on *Reduced set* 2 (*N*=19), IDA and MSA with CS-compatible records. It can be observed that the two *Cloud to IDA* fragility curves are confined between the IDA and MSA results; with the fragility based on *Reduced set* 2 closer to the "best-estimate" MSA results for the range of IM values of high probability content for risk evaluation. Instead, the fragility based on *Reduced set* 1 is slightly closer to the IDA fragility.

Figure 4.16 shows the comparison between the IDA and *Cloud to IDA* procedures for all the three record sets (*Reduced set 1*, *Reduced set 2*, and *Complete*; the lines types for each procedure are distinguished by their thickness: the larger the set of records the thicker the line). For each given record set, the fragility curves obtained based on IDA and *Cloud to IDA* procedures are almost identical. In the context of this study, the *Cloud to IDA* procedure demonstrates its capability of improving the computational efficiency significantly without sacrificing the accuracy with respect to the original IDA method.

Table 4.2 shows the statistical parameters for the fragility curves, where η is the median value of the fragility curve and β is its logarithmic standard deviation. It also shows the number of analyses required for each of the alternative non-linear dynamic analysis procedures. Moreover, the table illustrates the mean annual frequencies of exceeding the near-Collapse limit state (i.e., risk obtained by integrating the fragility and site-specific hazard curve) denoted by λ_{LS} corresponding to the Robust Fragility and the Robust Fragility plus/minus two standard deviations. $\tilde{R}_F$ denotes the risk obtained by integrating Robust Fragility and site-specific hazard; $\tilde{R}_{F\pm2\sigma\chi}$ denotes risk calculated by integrating Robust Fragility plus/minus its two standard deviation confidence intervals and the site-specific hazard. The fragility curves obtained based on the Cloud Analysis considering the Collapse cases, *Cloud to IDA* based on *Reduced set 2* and MSA are quite close. Even *Cloud to IDA* based on *Reduced set 1* manages to provide very reasonable results with a smaller number of analyses with respect to *Reduced set 2*. It can also be observed that *Cloud to IDA* results for the complete record set are identical to that of the IDA for the same record set.

The number of analyses required for implementing IDA procedure is equal to the product of the number of the records and the number of the intensity levels (50×17, as it can be seen also in Figure 4.9). As far as it regards the computational effort related to the implementation of *Cloud to IDA* procedure, the number of analyses required is not fixed. Herein, it is equal to the number of records required for Cloud Analysis (i.e., 50) plus two times the number of the selected records (10×2 and 19×2 for Reduced sets 1 and 2, respectively). Overall, the *Cloud to IDA* fragilities with limited scaling (*Reduced sets* 1 and 2) manage to provide very reasonable results with a sensibly lower analysis effort compared to IDA and MSA. However, the prize for the lowest number of analyses without any scaling goes to Cloud Analysis considering the collapse cases.

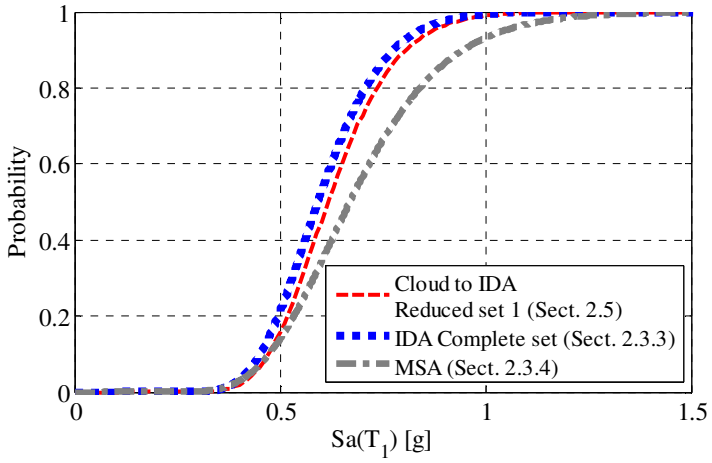

Figure 4.14: Comparison between the three non-linear dynamic procedures (*Cloud to IDA*, IDA and MSA with CS-compatible records) for the *Reduced set 1*.

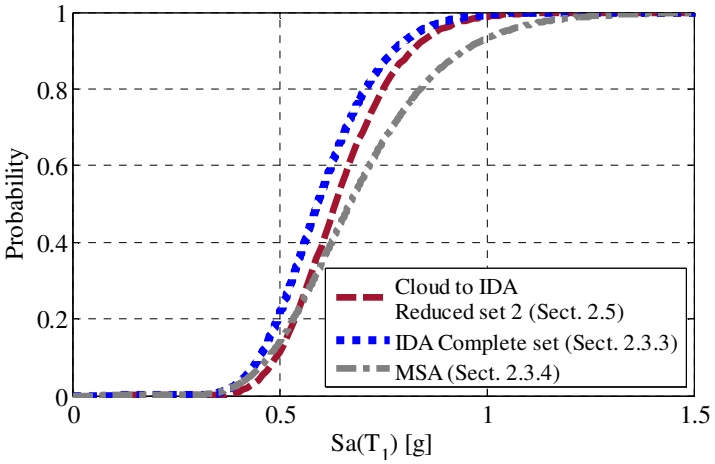

Figure 4.15: Comparison between the three non-linear dynamic procedures (*Cloud to IDA*, IDA and MSA with CS-compatible records) for the *Reduced set 2*.

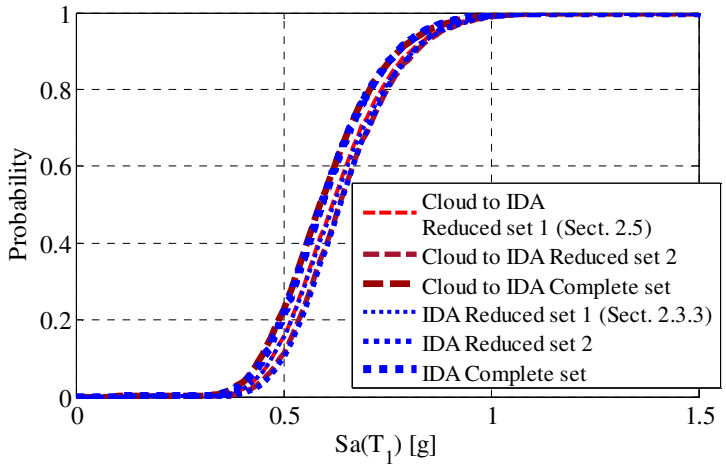

Figure 4.16: Comparison between IDA and *Cloud to IDA* procedures for the three record sets: *Reduced set 1*, *Reduced set 2*, and the Complete set (FEMA).

Table 4.2: Statistical parameters for fragility curves, number of analyses and mean annual frequencies of exceeding the limit state for the alternative nonlinear dynamic procedures.

Methodology	η [g]	β	Number of analyses	λ_{LS} using the Robust Fragility		
				$\tilde{R}_{F\text{-}2\sigma_\chi}$	$\tilde{R}_F$	$\tilde{R}_{F+2\sigma_\chi}$
Cloud Analysis (Complete set)	0.63	0.20	50	1.9×10^{-3}	2.5×10^{-3}	3.1×10^{-3}
Cloud to IDA Reduced set 1	0.62	0.21	50+10×2=70	1.8×10^{-3}	2.6×10^{-3}	3.5×10^{-3}
Cloud to IDA Reduced set 2	0.63	0.20	50+19×2=88	1.8×10^{-3}	2.4×10^{-3}	3.1×10^{-3}
IDA (Complete set)	0.59	0.21	50×17=850	2.4×10^{-3}	2.9×10^{-3}	3.4×10^{-3}
Cloud to IDA (Complete set)	0.59	0.21	50×3+1=151	2.4×10^{-3}	2.9×10^{-3}	3.4×10^{-3}
MSA (varying suites of CS-compatible records)	0.67	0.27	38×19=722	-	2.3×10^{-3}	-

4.4 CONCLUSIONS

Cloud to IDA is proposed as an efficient procedure with limited scaling of ground motion records that exploits the results of a simple Cloud Analysis for carrying out incremental dynamic analysis (IDA). The procedure is applicable when the adopted EDP is expressed in terms of a critical demand to capacity ratio that is equal to unity at the onset of the limit state.

There is indeed a natural link between Cloud and IDA procedures. The Cloud data can be viewed as the first points on the various IDA curves. On the other

hand, an IDA curve can be obtained theoretically with only two data points, consisted of pairs of intensity versus critical demand to capacity values, if the interval of values covered by the two points covers the demand to capacity ratio equal to one. In the *Cloud to IDA* procedure, the intensity levels to scale to are chosen strategically with the aim of performing the minimum number of analyzes and minimum amount of scaling necessary. To this end, one can exploit the simple linear (logarithmic) regression predictions made based on the results of the structural analysis to the un-scaled registered records (a.k.a., the simple Cloud Analysis) to choose landmark IM levels for scaling. In this context, those records that are going to be potentially scaled up/down by a factor close to unity are identified from the pool of original records in order to avoid excessive scaling of the records (the *Reduced sets 1* and *2* in this chapter).

The results indicate that the risk estimates obtained based on the *Reduced sets 1* and *2* are very close to those obtained based on the Cloud Analysis considering the collapse cases and MSA based on varying suits of CS-compatible records (the "best-estimate" herein). The same observation holds when comparing the statistics of the corresponding fragility curves. This is while the IDA-based fragility reveals a slight shift to the left compared to the other more "scaling-conscious" methods. Nevertheless, the risk results obtained are in overall good agreement between the alternative dynamic analysis methods. This work employs the Robust Fragility concept to consider the uncertainty in the estimation of fragility model parameters. This leads to definition of a confidence interval with a prescribed probability content around the estimated fragility curves. The definition of an error margin for the estimated fragility makes it possible to quantify the difference between the fragility curves obtained based on alternative dynamic procedures in terms of the number of standard deviations. Moreover, it allows for mapping the confidence band for the fragility to the risk level.

In synthesis, the proposed *Cloud to IDA* procedure leads to results (in terms of risk) very close to the "best-estimate" MSA with varying suits of CS-compatible records, when specific attention is made to choose records that require limited scaling. On the other hand, the proposed procedure lead to results that are identical to IDA, when the same set of records are used. All of this is possible with a number of analyses that is sensibly lower (almost an order of magnitude) with respect to IDA and MSA. It is worth emphasizing that the use of DCR_{LS} as

the performance variable directly is indispensable for the proposed *Cloud to IDA* procedure.

4.5 REFERENCES

[1] Miano. A., Jalayer. F., Ebrahimian, H., and Prota, A., 2017. Cloud to IDA: Efficient Fragility Assessment with Limited Scaling. Earthquake Engineering and Structural Dynamics (Under Review).

[2] Jalayer, F., Elefante, L., Iervolino, I., and Manfredi, G., 2011. Knowledge-based performance assessment of existing RC buildings. Journal of Earthquake Engineering; 15 (3): 362-389.

[3] Calvi, G.M., Pinho, R., Magenes, G., Bommer, J.J., Restrepo-Vélez, L.F., and Crowley, H., 2006. Development of seismic vulnerability assessment methodologies over the past 30 years. ISET J Earth Technology; 43(3): 75-104.

[4] Cornell, C.A., Krawinkler, H., 2000. Progress and challenges in seismic performance assessment. PEER Center News; 3 (2): 1-3.

[5] Villaverde, R., 2007. Methods to assess the seismic collapse capacity of building structures: State of the art. Journal of Structural Engineering; 133 (1): 57-66.

[6] Vamvatsikos, D., and Cornell, C.A., 2002. Incremental dynamic analysis. Earthquake Engineering and Structural Dynamics; 31 (3): 491-514.

[7] Vamvatsikos, D., and Cornell, C.A., 2004. Applied incremental dynamic analysis. Earthquake Spectra; 20(2): 523-553.

[8] Jalayer, F., and Cornell, C.A., 2003. A Technical Framework for Probability-Based Demand and Capacity Factor Design (DCFD) Seismic Formats. Pacific Earthquake Engineering Center (PEER) 2003/08.

[9] Jalayer, F., and Cornell, C.A., 2009. Alternative non-linear demand estimation methods for probability-based seismic assessments. Earthquake Engineering and Structural Dynamics; 38 (8): 951-972.

[10] Bazzurro, P., Cornell, C.A., Shome, N., and Carballo, J.E., 1998. Three proposals for characterizing MDOF nonlinear seismic response. Journal of Structural Engineering (ASCE); 124 (11): 1281-1289.

[11] Cornell, C.A., Jalayer, F., Hamburger, R.O., and Foutch, D.A., 2002. Probabilistic basis for 2000 SAC federal emergency management agency steel moment frame guidelines. Journal of Structural Engineering (ASCE); 128 (4): 526-533.

[12] Elefante, L., Jalayer, F., Iervolino, I., and Manfredi, G., 2010. Disaggregation-based response weighting scheme for seismic risk assessment of structures. Soil Dynamics and Earthquake Engineering; 30(2): 1513-1527.

[13] Ebrahimian, H., Jalayer, F., Asprone, D., Lombardi, A.M., Marzocchi, W., Prota, A., and Manfredi, G., 2014. A performance-based framework for adaptive seismic aftershock risk assessment. Earthquake Engineering and Structural Dynamics; 43 (14): 2179-2197.

[14] Jalayer, F., De Risi, R., and Manfredi, G., 2015. Bayesian Cloud Analysis: efficient structural fragility assessment using linear regression. Bulletin of Earthquake Engineering; 13 (4): 1183-1203.

[15] Jalayer, F., Ebrahimian H., Miano A., Manfredi G. and Sezen H., 2017. Analytical fragility assessment using un-scaled ground motion records. Earthquake Engineering and Structural Dynamics; https://doi.org/10.1002/eqe.2922.

[16] Jalayer, F., and Ebrahimian, H., 2017. Seismic risk assessment considering cumulative damage due to aftershocks. Earthquake Engineering and Structural Dynamics; 46(3): 369-389. https://doi.org/10.1002/eqe.2792.

[17] Vamvatsikos, D., and Cornell, C.A., 2005. Direct estimation of seismic demand and capacity of multi degree-of-freedom systems through incremental dynamic analysis of single degree of freedom approximation. Journal of Structural Engineering; 131(4): 589-599.

[18] Dolšek, M., and Fajfar, P., 2005. Simplified non-linear seismic analysis of infilled reinforced concrete frames. Earthquake Engineering and Structural Dynamics; 34(1): 49-66.

[19] Han, S.W., and Chopra, A.K., 2006. Approximate incremental dynamic analysis using the modal pushover analysis procedure. Earthquake Engineering and Structural Dynamics; 35(15): 1853-1873.

[20] Azarbakht, A., and Dolšek, M., 2007. Prediction of the median IDA curve by employing a limited number of ground motion records. Earthquake Engineering and Structural Dynamics; 36(15): 2401-2421.

[21] Azarbakht, A., and Dolšek M., 2010. Progressive incremental dynamic analysis for first-mode dominated structures. Journal of Structural Engineering; 137(3): 445-455.

[22] Dhakal, R.P., Mander, J.B., and Mashiko, N., 2006. Identification of critical ground motions for seismic performance assessment of structures. Earthquake Engineering and Structural Dynamics; 35(8): 989-1008.

[23] Baker, J.W., and Cornell, C.A., 2005. A vector-valued ground motion intensity measure consisting of spectral acceleration and epsilon, Earthquake Engineering and Structural Dynamics; 34: 1193-1217.

[24] Lin, T., and Baker, J.W., 2013. Introducing Adaptive Incremental Dynamic Analysis: A new tool for linking ground motion selection and structural response assessment. In: Proceedings of the 11th International Conference on Structural Safety and Reliability (ICOSSAR 2013), Deodatis G, Ellingwood B, Frangopol D. (eds.). The International Association for Structural Safety and Reliability: New York, NY, 2013.

[25] Lin, T., Harmsen, S.C., Baker, J.W, and Luco N., 2013. Conditional Spectrum computation incorporating multiple causal earthquakes and ground motion prediction models. Bulletin of Seismological Society of America; 103(2A): 1103-1116.

[26] Lin, T., Haselton, C.B., and Baker, J.W., 2013. Conditional spectrum-based ground motion selection. Part I: Hazard consistency for risk-based assessments. Earthquake Engineering and Structural Dynamics; 42(12): 1847-1865.

[27] Jayaram, N., Lin T., and Baker, J.W., 2011. A computationally efficient ground-motion selection algorithm for matching a target response spectrum mean and variance. Earthquake Spectra; 27(3): 797-815.

[28] FEMA P440A. Effects of strength and stiffness degradation on seismic response. Washington (DC): Federal Emergency Management Agency; 2009.

[29] FEMA P695. Quantification of Building Seismic Performance Factors. Washington (DC): Federal Emergency Management Agency; 2009.

[30] FEMA P-58-1. Seismic assessment performance of buildings, Volume 1-Methodology. Washington (DC): Federal Emergency Management Agency; 2012.

[31] ASCE/SEI 41-13. Seismic evaluation and retrofit of existing buildings. American Society of Civil Engineers: Reston, VA, 2014.

[32] FEMA 356. Prestandard and Commentary for the Seismic Rehabilitation of Buildings. Washington (DC): Federal Emergency Management Agency; 2000.

[33] CEN. Eurocode 8: Design of structures for earthquake resistance, Part 3: Assessment and retrofitting of buildings. EN 1998-1 CEN Brussels, April 2004.

[34] Baker, J.W., 2015. Efficient analytical fragility function fitting using dynamic structural analysis. Earthq Spectra. 2015; 31(1): 579-599.

[35] Jalayer, F., Franchin, P., and Pinto, P.E., 2007. A scalar damage measure for seismic reliability analysis of RC frames. Earthquake Engineering and Structural Dynamics; 36(13): 2059-2079.

[36] Miano, A., Jalayer, F., and Prota, A., 2016. Cloud to IDA: a very efficient solution for performing Incremental Dynamic Analysis. AICAP 2016 Congress, Italian concrete days, Rome, Italy, 27-28 October 2016.

[37] Ebrahimian, H., Jalayer, F., and Manfredi, G., 2015. Seismic retrofit decision-making of bridges based on life-cycle cost criteria. In: Proceedings of the 5th ECCOMAS Thematic Conference on Computational Methods in Structural Dynamics and Earthquake Engineering (COMPDYN 2015), M. Papadrakakis, V. Papadopoulos, V. Plevris (eds.), Crete Island, Greece, 25-27 May 2015.

[38] Miano, A., Sezen, H., Jalayer, F., and Prota, A., 2017. Performance based comparison of different retrofit methods for reinforced concrete structures. In: Proceedings of the 6th ECCOMAS Thematic Conference on Computational Methods in Structural Dynamics and Earthquake Engineering (COMPDYN 2017), Rhodes, Greece, 15-17 June 2017.

[39] Miano, A., Jalayer, F., and Prota, A., 2017. Considering Structural Modeling Uncertainties usign Bayesian Cloud Analysis. In: Proceedings of the 6th ECCOMAS Thematic Conference on Computational Methods in Structural Dynamics and Earthquake Engineering (COMPDYN 2017), Rhodes, Greece, 15-17 June 2017.

[40] McKenna, F., 2011. OpenSees: a framework for earthquake engineering simulation. Computing in Science and Engineering; 13(4): 58-66.

[41] Setzler, E.J. and Sezen, H., 2008. Model for the lateral behavior of reinforced concrete columns including shear deformations. Earthq Spectra; 24(2): 493-511.

[42] Sezen, H., 2008. Shear deformation model for reinforced concrete columns. Struct Eng Mech; 28(1): 39-52.

[43] Ditlevsen, O., and Madsen, H.O., 1996. Structural reliability methods. Wiley: New York.

[44] Galanis, P.H., and Moehle, J.P., 2015. Development of collapse indicators for risk assessment of older-type reinforced concrete buildings. Earthquake Spectra; 31 (4): 1991-2006.

[45] Gehl, P., Douglas, J., and Seyedi, D.M., 2015. Influence of the number of dynamic analyses on the accuracy of structural response estimates. Earthquake Spectra; 31(1): 97-113.

[46] Luco, N., and Cornell C.A., 2007. Structure-specific scalar intensity measures for near-source and ordinary earthquake ground motions. Earthquake Spectra; 23(2): 357-392.

[47] Jalayer, F., Beck, J., and Zareian, F., 2012. Analyzing the sufficiency of alternative scalar and vector intensity measures of ground shaking based on information theory. Journal of Engineering Mechanics; 138(3): 307-316.

[48] Ebrahimian, H., Jalayer, F., Lucchini, A., Mollaioli, F., and Manfredi G., 2015. Preliminary ranking of alternative scalar and vector intensity measures of ground shaking. Bulletin of Earthquake Engineering; 13(10): 2805-2840.

[49] Kohrangi, M., Bazzurro, P., Vamvatsikos, D., and Spillatura A., 2017 Conditional spectrum-based ground motion record selection using average spectral acceleration. Earthquake Engineering and Structural Dynamics; 46(10): 1667-1685.

[50] Shome, N., and Cornell, C.A., 1999. Probabilistic seismic demand analysis of nonlinear structures. Report No. RMS35, Stanford University, CA, 1999: 320 pp.

[51] Stoica, M., Medina, R.A., and McCuen, RH., 2007. Improved Probabilistic Quantification of Drift Demands for Seismic Evaluation. Structural Safety; 29(2): 132-45.

[52] Ebrahimian, H., Azarbakht, A.R., Tabandeh, A., and Golafshani AA., 2012. The exact and approximate conditional spectra in the multi-seismic-sources regions. Journal of Soil Dynamics and Earthquake Engineering; 39(1): 61-77.

[53] Jalayer, F., De Risi, R,. Elefante, L., and Manfredi G., 2013. Robust fragility assessment using Bayesian parameter estimation. Vienna Congress on Recent Advances in Earthquake Engineering and Structural Dynamics 2013 (VEESD 2013). C. Adam, R. Heuer, W. Lenhardt & C. Schranz (eds), Vienna, Austria, 28-30 August 2013, Paper No. 503.

Chapter 5

CONSIDERING STRUCTURAL MODELLING UNCERTAINTIES USING BAYESIAN CLOUD ANALYSIS

5.1 INTRODUCTION

Assessment of analytic structural fragility for existing buildings is one of the fundamental steps in the modern performance-based engineering [1]. This chapter deals with the quantification the impact of structural modelling uncertainty on the seismic performance assessment for existing building [2]. In fact, one main feature distinguishing the assessment of existing buildings from that of the new ones is the large amount of uncertainty present in determining the structural modeling parameters. In particular, considering the partial information available related to material properties, construction details and also the uncertainty in the capacity models, the impact of modelling uncertainties on the seismic performance assessment is a crucial issue for existing buildings. Thus, for this type of buildings, explicit consideration of modelling uncertainty in the process of the assessment of structural performance can lead to more accurate results.

In order to assess the performance of the existing buildings, as discussed in details in Chapter 3 and 4, there are alternative non-linear dynamic analysis procedures available in the literature, such as, Incremental Dynamic Analysis (IDA, [3]), Multiple-Stripe Analysis (MSA, [4-6]) and Cloud Analysis [4,7-10]. As previously presented in detail, Cloud Analysis is particularly efficient since it involves the non-linear analysis of the structure subjected to a set of un-scaled ground motion time-histories. A complete discussion about advantages and limits of the Cloud Analysis in presented in Chapter 3 and Chapter 4.

Herein, Cloud Analysis has been used, not only to model the record-to-record variability in ground motion, but also to propagate structural modelling

uncertainties such as uncertainty in component capacity [9,12] and the uncertainties in mechanical material properties and construction details [9,13]. One approximate way to consider the epistemic uncertainties in the fragility assessment is to consider the uncertainty in the evaluation of the median of the fragility curve (e.g., [11-12,14-18]). Such modelling of epistemic uncertainties, assuming that the median is unbiased and normally distributed, leads to an overall increase in the fragility dispersion and leaves the fragility median invariant. In other words, such procedure does not manage to capture the bias in median limit state probability due the effect of epistemic uncertainties. Simulation-based methods are arguably the most efficient and straightforward means for taking into account the epistemic uncertainties (see e.g., [19-20]). However, they fall short of modelling record-to-record variability when recorded ground motions are implemented (due to a lack of reference probability distributions for recorded ground motions). In the recent years, several alternative methods have been proposed that combine reliability methods such as the first order second moment (FOSM and MVFOSM, see for example [21]) methods, response surface methods [22], simulation-based methods (e.g., Monte Carlo, Latin Hypercube Sampling) with non-linear dynamic procedures such as IDA based on recorded ground motions in order to take into account also sources of uncertainties other than record-to-records variability [23-26].

In this chapter, the modified version of Cloud Analysis, proposed in Chapter 3, that considers the (eventual) cases of global dynamic instability, based on coupling the simple regression in the logarithmic space of structural response versus seismic intensity for a suite of registered records with logistic regression, has been implemented to consider both record-to-record variability and modelling uncertainties. This modified version of Cloud Analysis relies on adopting a critical demand to capacity ratio, which is equal to unity at the onset of limit state, as the damage measure/decision variable.

For each of the registered records within the suite of ground motion records, a different realization of the structural model has been generated through a standard Monte Carlo Simulation procedure. A Bayesian updating framework, presented in Chapter 3, which treats the structural response to the selected records as “data”, is adopted to take into account the uncertainty in the fragility parameters. One advantage in using the Bayesian framework is that it leads to

fragility estimation together with the definition of a prescribed confidence band. Consequently, the risk estimates can be provided as a range of values that map a certain probability content in terms of the confidence in the fragility estimate (e.g., plus/minus one or two standard deviations from the median that correspond to approximately 70% and 95% probability content, respectively, assuming Normality). There are no specific restrictions on the sample of "data" points other than being plausible independent "observations" (in reality they are calculated) of the structural response. Another advantage in using such framework is that it enables the formal introduction of prior information available about the fragility parameters (e.g., particularly useful for updating of existing fragility models).

The longitudinal frame of the seven-story existing building in Van Nuys, CA, presented in details in Chapter 1.6 and modeled in OpenSees considering the modeling aspects presented in Chapter 2, has been employed to demonstrate this procedure.

5.2 METHODOLOGY

The methodology for the assessment of the structural Robust Fragility and its prescribed confidence interval based on Cloud Analysis and considering explicitly the cases of "collapse" has been documented in details in Chapter 3.2, considering only record-to-record variability. The work proposed in this chapter employs this method to consider also the structural modeling uncertainties. Below, a brief description of this method is reported.

5.2.1 THE INTENSITY MEASURE AND THE STRUCTURAL PERFORMANCE VARIABLE

The critical demand to capacity ratio for a prescribed limit state [12] and denoted as DCR_{LS}, has been adopted as a proxy for the structural performance variable, as presented in details in Chapter 3.2.1. DCR_{LS} is defined as the demand to capacity ratio for the component or mechanism that brings the system closer to the onset of limit state *LS*. The formulation refers to Equation 3.1 and is based on the cut-set concept [27], which is suitable for cases where various potential failure mechanisms (both ductile and fragile) can be defined a priori. DCR_{LS} is always equal to unity at the onset of limit state. The component demand to capacity ratios

are expressed in terms of the maximum component chord rotation. This leads to a deformation-based DCR_{LS}. For the near collapse limit state it is defined as the point on the softening branch of the force-deformation curve of the component, where a 20% reduction in the maximum strength takes place [28]. The possible failure mechanisms associated with the near-collapse limit state correspond to ductile or brittle failures of the columns.

Finally, also herein as in Chapter 3.2.1, the global *Collapse* of the structure is identified explicitly by verifying the following two criteria: (1) accounting for the loss of load bearing capacity when 50% +1 of the columns of a story reach the chord rotation corresponding to the complete loss of vertical-load carrying capacity of the component [29]; (2) accounting for for global dynamic instability when maximum inter-story drift exceeds 10%.

5.2.2 THE "OBSERVED DATA" D

Let vector θ represent all the uncertain parameters considered in the problem (apart from the fragility model parameters and those related to the ground motion representation). For example, this vector may contain component capacity model parameters, construction detail parameters and parameters related to mechanical material properties. It is enough to note that any given realization θ_i of vector θ identifies in a unique manner the structural model. Ideally, a standard Monte Carlo simulation can be used for generating a set of i=1:N realizations of the vector θ.

In particular, for each of the registered records within the suite of ground motion records, a different realization of the structural model has been generated through a standard Monte Carlo Simulation procedure. This way, each realization of the vector θ (plausible structural model subjected) subjected to a registered record leads to the corresponding DCR value. The set of DCR values calculated this way are then used as "observed data" in order to update the probability distribution for the parameters of the prescribed fragility model (e.g., Lognormal).

5.2.3 CLOUD ANALYSIS CONSIDERING COLLAPSE CASES AND ROBUST FRAGILITY ASSESSMENT

A regression-based probability model is employed to describe the DCR_{LS} for a given IM=$S_a(T_1)$ level. Let DCR_{LS}={$DCR_{LS,i}$, i=1:N} be the set of critical demand

to capacity ratio for limit state *LS*, calculated through non-linear time-history analyses performed for a suite of *N* recorded ground motions, and $S_a=\{S_{a,i}, i=1:N\}$ be the set of corresponding spectral acceleration values (where $DCR_{LS,i}$ and $S_{a,i}$ are calculated for the *i*th ground motion record). The *Cloud data* or simply *data* hereafter refer to the set $\mathbf{D}=\{(S_{a,i}, DCR_{LS,i}), i=1:N\}$. The regression probabilistic model is described in Equation 3.2. This non-linear dynamic analysis procedure, known as the Cloud Analysis (discussed previously in detail in Chapter 3.2.3), graphically invokes the idea of the scatter plot of data pairs of structural performance variable and the intensity measure for a given ground motion record. The Cloud Analysis is particularly useful when one deals with un-scaled ground motion records. The structural fragility obtained based on the Cloud Analysis can be expressed as the probability that DCR_{LS} exceeds unity given S_a, following the Equation 3.3.

Cloud Analysis can still be carried out in the cases in which some records take the structure to verge upon "Collapse", as proposed in details in Chapter 3.2.4. In particular, the Cloud data can be partitioned into two parts: (a) *NoC* data which correspond to that portion of the suite of records for which the structure does not experience "Collapse", (b) *C* corresponding to the "Collapse"-inducing records. The structural fragility for a prescribed limit state *LS*, expressed in Equation 3.3, can be expanded with respect to *NoC* and *C* sets using Total Probability Theorem (see [5,30]), following Equation 3.4, introduced in Chapter 3.2.4, together with the explanation of all the different terms of Equation 3.4.

Finally, the Robust Fragility is presented in details in Chapter 3.2.5 and can be defined as the expected value for a prescribed fragility model taking into account the joint probability distribution for the (fragility) model parameters χ [9, 13, 31]. The Robust Fragility expression refers to Equation 3.10 (see Chapter 3.2.5).

5.2.4 IMPLEMENTING THE CONCEPT OF ROBUST FRAGILITY IN ORDER TO TAKE INTO ACCOUNT THE STRUCTURAL MODELING UNCERTAINTIES

This chapter implements the concept of Robust Fragility in order to efficiently propagate the sources of uncertainty related to both record-to-record variability and structural modelling, based on the results of a Cloud Analysis. In particular, the Cloud procedure is embedded in a Bayesian updating framework that updates

the distribution of the fragility model parameters (based on the Cloud Analysis results) in order to lead to robust fragility estimates and the confidence bands. The flowchart in Figure 5.1 describes this procedure in a step-by-step manner:

Step 1: Perform the record selection. In this step, the record selection for Cloud Analysis should be performed, based on very few main rules. That is, the records should be selected in a way that they cover a vast range of spectral acceleration values and the records should be selected so that a significant proportion of records have DCR_{LS} greater than unity.

Step 2: Characterize the uncertainties vector θ and the associated joint PDF, where θ represents all the uncertain parameters in the problem related to structural modeling. For example, as previously explained, this vector may contain component capacity modelling parameters, construction detailing parameters, parameters related to mechanical material properties and parameters related to the ground motion representation. It is enough to note that any given realization θ_i of vector θ identifies in a unique manner the structural model.

Step 3: Generate n samples (with MC simulation, LHS, …, etc.) of the vector θ, where n is the number of the records. Note that for each of the registered records within the suite of ground motion records, a different realization of the structural model is generated through for example a standard Monte Carlo Simulation procedure or a Latin Hypercube Sampling.

Step 4: Subject each structural model configuration to one of the records within the set. In this way, each realization of the vector θ (plausible structural model subjected to a registered record) leads to a corresponding critical DCR_{LS} value.

Step 5: Form the set of the critical $DCR_{LS}=\{DCR_{LS,i},\ i=1:N_{records}\}$ and perform Cloud Analysis. As said in Section 5.2.3, Cloud Analysis is based on a regression-based probability model, that is employed to describe the DCR_{LS} for a given IM level. Let $DCR_{LS}=\{DCR_{LS,i},\ i=1:N\}$ be the set of critical demand to capacity ratio for limit state *LS*, calculated through non-linear time-history analyses performed for the set of N records, and $S_a=\{S_{a,i},\ i=1:N\}$ be the set of corresponding spectral acceleration values (where $DCR_{LS,i}$ and $S_{a,i}$ are calculated for the ith record). The *Cloud data* refer to the set $\mathbf{D}=\{(S_{a,i},\ DCR_{LS,i}),\ i=1:N\}$. If cases in which some records take the structure to verge upon "Collapse" are present, the Cloud data can be partitioned into two parts (e.g. No Collapse data and Collapse data). The

structural fragility can be expanded with respect to No Collapse and Collapse sets using Total Probability Theorem as explained in Equation 3.4

Step 6: Obtain the Robust Fragility and the desired confidence bands. This entails Updating the joint distribution ($\chi|D$) for the fragility model parameters χ, based on the cloud data D (see sect. 5.2.4) and simulating vector $\boldsymbol{\chi}_i$ based on its probability density function $f(\boldsymbol{\chi}|\mathbf{D})$. This leads to the solution of the integrals leading to the Robust Fragility and its standard deviation (Equations 3.10 and 3.11).

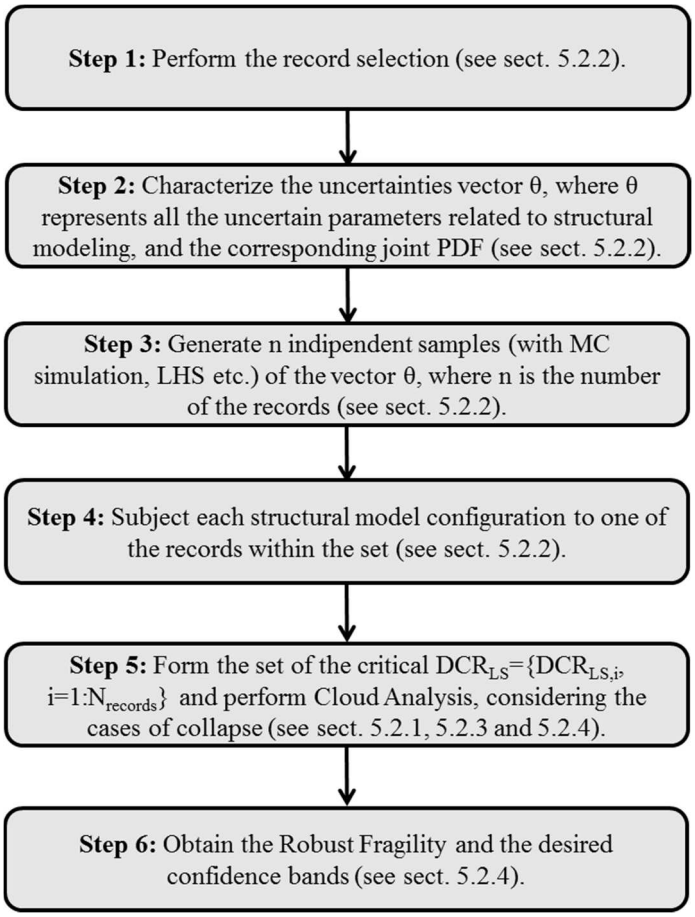

Figure 5.1 Step-by-step guide to implementing the Robust Fragility procedure for propagating both record-to-record variability and structural modelling uncertainties.

5.3 NUMERICAL APPLICATION

A reinforced concrete (RC) moment-resisting frame is considered herein as case study: the north longitudinal perimeter frame of the seven-story Holiday Inn hotel building in Van Nuys, California (presented in Chapter 1.6). All the details about the modelling issues have been presented in details in Chapter 2.

5.3.1 THE UNCERTAINTIES CHARACTERIZATION

Various sources of uncertainty are considered herein. In particular, the record-to-record variability (uncertainties in the representation of the ground motion), the uncertainties in component capacity models, and the uncertainties in the mechanical material properties and in the construction details (the latter is also referred to as structural "defects") are considered. In particular, for the mechanical material properties and the construction details, the prior probability distributions are updated based on the available data for the case study, employing a Bayesian framework (see [13] for detailed description of the updating procedure).

5.3.1.1 UNCERTAINTY IN THE REPRESENTATION OF GROUND MOTIONS

The record selection for Cloud Analysis is particularly important. In Chapter 3.2.3, some important points to consider when selecting records for Cloud Analysis are presented in details.

Here the two sets of 34 and 70 strong ground-motion records, presented in Chapter 3.3.1.1, are used (see Table 3.1 for the list of the records). The suite of 70 records covers a wide range of magnitudes between 5.5 and 7.9, and closest distance-to-ruptured area (denoted as R_{RUP}) up to around 40 km, as illustrated by the scatter diagram in Figure 3.2 (a). The associated spectral shapes are shown in Figure 3.2 (b). The soil average shear wave velocity in upper 30 m of soil, V_{s30}, at the Holiday Inn hotel's site is around 218 m/sec. Accordingly, all selected records are chosen from NEHRP site classes C-D. The lowest useable frequency is set at 0.25 Hz, ensuring that the low-frequency content is not removed by the ground motion filtering process. There is no specific consideration on the type of faulting; nevertheless, all selected records are from strike-slip or reverse faults (consistent with California faulting). The records are selected to be free field or on the ground level. The set of 34 ground-motion records is extracted from the set of the 70

records. The only criterion for this selection is to limit the number of records from a single seismic event to be one (to avoid intra-event correlations).

5.3.1.2 UNCERTAINTY IN THE COMPONENT CAPACITY MODELS

Component capacities are modelled herein as the product of predictive formulas expressed as η_{Ci} and unit-median Log Normal variables ε_{Ci} accounting for the uncertainty in component capacity [8,11], according to the general format:

$$C_i = \eta_{Ci} \cdot \varepsilon_{Ci} \tag{5.1}$$

The expression for median capacities corresponding to the considered mechanism are described below. It's important to highlight that only the shear capacity critical points are assumed as random variables and investigated as source of uncertainty. In fact, the critical points of the shear curve, chosen as random variables, come out from regressions, based on experimental tests. Instead, the flexural capacity points are based on a standard and complete section analysis, as presented in Section 2.2.1. The median of the lognormal distribution of the maximum shear strength, V_n, is calculated according to Equation 2.1 ($\eta_{Ci}=V_n$), while the relative COV has been provided in [32]. The median of the lognormal distribution of shear displacement corresponding to peak strength, $\Delta_{v,n}$, is calculated according to Equation 2.3 ($\eta_{Ci}=\Delta_{v,n}$), while the relative COV has been assumed equal to 0.15 due the lack of specific data.

The median of the lognormal distribution of total lateral displacement, Δ_a, is calculated according to Equation 2.4 ($\eta_{Ci}=\Delta_a$), while the relative COV has been taken as presented in [33].

Table 5.1 summarizes the component capacity variables, that have been considered herein, and the relative distributions.

Table 5.1: Logarithmic standard deviation values for component capacity models.

Log-normal variable	COV	References
V_n	0.15	[38]
$\Delta_{v,n}$	0.15	[40]
Δ_a	0.26	[41,43]

5.3.1.3 THE UNCERTAINTY IN THE MECHANICAL MATERIAL PROPERTIES AND IN THE CONSTRUCTION DETAILS

The probability distributions for the material mechanical properties and for the construction details (structural defects) are obtained using a Bayesian framework, updating the prior probability distributions with the available data for the specific case study [19]. The parameters identifying the prior probability distributions for the material mechanical properties (compressive concrete strength for beams and columns at different floors, steel yielding force for beams and columns, compressive concrete ultimate strain, steel hardening slope) have been based on the values provided in Table 5.2. The probability distributions for the material mechanical properties are later updated employing the Bayesian framework for inference (see [13] for details of the updating procedure).

Table 5.2 shows the statistics of the lognormal prior and posterior probability distributions for the material mechanical properties and the related references. Figure 5.2 (a) illustrates the prior and posterior probability distributions of the concrete strength *fc1* (see Table 5.2).

Table 5.2: The uncertainty characterization for the material mechanical properties.

Material	Prior distribution			Posterior distribution			References	Available data
	Type	Median	COV	Type	Median	COV		
f_{y1} (MPa)	LN	496	0.12	LN	488	0.07	[34,35]	[34,35]
f_{y2} (MPa)	LN	344	0.12	LN	339	0.07	[34,35]	[34,35]
f_{c1} (MPa)	LN	34.5	0.15	LN	39.1	0.11	[34]	[34,35]
f_{c2} (MPa)	LN	27.6	0.15	LN	31.5	0.11	[34]	[34,35]
f_{c3} (MPa)	LN	20.7	0.15	LN	23.5	0.11	[34]	[34,35]
e_{cu}	LN	0.006	0.40	LN	0.007	0.30	[44,45]	[34,35]
$\alpha_{hardening}$	LN	0.010	0.40	LN	0.011	0.31	[34]	[34]

With regard to the construction detailing parameters, it has been assumed herein that 50% of the inspections verify the design values indicated in the original documents. Tables 5.3 and 5.4 shows the prior and posterior probability distribution statistics for the spacing between the shear reinforcement for the columns, which is the only construction detailing variable assumed as uncertain herein. Figure 5.2 (b) illustrates the prior and posterior probability distributions for the spacing between the shear reinforcement together with updated

distribution based on the hypothesis that 50% of the inspections verify the design value (s=30.5cm). The updating procedure is described in detail in [13].

Table 5.3: The uncertainty in spacing of shear rebars: prior distribution.

Defect	Prior distribution	Values	Reference
Shear rebars spacing	Uniform	30-40cm	[34]

Table 5.4: The uncertainty in spacing of shear rebars: posterior distribution.

Defect	Posterior distribution	Median	COV
Shear rebars spacing	Lognormal	35.5cm	0.18

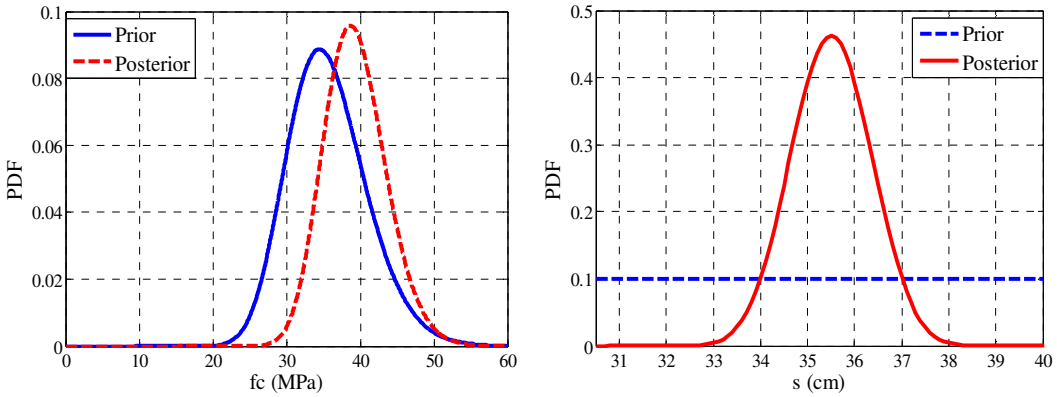

Figure 5.2 (a) The prior and updated probability distributions for the concrete strength *fc1* (see Table 5.2); (b) the uniform prior and updated probability distributions for the spacing of the shear rebars (see Tables 5.3 and 5.4).

5.3.2 CLOUD ANALYSIS

Figures 5.3 (a) show the scatter plots for Cloud data $\mathbf{D}=\{(S_{a,i}, DCR_{LS,i}), i=1:34\}$ for the case-study frame and for the set of the different realizations (each one is a simulated structural model through the standard Monte Carlo procedure plus a registered record). The grey-colored circles represent the *NoC* data, while the grey-colored with red edge squares indicate the *C* data or "collapse-cases" (see Section 5.2.3). In order to have a better representation of *NoC* data, an upper-bound limit of 5 is assigned to the horizontal DCR_{LS}-axis. It can be noted that, consistent with the Section 3.2.3 recommendations, the Cloud data not only

covers a vast range of spectral acceleration values, but it also provides numerous data points in the range of DCR_{LS}>1. Figure 5.3 (a) illustrates also Cloud Analysis regression prediction model (i.e., regression line and the estimated parameters, see Equation 3.2) fitted to the *NoC* data. The Lognormal distribution displayed in Figure 5.3 (a) denotes the distribution of DCR_{LS} given $S_a(T_1)$. Moreover, the line DCR_{LS}=1 corresponding to the onset of limit state (herein, Near-Collapse) is shown with red-dashed line. Finally, Figure 5.3 (a) shows the 16th, 50th and 84th percentiles of the performance variable as a function of spectral acceleration, with and without considering the collapse cases. Figure 5.3 (b) shows the same information for the larger set of 70 records/structural model realizations.

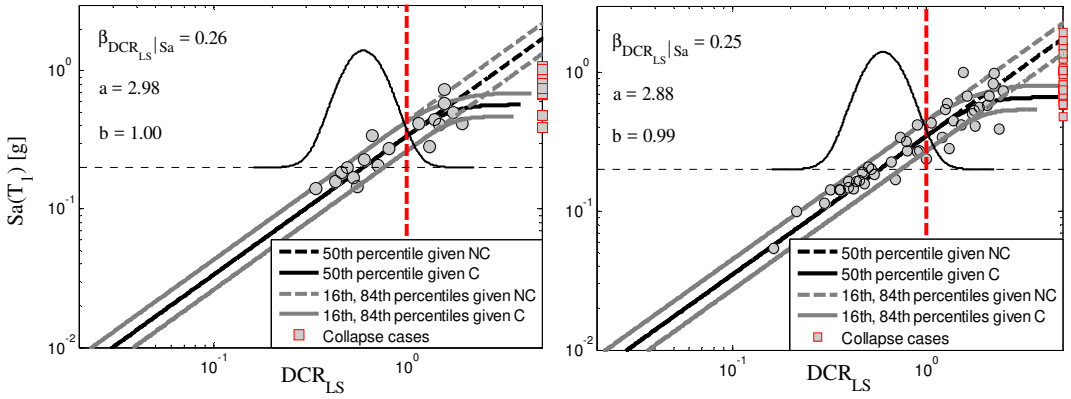

Figure 5.3 (a) Cloud data and regression for the set of 34 records/realizations; (b) Cloud data and regression for the set of 70 records/realizations.

It is worth noting that the structural model realizations can also be generated through a Latin Hypercube (LHS described briefly in the next section, [35-37]) sampling scheme. This is done herein but the corresponding Cloud Analysis results are not reported for brevity. However, the fragility and risk results are reported later.

5.3.3 IDA WITH LATIN HYPERCUBE SAMPLING (LHS)

The LHS belongs to the category of advanced stratified sampling techniques which result in a good estimate of statistical moments of response using small-sample simulation. The basic feature of LHS is that the range of univariate random

variables is divided into N intervals (N is a number of simulations); the values from the intervals are then used in the simulation process (random selection, median or the mean value). The selection of the intervals is performed in such a way that the range of the probability distribution function of each random variable is divided into intervals of equal probability, $1=N$. The samples are chosen directly from the distribution function based on an inverse transformation of the univariate distribution function. The representative parameters of variables are selected randomly, being based on random permutations of integers $k=1,2,..,N$. Every interval of each variable must be used only once during the simulation. The generation of the LHS is then completed by randomly pairing (without replacement) the resulting values for each of the random variables. Unfortunately, the nature of LHS does not allow us to determine a priori the appropriate sample size N to achieve a certain confidence level. Still, the use of a relatively high N that is substantially larger than the number of parameters will always result to reasonably accurate estimates for practical purposes. The optimal N to use is obviously a function of the number of random variables and their influence on the response is a subject of further research [24].

The LHS has been paired up with incremental dynamic analysis (IDA) in order to consider both the record-to-record variability and the epistemic uncertainties (eg, [23-25]). In this work, for the sake of comparison with the literature, Monte Carlo with LHS has been performed for $N=34$ and for $N=80$ realizations of the frame, a relatively high number that has been chosen to allow pinpoint accuracy in our estimates (the number of uncertain variable is 11). Thus, by performing IDA on each of the N realizations, 34×34=1156 and 80×34=2720 IDA curves have been obtained, respectively. Each IDA curve traces the variation in DCR_{LS} for a given realization of the structural model as a function of $Sa(T_1)$ as the record's amplitude is linearly scaled up. As explained in Sect. 3.4, the spectral acceleration values at $DCR_{LS}=1$, denoted as $Sa^{DCR=1}$, are used in order to obtain the IDA-based fragilities [12].

5.3.4 MEAN VALUE FIRST-ORDER SECOND-MOMENT (MVFOSM) METHOD

The MVFOSM method, which is based on the calculation of the first two moments of a nonlinear function, is an approximate method for propagating the

uncertainties (e.g. [24,38]). The number of simulations required is only $2K+1$, where K is the number of uncertain variables considered in the study. Let the log of the S_a capacity denoted as $\ln S_a^{DCR=1}$ be a function f of the uncertainties vector:

$$\ln S_a^{DCR=1} = f(\theta) = \mathrm{f}(\theta_1, \theta_2, ..., \theta_k) \tag{5.2}$$

where f is a function of the random variables for the given limit state and θ is the vector of the random uncertain modeling parameters. It should be noted that the Sa capacity is calculated from the median of IDA curves.

In the first place, the base-case value of f denoted as $\ln S_a^{DCR=1,0}$, that corresponds to all random variables being set equal to their mean $m_{\theta k}$ is calculated. The remaining $2K$ simulations are obtained by shifting each parameter θ_k from its mean by $\pm 1.7\sigma_{\theta k}$ [26], while all other variables remain equal to their mean $m_{\theta k}$. When the θ_k parameter is perturbed, the logs of the median Sa-capacities are denoted as $\ln S_a^{k+}$ and $\ln S_a^{k-}$, where the sign indicates the direction of the shift. Since the number of simulations required is $2K+1$ and $K=11$ in this study, $23\times34=782$ (where 34 is the number of records) IDA curves have been obtained, based on the previous recommendations.

According to MVFOSM, the nonlinear function f can be approximated using a Taylor expansion to obtain its first and second moments. Following the notation of Equation 5.2, the function $f = \ln S_a^{DCR=1}$ is expanded around the mean value denoted as $\bar{\theta}$ [39]:

$$f(\theta) \approx f(\bar{\theta}) + \sum_{k=1}^{K} (\theta_k - \mathrm{m}_{\theta_k}) \frac{df}{d\theta_k}\bigg|_{\bar{\theta}} + \frac{1}{2}\sum_{k=1}^{K} (\theta_k - \mathrm{m}_{\theta_k})^2 \frac{d^2 f}{d\theta^2_k}\bigg|_{\bar{\theta}} \tag{5.3}$$

The gradient and curvature of f can be approximated with a finite difference approach, which is why 2K+1 simulations were needed. The random parameters are set equal to their mean to obtain $\ln S_a^{DCR=1,0}$ and then each random parameter is perturbed as described above. Thus, the first and the second derivative of f with respect to θ_k, will be:

$$\frac{df}{d\theta_k} \approx \frac{\ln S_a^{k+} - \ln S_a^{k-}}{2 \cdot 1.7 \cdot \sigma_{\theta_k}}$$
$$\frac{d^2 f}{d\theta^2_k} \approx \frac{\ln S_a^{k+} - 2 \cdot \ln S_a^{DCR=1}{}_{,0} + \ln S_a^{k-}}{1.7 \cdot \sigma^2_{\theta_k}} \quad (5.4)$$

Truncating after the linear terms in Equation 5.3 provides a first-order approximation for the limit-state mean-log capacities, where they are going to be equal to the base-case values $\ln S_a^{DCR=1},_0$ (the linear term is going to be equal to zero). A more refined estimate is the mean-centered, second-order approximation, which according to Equation 5.3 can be estimated as [24]:

$$m_{\ln Sa^{DCR=1}} \approx \ln S_a^{DCR=1}{}_{,0} + \sum_{k=1}^{K} \frac{1}{2} \frac{d^2 f}{d\theta^2_k} |_{\bar{\theta}} \cdot \sigma_{\theta^2_k} \quad (5.5)$$

Thus the median S_a capacity, assuming lognormality, comes out to be:

$$\hat{S}_a^{DCR=1} = \exp(m_{\ln Sa^{DCR=1}}) \quad (5.6)$$

while, using a first-order approximation, the standard deviation of the logs is estimated as:

$$\beta_{\ln Sa^{DCR=1}} \approx \sum_{k=1}^{K} (\frac{df}{d\theta_k} |_{\bar{\theta}})^2 \sigma_{\theta^2_k} \quad (5.7)$$

It should be noted that the above statistics refer to the *Sa* capacity as calculated from the median IDA curve and total dispersion will need to combine also the effect of record-to-record variability. In this work, the SRSS approach has been used in order to combine the dispersion due to the structural modeling uncertainties and the record-to-record variability.

5.3.5 FRAGILITY CURVES COMPARISON

Figure 5.4 illustrates the Cloud-based Robust Fragility curve (black solid line) and its plus/minus two standard deviation confidence bands (grey dashed lines). The Robust Fragility curve and its confidence interval is obtained following the procedure described in Section 5.2.3 and in Chapter 3.2.5 (see [9] for more details). As mentioned in Chapter 3.2.5, one distinct advantage gained by calculating the Robust Fragility lies in the estimation of its confidence band. In

Figure 5.4 the Cloud-based Robust Fragility curve is compared with the fragility curve obtained through Cloud Analysis (black dashed line) with the consideration only of the record to record (R2R) variability. Moreover, also the site-specific hazard (at T=1 sec, from USGS National Seismic Hazard Mapping Project website (http://earthquake.usgs.gov/hazards, red solid line) is shown in Figure 5.4. As it can be seen from Figure 5.4, Cloud-based Robust Fragility curve with the consideration of all the sources of uncertainty present a reduction both in median capacity and in the dispersion with respect to the fragility curve obtained through Cloud Analysis with the consideration only of the record-to-record variability.

Figure 5.5 illustrates the Cloud-based Robust Fragility curve (black solid line) with its plus/minus one standard deviation confidence bands (grey dashed lines) and the fragility curves (thin grey solid lines) obtained based on Cloud Analysis through the generation of different sets of realizations (10 different sets) of the structural model. It can be observed that the different simulations of the cloud-based fragility curves are contained within the plus/minus one standard deviation interval of the robust fragility curve. The fragility curve based on the Cloud Analysis of 70 records/structural model realizations is also shown in Figure 5.5 in solid blue lines. The figure also illustrates how the cloud-based fragility curves would shift if the LHS procedure is used for stratified sampling of the structural model parameters instead of the standard Monte Carlo procedure proposed herein (for both sets of 34 and 70 records plotted as black dotted and blue dotted lines, respectively). It can be observed that the differences between the number of records/extractions and the type of simulation (random versus stratified) is again contained within one standard deviations away from the Robust Fragility curve (obtained based 34 record/realizations and standard Monte Carlo sampling of the structural model parameters). This underlines the utility of the confidence bands, that represent a reliable interval, in which the “true” fragility curve would lie with a prescribed probability/confidence level. Moreover, it can be observed that the fragility curve based on 70 records/LHS-generated realizations marks an increase in the dispersion with respect to the rest of the curves.

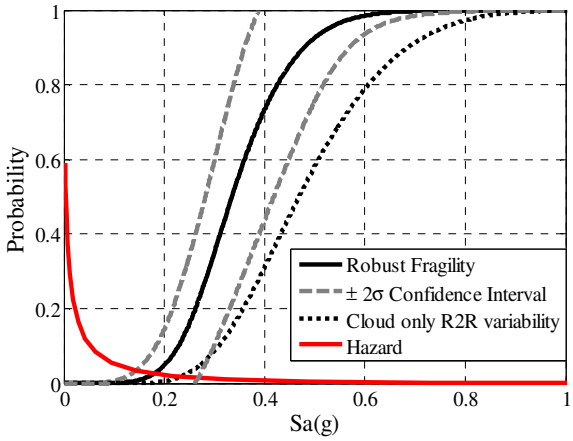

Figure 5.4: Robust Fragility and its plus/minus two standard deviation confidence interval and Cloud-based fragility curve, considering only the R2R variability.

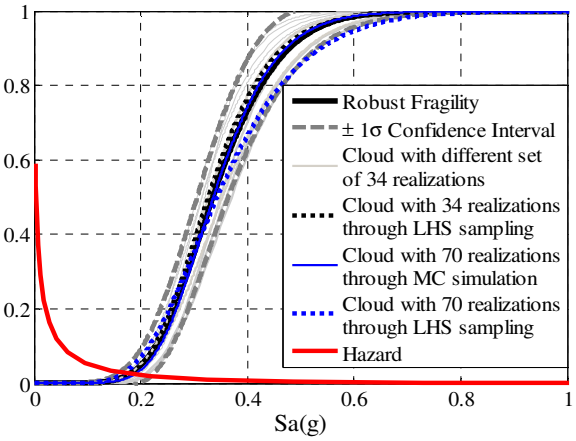

Figure 5.5: Robust Fragility and its plus/minus one standard deviation confidence interval, Cloud-based fragility curves based on 10 different 34 records/MC-based realizations, Cloud-based fragility curves based on 70 records/MC-based realizations, 34 records/LHS-based realizations and 70 records/LHS-based realizations of the uncertainties vector θ.

Figure 5.6 illustrates the comparison between the (cloud-based) Robust Fragility curve and its plus/minus two standard deviations interval, the IDA-based fragility curves obtained using the LHS, with 34 and 80 realizations of the structural model (plotted in blue solid and blue dashed lines, respectively), and

the fragility curve obtained through MVFOSM approach (in black dashed line). As it can be seen from Figure 5.6, the different fragility curves are close in terms of median capacity. The difference between the IDA-based/LHS fragilities and the IDA-based/MVFOSM fragility curves is contained within the plus/minus two standard deviations interval of the Robust Fragility. It can be observed that the Cloud-based Robust Fragility is quite close to the fragility curves obtained through the IDA-based/LHS and IDA-based/MVFOSM approaches, while the computational effort is sensibly lower. As shown in Table 5.5, the Cloud-based Robust Fragility requires number of analyses equal to the number of the records in the chosen set (34 and 70 for the case study). To implement IDA using LHS and MVFOSM, the necessary analyses are in the order of thousands and hundreds, respectively. In particular, for IDA paired up with LHS the number of required analysis is the product of the number of structural realizations, the number of the selected records and the number of steps for IDA procedure. For implementing the IDA paired up with the MVFOSM approach, the number of required analysis is the product of two times the number of the uncertain variables plus one (the base-case value of *f* that corresponds to all random variables being set equal to their mean), the number of the selected records and the number of steps for IDA procedure.

It is important to note that these results refer to the specific case study and additional comparisons are needed to validate these results. Based on the site-specific hazard shown in Figure 5.6, it can be noted that the difference between the Cloud-based Robust Fragility curve and IDA-based/LHS and IDA-based/MVFOSM fragility curves are more accentuated in the zone of very small hazard values. This observation is further validated by risk calculations reported in Table 5.5.

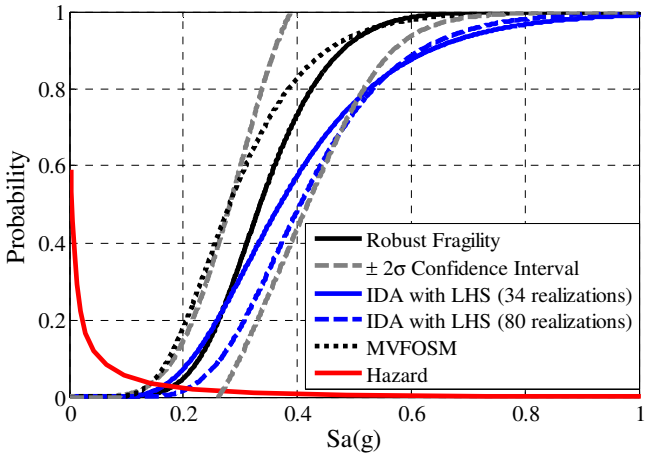

Figure 5.6: Comparison between Cloud-based Robust Fragility curve and its plus/minus two standard deviations intervals, IDA-based fragility curves obtained using LHS sampling with 34 and 80 realizations and IDA-based fragility curve obtained through MVFOSM approach.

Table 5.5 summarizes for all the procedures discussed herein, the number of analyses required and the mean annual frequencies of exceeding the Near-Collapse limit state (i.e., risk obtained by integrating the fragility and site-specific hazard curve) denoted by λ_{LS} corresponding to the different fragility curves.

In particular, R_F denotes the risk corresponding to the Robust fragility curve and $R_{F\pm 2\sigma\chi}$ define the risk values associated with Robust Fragility plus/minus its two standard deviation confidence intervals.

It can be noted that Cloud-based Robust Fragility curves (with 34 or 70 realizations through standard MC simulation or LHS sampling) with their plus/minus two standard deviation confidence bands provide reliable results in term of risk with respect to IDA-based LHS and MVFOSM approach fragility curves.

Table 5.5: Number of analyses required and the mean annual frequency of exceeding the limit state for the alternative procedures.

Type of procedure	*Number of analyses*	λ_{LS} using the Robust Fragility		
		$R_{F+2\sigma\chi}$	R_F	$R_{F-2\sigma\chi}$
RF with 34 realizations through MC sim	34	7.4×10^{-3}	1.1×10^{-2}	1.5×10^{-2}
RF with 34 realizations through LHS	34	7.8×10^{-3}	1.0×10^{-2}	1.4×10^{-2}
RF with 70 realizations through MC sim	70	7.9×10^{-3}	1.0×10^{-2}	1.2×10^{-2}
RF with 70 realizations through LHS	70	7.7×10^{-3}	1.0×10^{-2}	1.4×10^{-2}
MVFOSM approach	7820	-	1.5×10^{-2}	-
IDA with LHS (34 realizations)	11560	-	1.0×10^{-2}	-
IDA with LHS (80 realizations)	27200	-	9.0×10^{-3}	-

5.4 CONCLUSIONS

In this chapter, the modified version of Cloud Analysis, that considers the (eventual) cases of global dynamic instability, based on coupling the simple regression in the logarithmic space of structural response versus seismic intensity for a suite of registered records with logistic regression, is implemented to propagate both record-to-record variability and the structural modeling uncertainties. For each of the registered records within the suite of ground motion records, a different realization of the structural model is generated through a standard Monte Carlo Simulation procedure. The Bayesian version of the Cloud method is employed, in which the uncertainty in the structural fragility model parameters is considered. This leads to a Robust Fragility estimate and a desired confidence interval defined around it. The longitudinal frame of the Van Nuys Holiday Inn hotel building, modeled with the consideration of the flexural-shear-axial interaction, is employed to demonstrate this procedure. The selection of the suite of ground motion records for the case study has been based on a set of criteria that ensure the statistical significance of the linear regression in predicting the structural response as a function of the intensity measure.

It is observed that, for the case study frame, Cloud-based Robust Fragility curve with the consideration of both record-to-record variability and structural modelling uncertainties leads to a reduction both in median and in the dispersion of the fragility curve with respect to the Cloud-based fragility considering only R2R variability. Moreover, the Cloud-based Robust Fragility curve is very close

to the results provided by IDA-based LHS and MVFOSM fragility curves, while the computational effort is sensibly lower. These observations refer to the specific case study and additional comparisons needed to validate these results. Based on the site-specific hazard, it can be noted that the difference between the Cloud-based Robust Fragility curve and the IDA based fragility curves obtained using the LHS and the MVFOSM approach are more accentuated in the zone of very small hazard values. Thus, it can be noted that Cloud-based Robust Fragility curves (with 34 or 70 realizations through standard MC simulation or LHS sampling) with their plus/minus two standard deviation confidence bands provide reliable results in term of risk with respect to IDA-based LHS and MVFOSM fragility curves. Consequently, and with specific reference to the case-study frame, the Cloud-based Robust Fragility procedures provides --in an extremely efficient manner-- reliable risk estimates.

5.5 REFERENCES

[1] Cornell, C.A., and Krawinkler, H., 2000. Progress and challenges in seismic performance assessment. PEER Center News; 3 (2): 1-2

[2] Miano, A., Jalayer, F., and Prota, A., 2017. Considering Structural Modeling Uncertainties using Bayesian Cloud Analysis. In: Proceedings of the 6th ECCOMAS Thematic Conference on Computational Methods in Structural Dynamics and Earthquake Engineering (COMPDYN 2017), Rhodes, Greece, 15-17 June 2017.

[3] Vamvatsikos, D., and Cornell, C.A., 2002. Incremental dynamic analysis. Earthquake Engineering and Structural Dynamics; 31 (3): 491-514.

[4] Bazzurro, P., Cornell, C.A., Shome, N. and Carballo, J.E., 1998. Three proposals for characterizing MDOF nonlinear seismic response. Journal of Structural Engineering (ASCE); 124 (11): 1281-1289.

[5] Jalayer, F., and Cornell, C.A., 2009. Alternative non-linear demand estimation methods for probability-based seismic assessments. Earthquake Engineering & Structural Dynamics 38(8): 951-972.

[6] Baker, J.W., 2007. Probabilistic structural response assessment using vector-valued intensity measures. Earthquake Engineering & Structural Dynamics, 36(13), 1861-1883.

[7] Shome, N., Cornell, C.A., Bazzurro, P., and Carballo, J.E., 1998. Earthquakes, records, and nonlinear responses. Earthquake Spectra, 14(3), 469-500.

[8] Jalayer, F., 2003. Direct Probabilistic seismic analysis: implementing non-linear dynamic assessments. Ph.D. dissertation, Stanford University, California.

[9] Jalayer, F., De Risi, R., and Manfredi, G., 2015. Bayesian Cloud Analysis: efficient structural fragility assessment using linear regression. Bulletin of Earthquake Engineering, 13(4), 1183-1203.

[10] Jalayer, F., Ebrahimian, H., Miano, A., Manfredi, G. and Sezen, H., 2017. Analytical fragility assessment using un-scaled ground motion records. Earthquake Engineering & Structural Dynamics; https://doi.org/10.1002/eqe.2922.

[11] Cornell, C.A., Jalayer, F., Hamburger, R.O., and Foutch, D.A., 2002. Probabilistic basis for 2000 SAC federal emergency management agency steel moment frame guidelines. Journal of Structural Engineering, 128(4), 526-533.

[12] Jalayer, F., Franchin, P., and Pinto, P.E., 2007. A scalar damage measure for seismic reliability analysis of RC frames. Earthquake Engineering and Structural Dynamics; 36 (13): 2059–2079.

[13] Jalayer, F., Elefante, L., Iervolino, I., and Manfredi, G., 2011. Knowledge-based performance assessment of existing RC buildings. Journal of Earthquake Engineering; 15 (3): 362-389.

[14] Hickman, J.W., 1983. PRA procedures guide: a guide to the performance of probabilistic risk assessments for nuclear power plants. NUREG/CR-2300, U.S. Nuclear Regulatory Commission, Washington, DC.

[15] Kennedy, R.P., and Ravindra, M.K., 1984. Seismic fragilities for nuclear power plant risk studies. Nuclear Engineering and Design, 79(1), 47-68.

[16] Reed, J.W., and Kennedy, R.P., 1994. Methodology for developing seismic fragilities. Final Report TR-103959, EPRI.

[17] Ellingwood, B.R., Celik, O.C., and Kinali, K., 2007. Fragility assessment of building structural systems in Mid - America. Earthquake Engineering and Structural Dynamics 2007; 36 (13): 1935-1952.

[18] Celik, O.C., and Ellingwood, B.R., 2010. Seismic fragilities for non-ductile reinforced concrete frames–Role of aleatoric and epistemic uncertainties. Structural Safety 32(1): 1-12.

[19] Jalayer, F., Iervolino, I., and Manfredi, G., 2010. Structural modeling uncertainties and their influence on seismic assessment of existing RC structures. Structural Safety; 32 (3): 220-228.

[20] Franchin, P., Pinto, P.E., and Rajeev, P., 2010. Confidence factor?. Journal of Earthquake Engineering, 14(7), 989-1007.

[21] Melchers, R.E. (1987). Structural reliability. Horwood.

[22] Schotanus, M.I.J., Franchin, P., Lupoi, A., and Pinto, P.E., 2004. Seismic fragility analysis of 3D structures. Structural Safety, 26(4), 421-441.

[23] Dolsek, M., 2009. Incremental dynamic analysis with consideration of modeling uncertainties. Earthquake Engineering & Structural Dynamics, 38(6), 805-825.

[24] Vamvatsikos, D., and Fragiadakis, M., 2010. Incremental dynamic analysis for estimating seismic performance sensitivity and uncertainty. Earthquake Engineering and Structural Dynamics, 39(2), 141-163.

[25] Celarec, D., and Dolšek, M., 2013. The impact of modelling uncertainties on the seismic performance assessment of reinforced concrete frame buildings. Engineering Structures, 52, 340-354.

[26] Liel, A.B., Haselton, C.B., Deierlein, G.G., and Baker, J.W., 2009. Incorporating modeling uncertainties in the assessment of seismic collapse risk of buildings. Structural Safety, 31(2), 197-211.

[27] Ditlevsen, O., and Madsen, H.O., 1996. Structural reliability methods. Wiley: New York.

[28] Eurocode 8, 2007. Design of structures for earthquake resistance.

[29] Galanis, P.H., and Moehle, J.P., 2015. Development of Collapse Indicators for Risk Assessment of Older-Type Reinforced Concrete Buildings. Earthquake Spectra, 31(4), 1991-2006.

[30] Shome, N., and Cornell, C.A., 1999. Probabilistic seismic demand analysis of nonlinear structures. Report No. RMS35, Stanford University, CA.

[31] Jalayer, F., and Ebrahimian, H., 2016. Seismic risk assessment considering cumulative damage due to aftershocks. Earthquake Engineering & Structural Dynamics.

[32] Sezen, H., and Moehle, J.P., 2004. Shear strength model for lightly reinforced concrete columns. Journal of Structural Engineering, 130(11), 1692-1703.

[33] Elwood, K., and Moehle, J. P., 2003. Shake table tests and analytical studies on the gravity load collapse of reinforced concrete frames (No. 1). Pacific Earthquake Engineering Research Center.

[34] Krawinkler, H., 2005. Van Nuys hotel building testbed report: exercising seismic performance assessment, Technical Report PEER 2005/11, Berkeley, USA.

[35] Helton, J.C., and Davis, F.J., 2003. Latin hypercube sampling and the propagation of uncertainty in analyses of complex systems. Reliability Engineering & System Safety, 81(1), 23-69.

[36] McKay, M.D., Conover, W.J., and Beckman, R., 1979. A comparison of three methods for selecting values of input variables in the analysis of output from a computer code. Technometrics; 21(2):239–245.

[37] Novák, D., Vořechovský, M., and Teplý, B., 2014. FReET: Software for the statistical and reliability analysis of engineering problems and FReET-D: Degradation module. Advances in Engineering Software, 72, 179-192.

[38] Baker, J.W., and Cornell, C.A., 2008. Uncertainty propagation in probabilistic seismic loss estimation. Structural Safety, 30(3), 236-252.

[39] Menum, C., 2000. CE 204: Notes of Structural Reliability. Stanford University, California.

Chapter 6

PERFORMANCE BASED ASSESSMENT METHODOLOGY FOR RETROFIT OF BUILDINGS

6.1 INTRODUCTION

The earthquakes that hit different seismic regions around the world have shown the vulnerability of existing nonductile reinforced concrete (RC) frame buildings, as previously discussed. These nonductile concrete frame structures are much more susceptible to collapse than modern code-conforming frames [1-2]. Since such buildings comprise large percentage of existing building stock, efficient assessment methods are needed to compare different retrofit methods and to predict the collapse risk of existing structures in seismic regions [3-4]. Many conventional retrofit methods, such as concrete or steel jacketing of the columns, addition of shear walls and new methods often based on new materials, such as fiber reinforced polymers (FRP), have been proposed [5-6]. These methods can be applied considering the desired performance level, requirements of new seismic codes reduction in probability of collapse, optimization of cost and/or minimization of losses.

As discussed in the precedent chapters, performance-based assessment paradigm has been a persistent research theme over the past decade within the earthquake engineering community in order to develop seismic fragilities [7-9] and earthquake loss estimation [10-12]. Performance based design philosophy allows engineers to assess a specific structural performance level for a given earthquake hazard level at a local site. Nonlinear dynamic analysis procedures can be used to perform probabilistic seismic assessment, using recorded ground motions. These procedures can be used to estimate parameters required for specific probabilistic assessment criteria, such as Demand and Capacity Factored

Design (DCFD, see [13-14]), and also to make direct probabilistic performance assessment using numerical methods [13, 15-18]. In particular, herein, Cloud Analysis [19-20], discussed in the previous chapters, is chosen as nonlinear dynamic analysis procedure. In addition, as described in [21] and in the previous chapters, the critical demand to capacity ratio (*DCR*) is adopted as the structural response parameter. The structural response parameter or *DCR*, that is equal to unity at the onset of a specific performance level, can be caused by different potential failure mechanisms (both brittle and ductile). Moreover, following the methods in ASCE 41-13 [22], three different performance levels are considered in this work, i.e., immediate occupancy, life safety and collapse prevention performance levels.

In this chapter, the north longitudinal frame of the seven stories hotel building in Van Nuys, California, presented in Chapter 1.6, is modeled as a case study, including the effect of flexural-shear-axial load interaction to be able to capture column shear and axial failures, as described in Chapter 2. The RC frame building suffered significant damage during the 1994 Northridge earthquake. Detailed seismic evaluations performed by [23-24] confirmed structural vulnerability of the nonductile moment frame resisting system of the building. Krawinkler [25] also performed a detailed performance based assessment of the building and compared the effectiveness of different retrofit options.

The goal of the work presented in this chapter is to propose a nonlinear performance-based methodology to evaluate different retrofit methods considering hazard level, target performance levels, and also life cycle cost estimates [26-28]. The methodology is illustrated using three retrofit strategies for the analysed frame, used to improve the seismic performance of the frame [26-27]. In particular, strictly speaking, performance-based retrofit design should lead to the optimal retrofit strategy by comparing the expected loss during the service life of the structure for each viable retrofit option, based on risk-related safety-checking criteria. In summary, the performance-based procedure implemented in this paper identifies the most economic retrofit solution that satisfies structural safety requirements for a given performance level. However, the novelty of the proposed research is not in the evaluation of the specific retrofit solutions for the case study, but in the critical process proposed to evaluate the effectiveness of different retrofit methods using a performance based approach.

The process has been developed with reference only to the record to record variability, while at the end of the chapter a brief insight about the consideration of the structural modeling uncertainties in the definition of the structural performance is proposed with reference to the transverse frame of the case study building.

6.2 METHODOLOGY

6.2.1 THE STRUCTURAL PERFORMANCE VARIABLE

The critical demand to capacity ratio for a prescribed limit state [21], denoted as DCR_{LS}, has been adopted as a proxy for the structural performance variable. DCR_{LS} is defined as the demand to capacity ratio for the component or mechanism that brings the system closer to the onset of limit state *LS*. The formulation refers to Equation 3.1 and is based on the cut-set concept [29], which is suitable for cases where various potential failure mechanisms (both ductile and fragile) can be defined a priori. DCR_{LS} is always equal to unity at the onset of limit state and is always the maximum demand over capacity ratio among all the structural members. The demand is the same between the different limit states, while the capacity changes for each limit state. In this chapter, based on the goal to retrofit the American case study building, following the American codes approach (see ASCE 41-13, [22]) and differently from the previous chapters, the capacity values refer to specific Performance Levels (PLs) identified in the codes [22]. Obviously, the meaning of *DCR* is the same using limit states or performance levels; so coherently with the ASCE 41-2013 [22] approach, the critical DCR_{LS} is going to be called DCR_{PL}. The performance levels chosen in this work are the Immediate Occupancy PL, Life Safety PL and Collapse Prevention PL, but, as previously discussed, the procedure can be used for any other prescribed performance levels/limit states. As suggested in Table C2.1 of ASCE 41-13 [22], the three considered performance levels are related to the achievement of the following objectives: a) yielding of the columns correspond to *Immediate Occupancy* performance level corresponding to hazard level identified with return period T_R=72 years; b) the ductile or brittle failures of the columns correspond to *Life Safety* performance level corresponding to hazard level identified with return

period T_R=225 years; and c) the collapse of the columns correspond to *Collapse Prevention* performance level corresponding to hazard level identified with return period T_R=975 years. Based on these considerations, the DCR_{PL} are defined as follows:

Immediate Occupancy Performance Level: D is the demand expressed in terms of maximum chord rotation for the component, denoted as $\theta_{D,\max}$, and computed from nonlinear dynamic analysis. *C* is the component chord rotation capacity, denoted as $\theta_{C,\text{yielding}}$, and identified as the deformation capacity corresponding to the point in the force-deformation curve of the member (considering the nonlinear deformations associated with flexure, shear and bar-slip) in which the longitudinal steel rebar in the member starts to yield in tension.

Life Safety Performance Level: D is the demand expressed in terms of maximum chord rotation for the component, denoted as $\theta_{D,\max}$, and computed from nonlinear dynamic analysis. *C* is the component chord rotation capacity, denoted as $\theta_{C,\text{ultimate}}$, and identified as deformation capacity corresponding to the point in the force-deformation curve of the member, where a 20% reduction in the maximum strength takes place.

Collapse Prevention Performance Level: D is the demand expressed in terms of maximum chord rotation for the component, denoted as $\theta_{D,\max}$, and computed from nonlinear dynamic analysis. *C* is the component chord rotation capacity, denoted as $\theta_{C,\text{axial}}$, and identified as the deformation capacity corresponding to the point in the force-deformation curve of the member associated with the complete loss of vertical-load carrying capacity (to account for the loss of load bearing capacity).

6.2.2 CLOUD ANALYSIS CONSIDERING COLLAPSE AND/OR GLOBAL DYNAMIC INSTABILITY

As mentioned before, this work exploits the non-linear dynamic analysis as a tool for design and selection of the optimal retrofit strategy and technique. In particular, the structural fragility is calculated based on the critical demand to capacity ratios DCR_{PL} for a suite of un-scaled ground motion records for the above-mentioned three performance objectives (a.k.a., the *Cloud Analysis,* see Chapter 3.2 for all the details). For a suite of ground motions, the cloud data

encompasses pairs of ground motion intensity measure (IM) and its corresponding structural performance variable DCR_{PL} (see Equation 3.2). Herein, IM is adopted as the spectral acceleration at the first-mode period, $S_a(T_1)$. Cloud Analysis can still be carried out in the cases in which some records take the structure to verge upon "Collapse", as presented in details in Chapter 3.2.4. Here, as presented also in precedent chapters, the criteria established by Galanis and Moehle [30] for defining global structural collapse is adopted, where the structural collapse occurs when one of the two following conditions has reached: 1) 50% +1 of the columns in only one story reach θ_{axial}; and 2) the maximum lateral interstory drift exceeds 10%. Therefore, the cloud data is divided into two parts: a) *NoC* data which correspond to that portion of the suite of records for which the structure does not experience global "*Collapse*", and b) *C* data for which the structure will experience "Collapse". The fragility, presented in details in Chapter 3.2.4 and defined as the probability of exceeding the limit state PL given IM, more conveniently expressed as the probability that DCR_{PL} exceeds unity given IM, can be expanded with respect to *NoC* and *C* portions of Cloud data using total probability theorem [18, 20, 31], following Equation 3.4.

6.2.3 PERFORMANCE-BASED SAFETY-CHECKING FRAMEWORK

As described in [14], a framework for probability-based demand and capacity factor design (*DCFD*) seismic safety evaluation is implemented in order to verify the structural safety at each performance level. The *DCFD* format is based on a closed-form analytical expression for the mean annual frequency of exceeding a structural performance level. The threshold for each performance level is identified by a critical demand to capacity ratio DCR_{PL} calculated for the prescribed performance level (e.g., immediate occupancy, life safety or collapse prevention) and set equal to unity. According to *DCFD*, the structure in question satisfies the safety requirements for a prescribed performance level *PL* if the seismic demand corresponding to an acceptable probability/risk level is less than or equal to the seismic capacity for that *PL*. Herein, an intensity-based version of this format is adopted where the safety criteria is expressed in term of the seismic intensity measure (see [14-32]):

$$S_a(P_o) \leq S_a^{PL} \tag{6.1}$$

where $S_a(P_o)$ or the IM-based *factored demand* (denoted generically later as D_{PL}, where *PL=IO, LS, CP*) is the spectral acceleration value corresponding to the acceptable probability level P_o, based on the site-specific mean hazard curve for the fundamental period of the selected building. The hazard curve is approximated by a power-law type of expression in the region of spectral acceleration values of interest:

$$S_a(P_o) = \lambda^{-1}{}_{S_a}(P_o) \;\; ; \;\; \lambda_{S_a}(S_a) \approx k_o \cdot S_a^{-k} \tag{6.1}$$

where k_o and k are the fit parameters with k that is the slope of this approximate curve. S_a^{PL} (denoted as C_{PL}, where *PL=IO, LS, CP*) is the IM-based *factored capacity* and is calculated as:

$$S_a^{PL} = \eta(S_a^{DCR_{PL}=1}) \cdot \exp\left(-\frac{k}{2}\beta(S_a^{DCR_{PL}=1})^2\right) \tag{6.2}$$

where $S_a^{DCRPL=1}$ is the spectral acceleration at the onset of performance level *PL* (i.e., DCR_{PL}=1); $\eta(S_a^{DCRPL=1})$ and $\beta(S_a^{DCRPL=1})$ are the median and logarithmic standard deviation of the fragility curve for performance level PL. The fragility is defined as P($DCR_{PL} > 1 | S_a$) or equivalently in IM-based terms as P($S_a^{DCRPL=1} \leq S_a$) is assumed to be a lognormal cumulative distribution function (CDF) with median $\eta(S_a^{DCRPL=1})$ and logarithmic standard deviation $\beta(S_a^{DCRPL=1})$ estimated as:

$$\eta(S_a^{DCR_{PL}=1}) = S_a^{50th} \;\; ; \;\; \beta(S_a^{DCR_{PL}=1}) = \frac{1}{2}\ln\frac{S_a^{84th}}{S_a^{16th}} \tag{6.3}$$

where S_a^{16th}, S_a^{50th}, S_a^{84th} are the values of S_a corresponding to probability values equal to 0.16, 0.50 and 0.84, respectively. So, the capacity factor, $\exp(k\beta^2(S_a^{DCRPL=1})/2)$, is a reduction factor that considers the record-to-record variability in the structural performance capacity (in IM-based terms). In other words, the factored capacity is always less than or equal to the median capacity.

6.3 CASE STUDY RESULTS FOR THE LONGITUDINAL FRAME

The reinforced concrete (RC) moment-resisting frame, considered herein as case study, is the north longitudinal perimeter frame of the seven-story Holiday Inn hotel building in Van Nuys, California (presented in Chapter 1.6). All the

details about the modelling issues have been presented in details in Chapter 2 (see also [33-34]). All the details about the failure mechanisms of all the columns of the frame are presented in Table 2.1.

6.3.1 MODELS FOR RETROFITTED FRAMES

The main goal of the retrofit design is to prevent premature failure of brittle elements and to increase their ductility and strength. In addition, the lateral displacements need to be as uniform as possible over the height of the structure to avoid concentration of inelastic deformations in a single story to prevent soft story mechanism. To control lateral drift by keeping them below the target displacement, one of the effective strategies for moment frame concrete structures is to add lateral stiffness, e.g., by adding a shear wall, to reduce the period and decrease the resulting building displacements. Another effective way to increase overall ductility and strength of the frame is to increase flexural and shear strength and deformation capacity of individual lateral load resistant members. This can be achieved by better confining the columns and shifting the failure mode from brittle shear to ductile flexural mode, e.g., by enlarging the cross section of concrete jacketing. In some cases, to avoid the restriction of use of building for a long time, addition of new lateral load resistance system or member replacement may be difficult or impossible to implement. In these cases, the ease and quick application of fiber reinforced polymers (FRP) can be very useful. In general, there are many practical retrofit options [5-6].

However, in this work three common strategies are considered to show the effectiveness of different retrofit options, while stressing the critical process of performance based assessment: 1) RC jacketing of the columns, 2) addition of new shear walls into the frame, and 3) FRP wrapping of the columns. A target drift capacity is herein adopted as retrofit design criterion. This criterion is very helpful in terms of feeding an intelligent first guess into the procedure. Such a first guess is assessed based on performance-based criteria [22, 35-36]. Anyway, the performance-based procedure implemented in this paper identifies the most economic retrofit solution that satisfies structural requirements for a given performance level.

6.3.1.1 REINFORCED CONCRETE JACKETING

The first retrofit option considered is the reinforced concrete jacketing of the columns in the longitudinal frame of the Holiday Inn hotel building. Three different schemes of RC jacketing of the columns are selected, based on the consideration that the retrofit of a building should be seen as an iterative process: a) all columns of the frame are RC jacketed; b) all columns of the first four floors of the frame are RC jacketed; c) all columns of the first five floors of the frame are RC jacketed.

Figure 6.1 (a) shows the retrofitted cross section of a middle column in the fourth story. The longitudinal reinforcement in the RC jacket is supposed to be continuous through the floor system. The size of all retrofitted columns increased from 356 mm x 508 mm to 508 mm by 660 mm with a jacket thickness of 76 mm. Column concrete used for jacketing has nominal strength f'_c of 34.5 MPa in the first and second stories, and 27.6 MPa from the third story to the seventh. Steel rebar in all jackets has a yield strength of 414 MPa (Grade 60). Column jackets include ten 28.7 mm diameter (No.9) bars between ground and second floors; eight No.9 bars between second and fourth floors; ten No.7 bars between fourth and fifth floors; and eight No.7 bars between fifth and seventh floors. The ties are No.4 bars spaced at 305 mm on center between ground and third floors, and No.3 bars spaced at 305 mm on centre above the third floor. The retrofit design and reinforcement details meet the seismic provisions of ACI 318-14 [37]. Original reinforcement in existing columns is neglected in the analysis since the response of all jacketed columns is governed by flexure. Table 6.1 shows the change in failure modes for the four lower stories before and after the retrofit (coherently with scheme b) because in the bare frame the main failure mechanisms happen in the lower stories, although also the superior columns are retrofitted in the other two schemes. The first period of the frame shifted from 1.17 seconds for the bare frame to 0.93, 0.97 and 0.95 seconds for schemes a, b, and c, respectively.

6.3.1.2 SHEAR WALL

The second retrofit method involved is the addition of a new shear wall into the frame. The wall is centred on the frame and is doweled into the existing columns and beams. Figure 6.1 (b) shows the shear wall cross section in the fourth floor. The boundary elements of the wall over the height of the entire frame are designed to be the retrofitted existing columns. After the RC jacketing, all

boundary elements are 508 mm wide by 660 mm deep, i.e., oriented to bend in their weak direction when resisting lateral forces in the plane of the frame. Column concrete used for jacketing has nominal strength f'_c of 34.5 MPa in the first and second stories, and 27.6 MPa from the third story to roof. Grade 60 column reinforcing steel is used for jacketing (f_y=414 MPa). The shear wall outside boundary elements has a constant thickness of 200 mm. The horizontal and vertical reinforcement ratios are determined following the minimum requirements in ACI 318-14 [37]. The fundamental period of the retrofitted frame is 0.46 sec.

6.3.1.3 FRP WRAPPING

In the third retrofit application, the nonductile concrete columns of the frame are wrapped with carbon fiber reinforced polymer composite (CFRP) as shown in Figure 6.1 (c). The columns are wrapped following four schemes: a) all columns are wrapped with only one layer of uni-axial transverse CFRP; b) all columns of the first four floors are FRP wrapped; c) all columns of the first five floors of the frame are FRP wrapped; d) all columns are FRP wrapped, but for the central columns in the first floor two FRP layers are used.

The single layer of uni-axial transverse CFRP has a thickness of 0.164 mm, based on the recommendation of a producer in Europe. The calculation of the shear strength and ductility increase are calculated using the Eurocode 8 [38] and Italian Guidelines [39]. The first period of the FRP retrofitted frames is about 1.13 sec for all the schemes. The FRP retrofitted models do not include fracture or debonding of the fiber wrap since these failure modes are assumed to be prevented during design procedures. Table 6.1 shows, for schemes a, b and c, that FRP wrapping can shift the brittle failure modes to more ductile flexure failures.

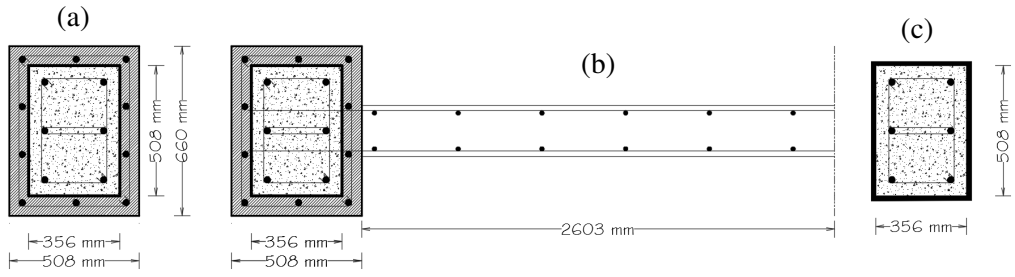

Figure 6.1: Retrofit options considered: (a) RC jacketing of columns, (b) shear wall addition and (c) FRP wrapping of columns

Table 6.1: Comparison of the shear strength V_n, yield strength V_y and flexural strength V_p for the bare frame and category (*Cat.*) classification before and after retrofit for the columns in the first four stories.

Column	Bare frame						Retrofitted frame			
	V_y (kN)	V_n (kN)	V_p (kN)	V_p/V_n	V_y/V_n	Cat.	RC jacketing V_p/V_n	Cat.	FRP wrapping V_p/V_n	Cat.
1, 9	201	233	210	0.90	0.86	IV	0.66	V	0.63	V
2, 8	212	245	244	1.00	0.87	III	0.66	V	0.73	IV
3 to 7	212	245	244	1.00	0.87	III	0.66	V	0.73	IV
10, 18	158	189	176	0.93	0.84	IV	0.82	IV	0.63	V
11, 17	295	279	325	1.16	1.06	I	0.79	IV	0.88	IV
12 to 16	248	281	266	0.95	0.88	IV	0.79	IV	0.72	IV
19, 27	143	171	162	0.95	0.84	IV	0.86	IV	0.64	V
20, 26	268	260	309	1.19	1.03	I	0.83	IV	0.92	IV
21 to 25	224	260	249	0.96	0.86	IV	0.83	IV	0.74	IV
28, 36	138	164	154	0.94	0.84	IV	0.77	IV	0.63	V
29, 35	163	175	168	0.96	0.93	III	0.76	IV	0.66	V
30 to 34	163	176	168	0.96	0.93	III	0.76	IV	0.66	V

6.3.2 PUSHOVER RESULTS

Nonlinear static or pushover analysis of the frame is performed to determine its overall frame stiffness, strength and damage progression under increasing lateral forces. In this research, lateral load is applied using an inverse triangular load distribution using a force base approach in OpenSees [40]. The response in terms of lateral loads (e.g., base shear) and maximum interstory drift is monitored. In Figure 6.2, the static pushover results are presented for the bare frame and for all the retrofitted frame models. The events of the first column yielding, attainment of the first column ultimate capacity and the axial failure of the first column are shown in Figure 6.2 for each model. As explained above, the failure mechanisms of first yielding, first ultimate capacity and first axial failure can be defined to correspond, respectively, to immediate occupancy, life safety and collapse prevention performance levels, as described in ASCE 41-13 [22]. According to FEMA 356-97 [41], these three performance levels are identified by the lateral drift thresholds of 1%, 2% and 4%.

Figure 6.2 shows that, in particular for the bare frame, these limits at first yielding, first ultimate capacity and first axial failure, match relatively well with the pushover results.

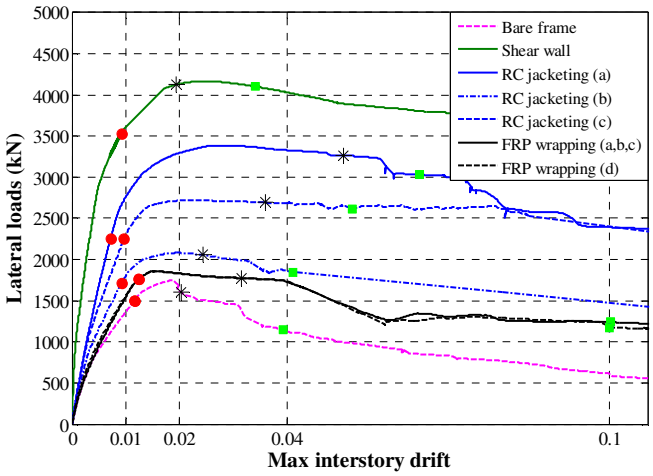

Figure 6.2: Pushover curves for bare frame and retrofitted frames (circles show the first member yielding, stars show the first ultimate capacity achievement and squares show the first axial failure in the frame).

Table 6.2 shows the calculated yield strength, V_y; maximum strength, V_{max}; ultimate strength, V_u; axial strength, V_a and global ductility for each of the frame model. Ductility, μ, is calculated as the ratio of maximum interstory drift of the frame at the collapse level and maximum interstory drift at the first member yielding.

Table 6.3 compares strength and ductility at first yielding, first column ultimate capacity and first column axial failure for each model, where μ_u and μ_a are the ductility values at the first ultimate capacity achievement and at the first axial failure in the frame. This allows for direct comparison of structural performance of each of the retrofit strategies.

Moreover, Table 6.3 shows that the addition of shear wall increases the strength most while the largest ductility increase is achieved when columns are jacketed or FRP wrapped.

Table 6.2: Yield strength (V_y), maximum strength (V_{max}), ultimate strength (V_u), axial strength (V_a) and global ductility for each model.

Case	V_y (kN)	V_{max} (kN)	V_u (kN)	V_a (kN)	Ductility μ
Bare frame	1499	1744	1603	1152	3.38
RC jacketing (a)	2252	3385	3265	3033	9.03
RC jacketing (b)	1715	2080	2059	1850	4.55
RC jacketing (c)	2249	2720	2694	2617	5.50
Shear wall	3525	4169	4125	4102	10.75
FRP wrapping (a,b,c)	1759	1863	1776	1240	8.05
FRP wrapping (d)	1759	1863	1776	1175	8.05

Table 6.3: Comparison of response of bare and retrofitted frames in terms of strength and ductility at first yielding, first ultimate capacity achievement and first axial failure in the frame.

Case	First yielding	First ultimate failure		First axial failure	
	Strength $V_y/V_{y\ bare\ frame}$	Strength $V_u/V_{u\ bare\ frame}$	Strength $V_a/V_{a\ bare\ frame}$	Strength $V_a/V_{a\ bare\ frame}$	Strength $V_y/V_{y\ bare\ frame}$
RC jacketing (a)	1.50	2.04	2.63	2.63	1.50
RC jacketing (b)	1.15	1.28	1.61	1.61	1.15
RC jacketing (c)	1.50	1.68	2.27	2.27	1.50
Shear wall	2.35	2.57	3.56	3.56	2.35
FRP wrapping (a,b,c)	1.17	1.11	1.08	1.08	1.17
FRP wrapping (d)	1.17	1.11	1.02	1.02	1.17

6.3.3 CLOUD ANALYSIS

A set of 70 strong ground-motion records are selected from the NGA-West2 database [20, 42] in order to implement Cloud Analysis, as presented in details in Chapter 3.3.1.1. This suite of records covers a wide range of magnitudes between 5.5 and 7.9, and closest distance-to-ruptured area (denoted as R_{RUP}) up to around 40 km, as illustrated by the scatter diagram in Figure 3.1 (a). The spectral acceleration spectra for the selected suite of ground motion records are shown in Figure 3.1 (b). All the other details about the records set (e.g. shear wave velocity, type of fault etc.) are presented in Chapter 3.3.1.1.

Cloud Analysis has been implemented based on this set of records for the case study frame. Cloud Analysis provides estimates of the two statistical parameters of demand given the spectral acceleration, namely the median given spectral acceleration $\eta_{DCRPL|Sa}$ and the constant logarithmic standard deviation given spectral acceleration $\beta_{DCRPL|Sa}$.

The Cloud response is obtained by applying original ground motions to the structure. Once the ground motion records are applied to the structure, the resulting $DCR_{PL}=D/C$ are calculated for each performance level.

Figures 6.3, 6.4, 6.5 and 6.6 show the Cloud Analysis results for the different performance levels for the bare frame and for one scheme of each retrofit option. The gray-colored circles represent the *NoC* data, while the gray colored with red edge squares represent the *C* data (Section 6.2.2).

Figures also illustrate the 16th, 50th and 84th percentiles of the performance variable as a function of *Sa* and calculated from Eq. (6) and report the parameters of the logarithmic linear regression (considering only the *NoC*), namely, *log a*, *b* and standard deviation $\beta_{DCRPL|Sa,\ NoC}=\beta$.

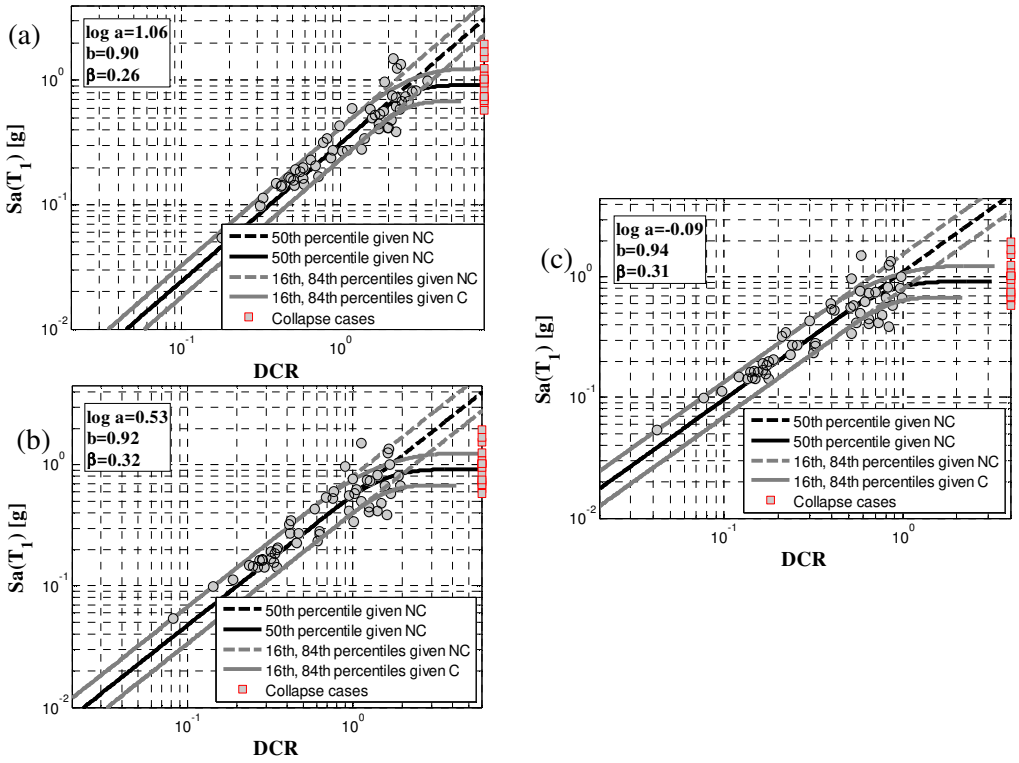

Figure 6.3: Cloud regression for bare frame: a) immediate occupancy *PL*, b) life safety *PL*, and c) collapse prevention *PL*.

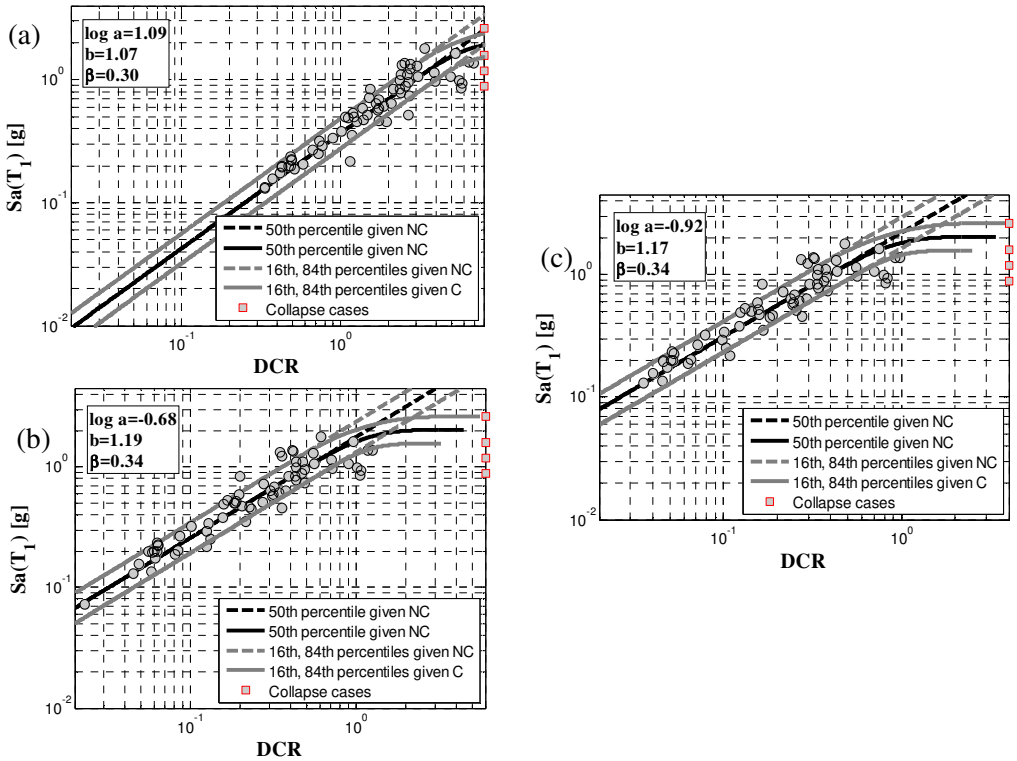

Figure 6.4: Cloud regression for RC jacketing (scheme a): a) immediate occupancy *PL*, b) life safety *PL*, and c) collapse prevention *PL*.

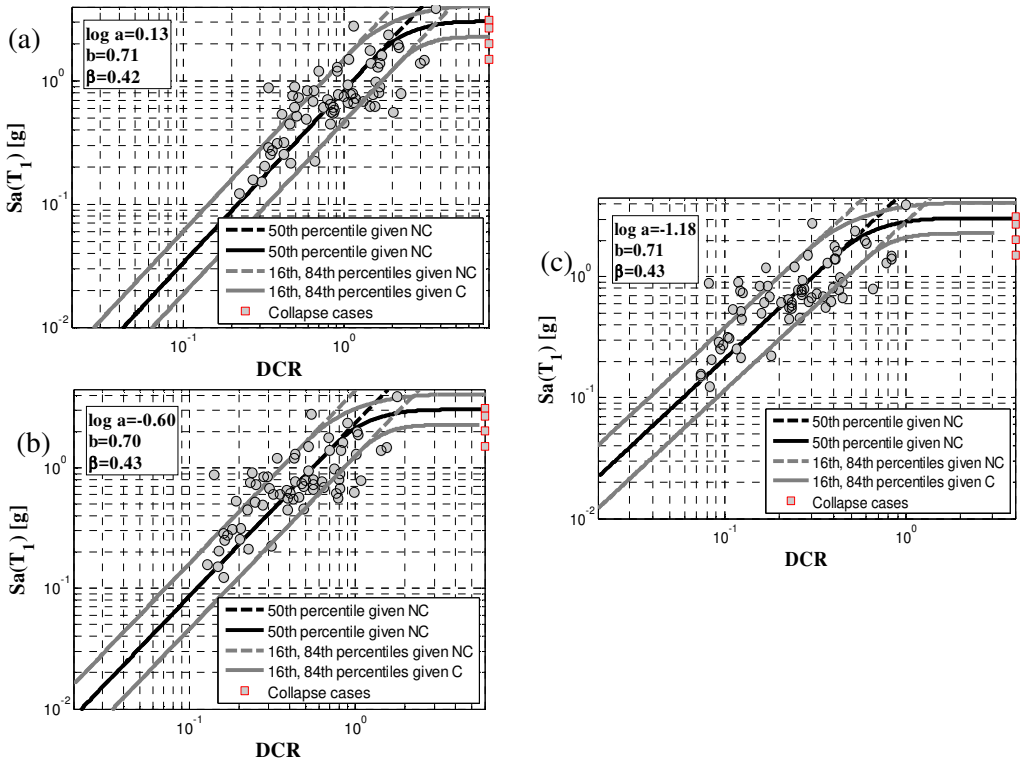

Figure 6.5: Cloud regression for shear wall: a) immediate occupancy *PL*, b) life safety *PL*, and c) collapse prevention *PL*.

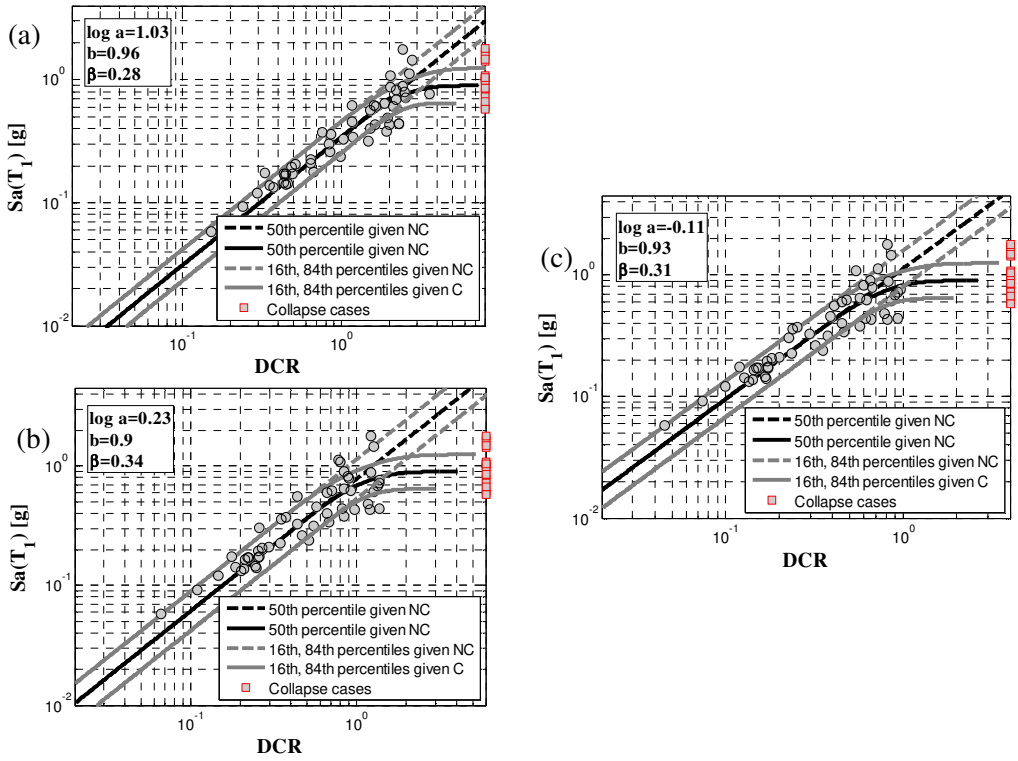

Figure 6.6: Cloud regression for FRP wrapping (scheme a): a) immediate occupancy *PL*, b) life safety *PL*, and c) collapse prevention *PL*.

6.3.4 PERFORMANCE-BASED SAFETY-CHECKING

The framework for probability-based Demand and Capacity Factor Design (*DCFD*) seismic safety evaluation (see Section 6.2.3) is presented here to verify the structural safety at each performance level. Figures 6.7, 6.8 and 6.9 show the mean hazard curve (https://www.usgs.gov), the fragility curves and the calculation of D_{PL} $S_a(P_o)$ and $C_{PL}=S_a^{PL}$. Tables 6.4 and 6.5 show the statistical parameters for fragility curves and the comparison between D_{PL} and C_{PL}, respectively, for each modeling option in each performance level.

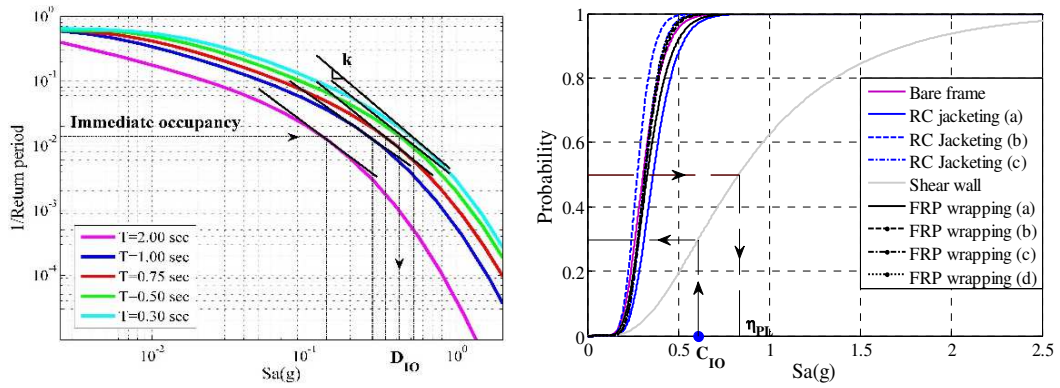

Figure 6.7: Hazard and fragility curves for immediate occupancy performance level (*PL=IO*).

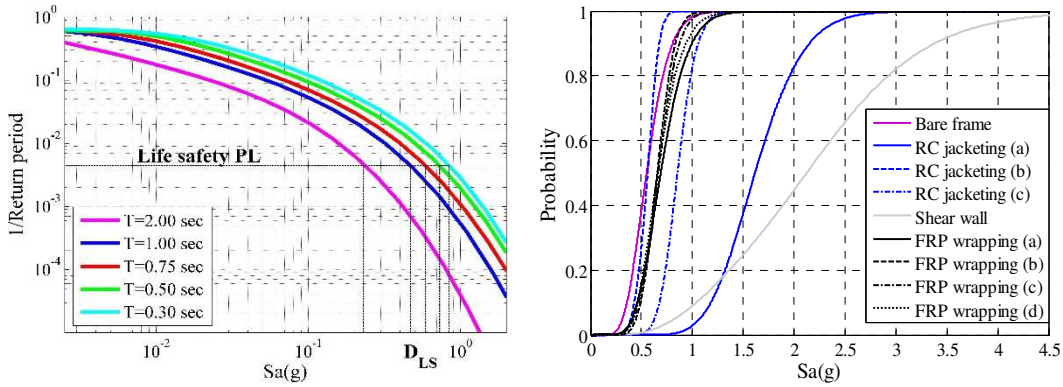

Figure 6.8: Hazard and fragility curves for life safety performance level (*PL=LS*).

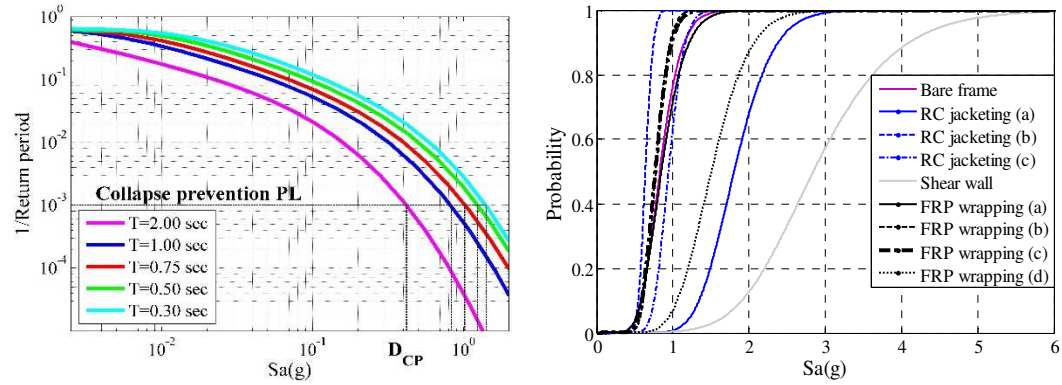

Figure 6.9: Hazard and fragility curves for collapse prevention performance level (*PL=CP*).

Table 6.4: Statistical parameters for fragility curves.

	Immediate occupance PL		Life safety PL		Collapse prevention PL	
Model	η (g)	β	η (g)	β	η (g)	β
Bare frame	0.30	0.29	0.55	0.32	0.82	0.27
RC jacketing (a)	0.37	0.28	1.61	0.23	1.81	0.22
RC jacketing (b)	0.29	0.26	0.56	0.21	0.65	0.20
RC jacketing (c)	0.32	0.22	0.83	0.22	0.95	0.24
Shear wall	0.84	0.57	2.12	0.44	2.84	0.29
FRP wrapping (a)	0.34	0.29	0.68	0.29	0.85	0.27
FRP wrapping (b)	0.32	0.24	0.67	0.20	0.79	0.17
FRP wrapping (c)	0.32	0.24	0.67	0.23	0.78	0.19
FRP wrapping (d)	0.32	0.23	0.66	0.27	1.49	0.27

Table 6.5: Comparison between DPL and CPL for each modelling option in each performance level.

Model	$Sa\ (T_1)$	D_{IO} (g)	C_{IO} (g)	D_{LS} (g)	C_{LS} (g)	D_{CP} (g)	C_{CP} (g)
Bare frame	1.17	0.27	0.27	0.45	0.48	0.78	0.73
RC jacketing (a)	0.93	0.30	0.34	0.51	1.51	0.89	1.68
RC jacketing (b)	0.97	0.28	0.28	0.48	0.53	0.86	0.62
RC jacketing (c)	0.95	0.29	0.31	0.50	0.78	0.87	0.87
Shear wall	0.54	0.44	0.61	0.75	1.65	1.28	2.48
FRP wrapping (a)	1.13	0.27	0.32	0.45	0.62	0.78	0.76
FRP wrapping (b)	1.13	0.27	0.34	0.45	0.65	0.78	0.73
FRP wrapping (c)	1.13	0.27	0.33	0.45	0.63	0.78	0.70
FRP wrapping (d)	1.13	0.27	0.30	0.45	0.61	0.78	1.33

Each retrofit strategy can improve the performance of the existing building differently based on how much it can increase the ductility and strength and avoid the brittle mechanisms. For the immediate occupancy *PL*, the frame with shear wall achieves the biggest factored capacity, that is about four times that of the bare frame, while the other retrofit schemes do not lead to significant increase in capacity. For the life safety and the collapse prevention *PLs,* different schemes belonging to the different retrofit options (shear wall, RC jacketing and FRP wrapping) are able to lead to a factored capacity sensibly higher than the corresponding factored demand. However, the retrofit schemes not able to satisfy the condition that the demand is lower than the capacity for all the performance levels are not used in the comparison in terms of life cycle cost.

6.4 LIFE CYCLE COST ANALYSIS

The expected life cycle cost is an important parameter for measuring the effectiveness and convenience of each retrofit option. In this paper, the expected life cycle cost is estimated from Equation 6.5 [43].

$$\mathbb{E}[C] = C_0 + C_R + C_M \tag{6.4}$$

where C_0 is the initial construction or upgrade installation cost, C_R is the repair cost taking into account also the loss of revenue due to downtime, and C_M is the annual maintenance costs.

The cost for the installation of different retrofit systems, C_0, includes both structural and non-structural component costs [44]. For the FRP retrofit, crack injections, sand blasting, primer, putty, saturant, demolition and reconstruction of partitions and partition paintings are included. For the shear wall retrofit, rebar installation, formwork, concrete casting, foundation strengthening, demolition and reconstruction of partitions and partition paintings are included. The cost for RC jacketing retrofit includes rebar installation, formwork, concrete casting, demolition and reconstruction of partitions and partition paintings. Moreover, for all the retrofit options, also the indirect costs due to the installation of the different retrofit options are included in C_0, based on the retrofit operations time frame reported in [45]. In particular, the down-time costs, which are the costs related to the reduced functionality of the building during the retrofit actions, are calculated as the product of the number of rooms out of service (in this case hotel rooms),the price of the room given the specific location, the average density of the rooms and the time (in days) in which the rooms are out of service.

The repair cost C_R can be calculated from Equation 6.6 [46]:

$$C_R = \sum_{t=0}^{T} \sum_{pl=1}^{N_{PL}} PLC \cdot e^{-\lambda_d t} \left[P\left(PL \mid [t, t+1]\right) - P\left(PL+1 \mid [t, t+1]\right) \right] \tag{6.5}$$

where N_{PL} is the number of prescribed performance levels ordered from serviceability up to collapse, and pl accounts for the performance level under consideration; PLC is the expected cost of restoring the structure from the plth performance level back to its intact state including eventual loss of revenue caused by interruption for repair operations; λ_d is the annual discount rate and $\exp(-\lambda_d t)$ denotes the change in the monetary-based evaluations per time; $P(PL|[t, t+1])$ is

the probability of exceeding the performance level *pl* in time interval [t, t+1]. $P(PL[t, t+1])$ can be calculated based on the assumption of a homogenous Poisson Process:

$$P\left(PL\,|\,[t,t+1]\right)=\lambda_{pl}\exp\left(-\lambda_{pl}t\right) \tag{6.6}$$

where λ_{pl} is the mean annual rate of exceeding the performance level *pl* and can be calculated from the following closed-form expression [14]:

$$\lambda_{pl}=\lambda_{S_a}\left(\eta(S_a{}^{DCR_{PL}=1})\right)\cdot\exp\left(\frac{k^2}{2}\beta(S_a{}^{DCR_{PL}=1})^2\right) \tag{6.7}$$

where $\lambda_{\mathrm{Sa}}(\eta(S_a{}^{DCRPL=1}))$ is the hazard value corresponding to the median spectral acceleration at the onset of *pl*. *PLC* is calculated as:

$$PLC=DTC\cdot e^{-\lambda_{\mathrm{d}}\tau_{pl}}+RC_{pl} \tag{6.8}$$

where *DTC* is the annual cost of downtime; τ_{pl} is the repair time [45] and RC_{pl} is the replacement cost associated with desired *pl*th performance level (herein, pl=1:N_{PL}=3). The cost of maintenance C_M can be estimated as:

$$C_{\mathrm{M}}=\int_0^{t_{life}}C_{\mathrm{m}}e^{-\lambda_{\mathrm{d}}t}dt=\frac{C_{\mathrm{m}}}{\lambda_{\mathrm{d}}}[1-e^{-\lambda_{\mathrm{d}}t_{life}}] \tag{6.9}$$

where C_m (Table 6.7) is the constant annual maintenance cost. Table 6.6 and Table 6.7 outline the values adopted for C_o [12, 44], *DTC* [47], RC_{IO}, RC_{LS}, RC_{CP} [12, 48] and C_m [46].

Figure 6.10 shows the expected life-cycle cost for bare frame and for the alternative retrofit schemes included in the comparison, i.e., the retrofit schemes for which the demand is lower than the capacity for all the performance levels (see Table 6.5).

It can be observed that FRP wrapping (d) is the most convenient option economically-speaking after 20 years, while RC jacketing (a) becomes the most convenient option after 50 years. In this context, the residual life should be established by the user in order to choose the best retrofit scheme. Making the assumption of a residual life greater than 50 years, RC jacketing (a) seems to be the most suitable strategy based on life cycle cost considerations, while if the residual life is fixed to be smaller than 50 years, FRP wrapping (d) becomes the best retrofit scheme.

Table 6.6: Life-cycle cost analysis parameters: the initial construction or upgrade installation cost C_0, the annual cost of downtime DTC and the repair cost for the immediate occupancy performance level RC_{IO}.

Model	C_0 ($\cdot 10^5$, \$)	DTC ($\cdot 10^5$, \$/year)	RC_{IO} (\$/year)
Bare frame	4.80	2.73	$0.1 \cdot RC_{CP}$
RC jacketing (a)	5.58	2.73	$0.1 \cdot RC_{CP}$
RC jacketing (b)	5.36	2.73	$0.1 \cdot RC_{CP}$
Shear wall	6.35	2.73	$0.1 \cdot RC_{CP}$
FRP wrapping (d)	5.13	2.73	$0.1 \cdot RC_{CP}$

Table 6.7: Life-cycle cost analysis parameters: the repair cost for the life safety performance level RC_{LS}, the repair cost for the collapse prevention performance level RC_{CP} and the constant annual maintenance cost C_m.

Model	RC_{LS} (\$/year)	RC_{CP} ($\cdot 10^5$, \$/year)	C_m ($\cdot C_0$, \$/year)
Bare frame	$0.5 \cdot RC_{CP}$	6.25	0.01
RC jacketing (a)	$0.5 \cdot RC_{CP}$	6.25	0.01
RC jacketing (b)	$0.5 \cdot RC_{CP}$	6.25	0.01
Shear wall	$0.5 \cdot RC_{CP}$	6.25	0.01
FRP wrapping (d)	$0.5 \cdot RC_{CP}$	6.25	0.01

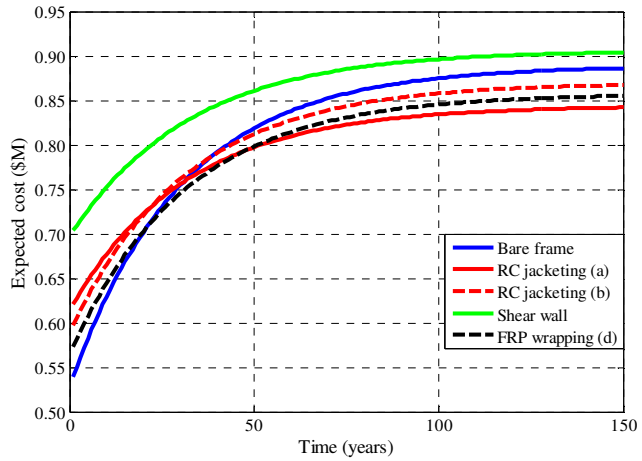

Figure 6.10: The expected life-cycle cost for bare frame and alternative retrofit schemes.

6.5 CASE STUDY RESULTS FOR THE TRANSVERSAL FRAME, CONSIDERING THE STRUCTURAL MODELING UNCERTAINTIES

In this last paragraph of the Chapter 6, a brief application is presented in order to show how the explicit consideration of the structural modelling uncertainties can influence the safety verification of a building. In particular, herein, as described in details for the longitudinal frame, alternative retrofit methods are evaluated for the transverse frame using the methodology previously presented. The objective of this paragraph is not to precisely quantify the effectiveness of the different retrofit strategies, identifying the optimal solution. Instead, the goal is to show how a frame that seems to don't need any retrofit using a standard assessment with the consideration only of the record to record variability, can become vulnerable and can need retrofit operations after the consideration of the structural modelling uncertainties. Therefore, the numerical application herein proposed wants to show how the impact of structural modelling uncertainty on the seismic performance assessment for existing building can be significant, giving more accurate results.

6.5.1 MODELING OF BARE FRAME AND RETROFITTED FRAMES

The east transverse perimeter frame of the seven-story Holiday Inn hotel building in Van Nuys, California (completely presented in Chapter 1.6) is considered as case study. All the details about the modelling issues have been presented in Chapter 2.

Three different retrofit schemes have been considered for this frame [28]. The first scheme is the reinforced concrete jacketing of all columns in the frame. The goal is to prevent shear damage in columns and to achieve flexural yielding and sufficient ductility (Figure 6.1 (a)). The second retrofit method is the addition of a new shear wall into the frame to increase the strength and stiffness and to reduce demand on the unstrengthened columns, limiting the lateral displacement. The wall is centred on the frame and is doweled into the existing columns and beams (Figure 6.1 (b)). In the third retrofit application, the columns of the frame are wrapped with carbon fiber reinforced polymer composite (CFRP) (Figure 6.1 (c))

in order to increase shear strength and to prevent shear failure in columns. The CFRP also improves the deformation capacity, by providing confinement.

6.5.2 CLOUD ANALYSIS, PERFORMANCE-BASED SAFETY-CHECKING AND LIFE CYCLE COST ANALYSIS RESULTS

A set of 70 strong ground-motion records, selected from the NGA-West2 database [20, 42] and presented in Section 6.3.1 and in Chapter 3.3.1., is used in order to implement Cloud Analysis. Figure 6.11 shows as example the Cloud Analysis results for the life safety performance level for each model (bare frame and retrofitted frames) and illustrate the 16th, 50th and 84th percentiles of the performance variable as a function of spectral acceleration. The same procedure has been implemented also for the other two performance levels.

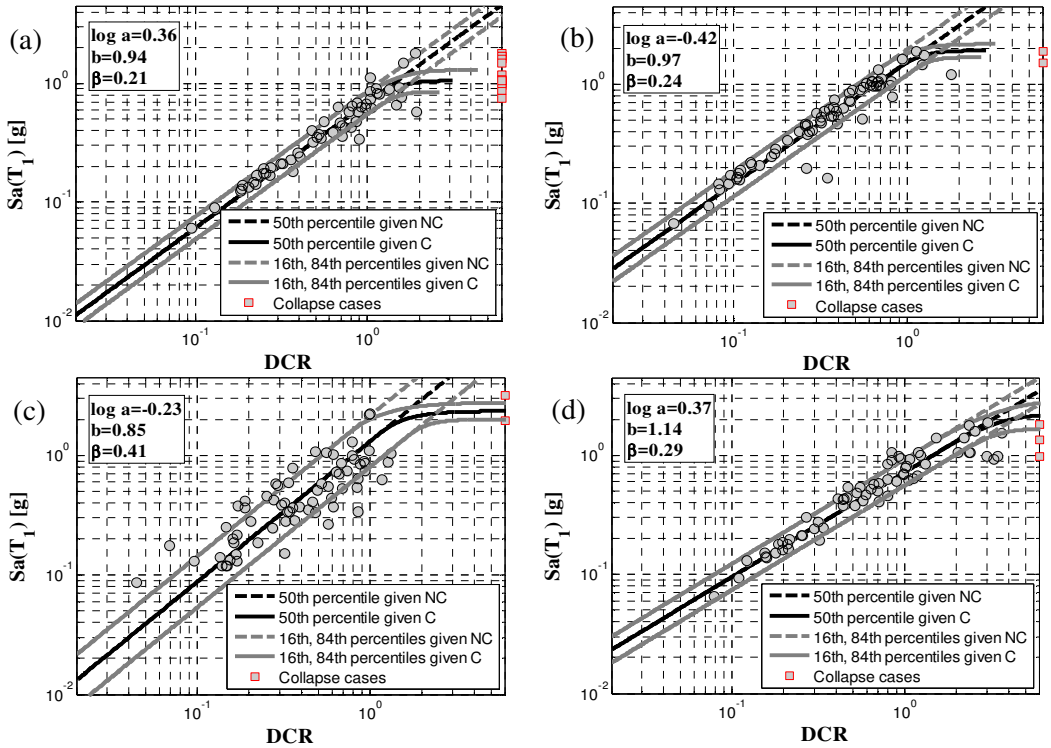

Figure 6.11: Cloud regression for *LS-PL*: (a) bare frame, (b) RC jacketing, (c) shear wall and (d) FRP wrapping.

Following the same procedure presented in detail for the longitudinal frame, the structural safety is herein verified for the transverse frame. Therefore, the

results of demand and capacity factor design (*DCFD*) seismic safety evaluation, are presented in order to verify the structural safety at each performance level. Table 6.7 shows the comparison between D_{PL} and C_{PL}, respectively, for each modeling option in each performance level. Figure 6.12 shows the fragility curves and the calculation of D_{PL} $S_a(P_o)$ and $C_{PL}=S_a^{PL}$ and the mean hazard curves (https://www.usgs.gov), used to calculate D_{PL}.

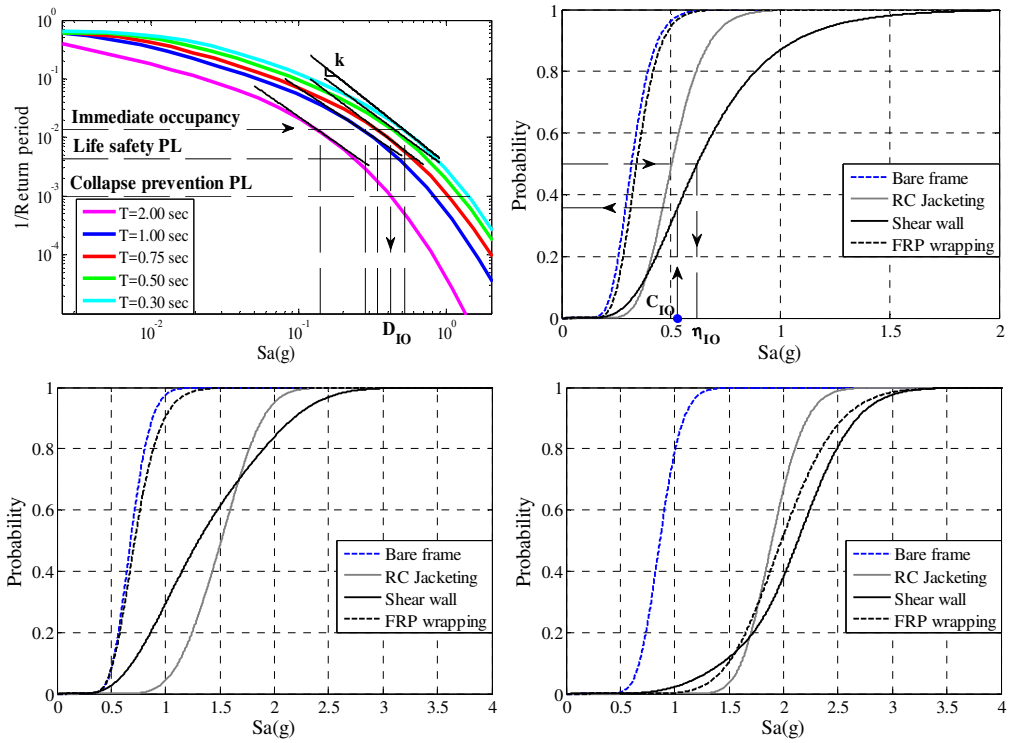

Figure 6.12: (a) Mean hazard curves; b) fragility curves for immediate occupancy performance level (*PL=IO*); b) fragility curves for life safety performance level (*PL=LS*); b) fragility curves for collapse prevention performance level (*PL=CP*).

Table 6.8: Comparison between D_{PL} and C_{PL} for each modelling option in each performance level for the transverse frame case study.

Model	$Sa\ (T_1)$ (g)	D_{IO} (g)	C_{IO} (g)	D_{LS} (g)	C_{LS} (g)	D_{CP} (g)	C_{CP} (g)
Bare frame	1.11	0.27	0.30	0.46	0.63	0.80	0.81
RC jacketing	1.01	0.28	0.47	0.48	1.43	0.84	1.84
Shear wall	0.40	0.47	0.53	0.79	1.02	1.33	1.98
FRP wrapping	1.04	0.27	0.33	0.47	0.65	0.82	1.83

6.5.3 CONSIDERING THE STRUCTURAL MODELING UNCERTAINTIES INSIDE THE FRAMEWORK

The comparison between the values of D_{PL} and C_{PL} for the bare frame shows that this frame should be safe as built and theoretically it would not need any retrofit operation. In fact, the values of C_{PL} are lightly bigger than the values of D_{PL}. The minimum ratio between C_{PL} and D_{PL} is only 1.01. This consideration is the basis to show the importance of modelling explicitly the contribution of the uncertainties related to structural parameters.

As shown in details in Chapter 5, in general, various sources of uncertainty are considered herein. In particular, the record-to-record variability (uncertainties in the representation of the ground motion), the uncertainties in the component capacity models and the uncertainties in the mechanical material properties and in the construction details (the latter is also referred to as structural "defects") are considered. The way of treating all these types of uncertainties is described in details in Chapter 5.3. In this application, only three parameters are considered as source of uncertainty: (a) the maximum shear strength, V_n; (b) the total lateral displacement, Δ_a; (c) the spacing of shear rebars, s. These three parameters are chosen out of all the other considered in the application presented in Chapter 5 because the results of that chapter show how they are some of the most important parameters in the modification of the structural response. The parameters (a) and (b) belong to the uncertainty in the component capacity models (see Chapter 5.3.1.2) and the component capacities are modelled herein as the product of predictive formulas expressed as η_{Ci} and unit-median Log Normal variables ε_{Ci} accounting for the uncertainty in component capacity [13, 49], according to the general format presented in Equation 5.1. Table 5.1 shows the two component capacity variables, considered herein, and the relative distributions. The parameter (c) belongs to the uncertainty in the material mechanical properties and in the construction details or structural defects (see Chapter 5.3.1.3). The probability distribution for the for the construction detail s is obtained using a Bayesian framework, updating the prior probability distributions with the available data for the specific case study [51], as presented in Chapter 5.3.1.3. In particular, with regard to the construction detailing parameter, s, it has been assumed herein that 50% of the inspections verify the design values indicated in

the original documents. Tables 5.3 and 5.4 shows the prior and posterior probability distribution statistics for the spacing between the shear reinforcement for the columns. Figure 5.2 (b) illustrates the prior and posterior probability distributions for the spacing between the shear reinforcement, *s*, together with updated distribution based on the hypothesis that 50% of the inspections verify the design value (s=30.5cm). The updating procedure is described in detail in [50].

However, the details of the complete methodology for considering the structural modeling uncertainties inside the probabilistic framework used in this thesis are shown in details in Chapter 5.2.

It's important to highlight that the structural modelling uncertainties are considered herein only with reference to the bare frame in order to show how a frame considered safe before the consideration of the structural modelling uncertainties can become unsafe after that explicit consideration of this type of uncertainty. However, for the retrofitted frames, the consideration of the structural modelling uncertainties is less critical, because the failure mechanisms after the retrofit operations are mainly flexural, so the contribution of the parameters considered uncertain herein becomes less decisive in the calculation of the demand and the capacity vectors. In some cases, as in the RC jacketing of the columns, in addition to the previous considerations, the spacing of the shear rebars, *s*, is designed in the retrofit option, so it is supposed to be relatively a not uncertain parameter. Anyway, a more accurate and complete assessment of all the possible source of uncertainties for the bare frame and for the retrofitted frames is out of the goals of this chapter and it can be further investigated in the future researchers.

Figure 6.13 shows as example the Cloud Analysis results for the life safety performance level for the bare frame model before and after the consideration of the structural modelling uncertainties. The figure also illustrates the 16^{th}, 50^{th} and 84^{th} percentiles of the performance variable as a function of spectral acceleration. The same procedure has been implemented also for the other two performance levels. The set of the records is the same of the one presented in Section 6.3.1.

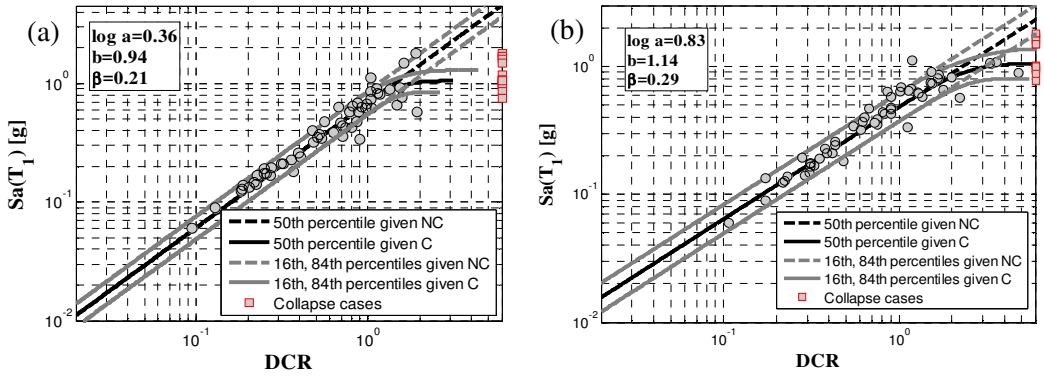

Figure 6.13: Cloud regression for *LS-PL*: (a) bare frame before the consideration of the structural modelling uncertainties; (b) bare frame after the consideration of the structural modelling uncertainties.

At this point, following the same procedure presented in details for the other case studies presented in this chapter, the structural safety is herein verified for the transverse frame after the consideration of the structural modelling uncertainties. So, the results of demand and capacity factor design (*DCFD*) seismic safety evaluation, are presented in order to verify the structural safety at each performance level. Table 6.8 shows the comparison between D_{PL} and C_{PL}, respectively, for the bare frame model before (only the record to record variability (R2R) is considered) and after (the record to record variability and the structural modelling uncertainties (R2R+SMU)) the consideration of the structural modelling uncertainties in each performance level. Figure 6.14 shows the fragility curves for each performance level (Immediate Occupancy (a), Life Safety (b), Collapse Prevention (c)) for the bare frame model before (before SMU in Figure 6.14) and after (after SMU in Figure 6.14) the consideration of the structural modelling uncertainties, showing the shift in the prediction of the capacity between the two curves. As it can be seen in Table 6.8, for the performance level of Life Safety and Collapse Prevention, the consideration of the structural modelling uncertainties modifies a condition of structural safety toward a condition of non structural safety.

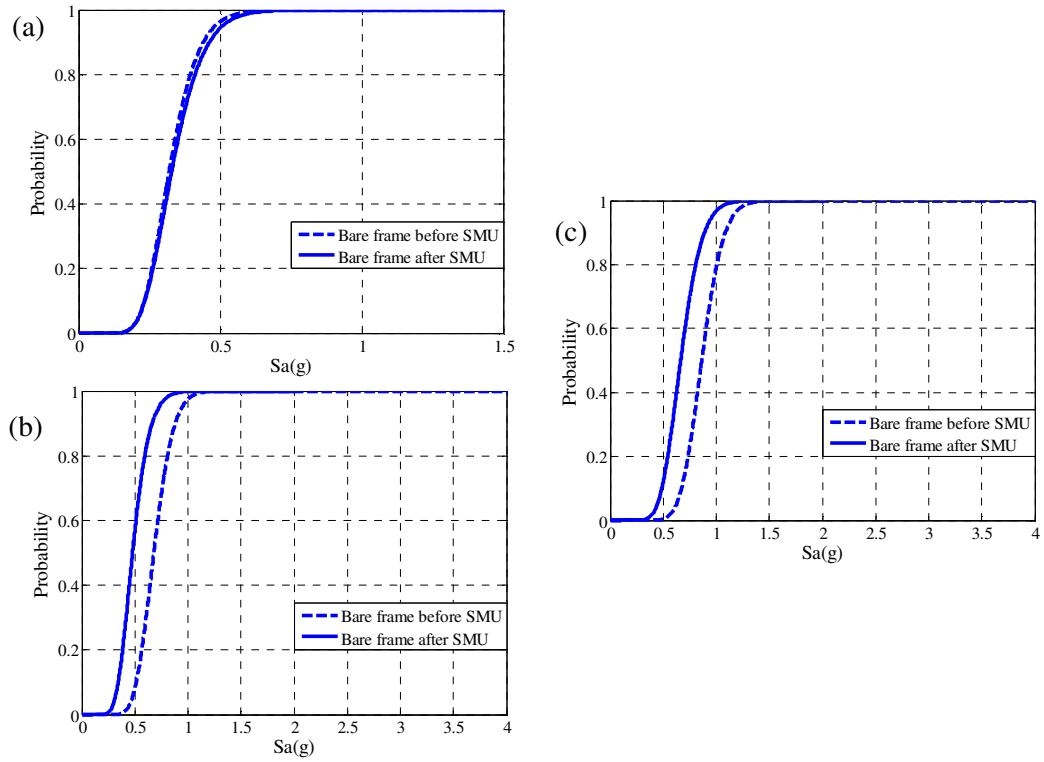

Figure 6.14: Fragility curve comparison for the bare frame model before and after the consideration of the structural modelling uncertainties: (a) immediate occupancy *PL*, (b) life safety *PL*, and (c) collapse prevention *PL*.

Table 6.9: Comparison between D_{PL} and C_{PL} for each performance level for the bare frame case study before and after the consideration of the structural modelling uncertainties.

Model	$Sa\ (T_1)$ (g)	D_{IO} (g)	C_{IO} (g)	D_{LS} (g)	C_{LS} (g)	D_{CP} (g)	C_{CP} (g)
Bare frame R2R	1.11	0.27	0.30	0.46	0.63	0.80	0.81
Bare frame R2R+ SMU	1.11	0.27	0.30	0.46	0.45	0.80	0.62

The last step of the procedure is the life cycle cost analysis. The same cost analysis parameters adopted for the longitudinal frame and presented in detail in Section 6.4 are used herein for the transverse frame. Figure 6.15 shows the expected life-cycle cost for bare frame and for the retrofitted frames, (a) before and (b) after the consideration of the structural modelling uncertainties for the bare frame.

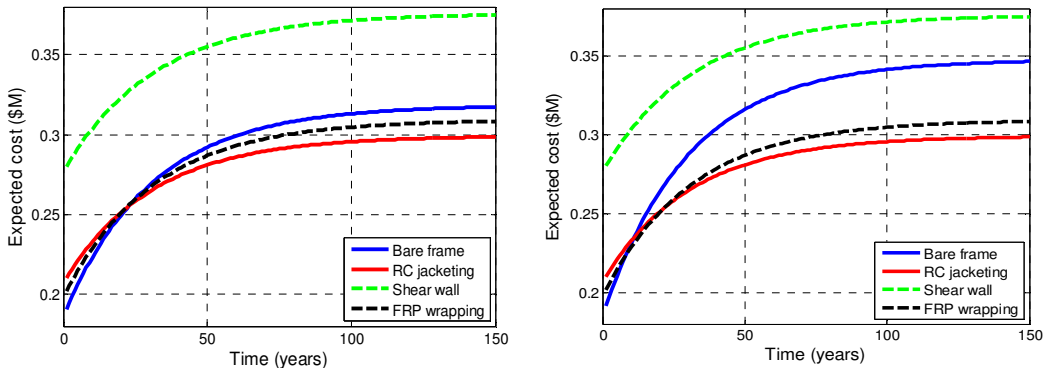

Figure 6.15: Expected life-cycle cost for bare frame and for the retrofitted frames, (a) before and (b) after the consideration of the structural modelling uncertainties for the bare frame.

It can be observed that, before the consideration of the structural modelling uncertainties for the bare frame, RC jacketing is the most convenient option economically-speaking after about 25 years, while also FRP wrapping becomes more convenient with respect to the bare frame after 25 years, while however is less convenient than the RC jacketing. In this context, the residual life should be established by the user in order to choose the best retrofit scheme. Making the assumption of a residual life greater than 25 years, RC jacketing seems to be the most suitable strategy based on life cycle cost considerations, while if the residual life is fixed to be smaller than 25 years, it seems that the best option is to don't retrofit the building frame.

Instead, after the consideration of the structural modelling uncertainties for the bare frame, FRP wrapping is the most convenient option economically-speaking after about 10 years, while RC jacketing (a) becomes the most convenient option after about 25 years. In this context, the residual life should be established by the user in order to choose the best retrofit scheme. Making the assumption of a residual life greater than 25 years, RC jacketing seems to be the most suitable strategy based on life cycle cost considerations, while if the residual life is fixed to be smaller than 25 years, FRP wrapping becomes the best retrofit scheme. Obviously, as previously discussed, the methodology for comparing the different retrofit options is implemented herein for the case study transverse frame with the goal of showing how the consideration of the structural modelling uncertainties in addition to the record to record variability can modify the results. However, as

presented in details in this chapter for the case study longitudinal frame, each retrofit strategy should be subjected to an iterative process, considering different schemes for each retrofit strategy in order to find better solutions, as it is necessary in a real decision making process.

6.6 CONCLUSIONS

In this chapter, a nonlinear performance based methodology is proposed to assess and compare different retrofit methods considering also life cycle cost analysis. The proposed methodology requires nonlinear dynamic analysis of the structures and development of fragility curves at the selected performance levels. To demonstrate the assessment process, alternative retrofit methods are compared for a case study, that is a longitudinal frame of an existing building, modeled considering the effect of flexural-shear-axial load interaction to capture column shear and axial failures. As nonlinear dynamic analysis, Cloud Analysis is used since it is particularly efficient, involving nonlinear analyses of the structure subjected to a set of un-scaled ground motion time histories. A framework for probability-based demand and capacity factor design (*DCFD*) seismic safety evaluation is implemented in order to verify the structural performance and safety at each chosen performance level.

The optimal retrofit strategy is chosen by comparing the expected loss during the service life of the structure for each retrofit option that satisfies structural safety requirements for a given performance level. However, for the case study longitudinal frame as the source of uncertainty, only the record-to-record variability, which is proved to be the dominant source of uncertainty, is considered herein. Based on the consideration that for existing buildings, the structural modeling uncertainties might be able to shift the results in terms of which retrofit strategy would be optimal, this issue is briefly investigated at the end of the chapter with reference to the case study transversal frame. It is showed how the consideration of the structural modeling uncertainties in addition to the record to record variability can modify the results (e.g. as in the case study for which a structural safety condition is shifted to a structural non safe condition).

Definitively, the main goals achieved in this chapter can be summarized as:

- A critical process is proposed to evaluate the effectiveness of different retrofit methods using a performance based approach.
- The proposed methodology requires detailed and accurate modeling of materials and beam-column frame members to capture the flexure, the shear and the flexure-shear failure modes in columns and potential collapse of the building frame.
- The proposed methodology proposes the critical demand to capacity ratio (DCR_{PL}) as structural performance parameter at each performance level and involves nonlinear dynamic analysis procedures using unscaled ground motions (Cloud Analysis).
- The proposed methodology can be used to select the optimal retrofit strategy by comparing the loss expected during the service life based on risk-related safety-checking criteria. In particular, the methodology identifies the most economic retrofit solution that satisfies structural safety requirements for a given performance level. The only compatibility requirement among alternative retrofit solutions is a uniform definition of the onset of performance level(s). Retrofit design criteria such as target drift capacity (adopted in this work) and target strength are very helpful in terms of feeding an intelligent "first guess" into the procedure. Such a first guess is going to be assessed based on performance-based criteria. In other words, the performance-based retrofit assessment procedure rules out the proposed strategies that do not meet the code-based (or desirable) structural safety criteria. In conclusion, the whole performance-based procedure can be formalized as an optimization procedure that minimizes/maximizes a utility function (e.g., economic losses, functional benefits, etc.) and satisfies code-based (or desirable) safety constraints.

6.7 REFERENCES

[1] Sezen, H., Whittaker, A., Elwood, K., and Mosalam, K, 2003. Performance of reinforced concrete buildings during the August 17, 1999 Kocaeli, Turkey earthquake, and seismic design and construction practise in Turkey, Engineering Structures, 25(1), 103-114.

[2] Liel, A.B., Haselton, C.B., Deierlein, G.G., and Baker, J.W., 2009. Incorporating modeling uncertainties in the assessment of seismic collapse risk of buildings, Structural Safety, 31(2), 197-211.

[3] Zareian, F., and Krawinkler, H., 2007. Assessment of probability of collapse and design for collapse safety, Earthquake Engineering & Structural Dynamics, 36(13), 1901-1914.

[4] Eads, L., Miranda, E., Krawinkler, H., and Lignos, D.G., 2013. An efficient method for estimating the collapse risk of structures in seismic regions. Earthquake Engineering & Structural Dynamics, 42(1), 25-41.

[5] Moehle, J.P., 2000. State of research on seismic retrofit of concrete building structures in the US. In US-Japan symposium and workshop on seismic retrofit of concrete structures.

[6] Thermou, G.E., and Elnashai, A.S., 2006. Seismic retrofit schemes for RC structures and local-global consequences, Progress in Structural Engineering and Materials, 8.1: 1-15.

[7] Celik, O.C. and Ellingwood, B.R., 2010. Seismic fragilities for non-ductile reinforced concrete frames–Role of aleatoric and epistemic uncertainties, Structural Safety 32(1), 1-12.

[8] Jeong, S.H., Mwafy, A.M., and Elnashai, A.S., 2012. Probabilistic seismic performance assessment of code-compliant multi-story RC buildings, Engineering Structures, 34, 527-537.

[9] Zareian, F., Kaviani, P., and Taciroglu, E., 2015. Multiphase Performance Assessment of Structural Response to Seismic Excitations, Journal of Structural Engineering, 141(11), 04015041.

[10] Aslani, H., and Miranda, E., 2005. Probabilistic earthquake loss estimation and loss disaggregation in buildings, dissertation, Stanford University.

[11] Goulet, C.A., Haselton, C.B., Mitrani-Reiser, J., Beck, J.L., Deierlein, GG., Porter, K. A., and Stewart, J.P., 2007. Evaluation of the seismic performance of a code-conforming reinforced-concrete frame building-from seismic hazard to collapse safety and economic losses. Earthquake Engineering & Structural Dynamics, 36(13), 1973-1997.

[12] Liel, A.B. and Deierlein G.G., 2013. Cost-benefit evaluation of seismic risk mitigation alternatives for older concrete frame buildings, Earthquake Spectra, 29(4), 1391-1411.

[13] Cornell, C.A., Jalayer, F., Hamburger, R.O., and Foutch, D.A., 2002. Probabilistic basis for 2000 SAC federal emergency management agency

steel moment frame guidelines, Journal of Structural Engineering, 128(4), 526-533.

[14] Jalayer F., and Cornell C.A., 2003. A technical framework for probability-based demand and capacity factor design (DCFD) seismic formats, Technical Report PEER 2003/08, Berkeley, USA.

[15] Shome N., Cornell C.A., Bazzurro P., and Carballo J.E., 1998. Earthquakes, records, and nonlinear responses, Earthquake Spectra, 14(3), 469-500.

[16] Vamvatsikos, D., and Cornell, C.A., 2002. Incremental dynamic analysis, Earthquake Engineering & Structural Dynamics, 31(3), 491-514.

[17] Baker, J.W., and Cornell, C.A., 2005. A vector-valued ground motion intensity measure consisting of spectral acceleration and epsilon, Earthquake Engineering & Structural Dynamics 34(10), 1193-1217.

[18] Jalayer, F. and Cornell C.A., 2009. Alternative non-linear demand estimation methods for probability-based seismic assessments, Earthquake Engineering & Structural Dynamics, 38(8), 951-972.

[19] Jalayer, F., De Risi, R., and Manfredi, G., 2015. Bayesian Cloud Analysis: efficient structural fragility assessment using linear regression, Bulletin of Earthquake Engineering, 13(4), 1183-1203.

[20] Jalayer, F., Ebrahimian, H., Miano, A., Manfredi, G., and Sezen H., 2017. Analytical fragility assessment using un-scaled ground motion records, Earthquake Engineering & Structural Dynamics, https://doi.org/10.1002/eqe.2922.

[21] Jalayer, F., Franchin, P., and Pinto, P., 2007. A scalar damage measure for seismic reliability analysis of RC frames. Earthquake Engineering & Structural Dynamics, 36(13), 2059-2079.

[22] American Society of Civil Engineers (ASCE), 2013. Seismic Evaluation and Retrofit of Existing Buildings, ASCE/SEI 41-13, Reston, VA, 2014.

[23] Islam, M.S., 1996. Analysis of the Northridge earthquake response of a damaged non-ductile concrete frame building, The structural design of tall buildings, 5(3), 151-182.

[24] Browning, J., Li, Y.R., Lynn, A., and Moehle, J.P., 2000. Performance assessment for a reinforced concrete frame building, Earthquake Spectra, 16(3), 541-555.

[25] Krawinkler, H., 2005. Van Nuys hotel building testbed report: exercising seismic performance assessment, Technical Report PEER 2005/11, Berkeley, USA.

[26] Miano, A., Sezen, H., Jalayer, F., Prota, A. Performance based assessment methodology for retrofit of buildings. *Earthquake Spectra*, (Under Review).

[27] Miano, A., Sezen, H., Jalayer, F., and Prota, A., 2017. Performance based comparison of different retrofit methods for reinforced concrete structures. In: Proceedings of the 6th ECCOMAS Thematic Conference on Computational Methods in Structural Dynamics and Earthquake Engineering (COMPDYN 2017), Rhodes, Greece, 15-17 June 2017.

[28] Miano, A., Sezen, H., Jalayer, F., and Prota, A., 2017. Probability based comparison of retrofit methods for existing nonductile concrete frames. In: Proceedings of the 4th Thematic Conference on Smart Monitoring, Assessment and Rehabilitation of Civil Structures (SMAR 2017), Zurich, Switzerland, 13-15 September 2017.

[29] Ditlevsen, O., and Madsen, H.O. Structural reliability methods. Wiley: New York, 1996.

[30] Galanis, P. H., and Moehle, J. P., 2015. Development of Collapse Indicators for Risk Assessment of Older-Type Reinforced Concrete Buildings, Earthquake Spectra, 31(4), 1991-2006.

[31] Shome, N., and Cornell, C.A., 1999. Probabilistic seismic demand analysis of nonlinear structures. Report No. RMS35, Stanford University, CA.

[32] Jalayer, F., Carozza, S., De Risi, R., Manfredi, G., and Mbuya, E., 2016. Performance-based flood safety-checking for non-engineered masonry structures, Engineering Structures, 106, 109-123.

[33] Setzler, E.J., and Sezen, H., 2008. Model for the lateral behavior of reinforced concrete columns including shear deformations, Earthquake Spectra, 24(2), 493-511.

[34] Sezen, H., 2008. Shear deformation model for reinforced concrete columns, Structural Engineering and Mechanics, 28(1), 39-52.

[35] Cornell, C.A. and Krawinkler H., 2000. Progress and challenges in seismic performance assessment. PEER Center News, 3(2), 1-2.

[36] Fardis, M.N., 2009. Seismic design, assessment and retrofitting of concrete buildings based on EN-Eurocode 8. Vol. 8, Springer Science & Business Media.

[37] American Concrete Institute (ACI), 2014. Building Code Requirements for Structural Concrete, ACI 318-14, Farmington Hills, MI.

[38] Eurocode 8, 2007. Design of structures for earthquake resistance, EN 1998-1 CEN Brussels, 2007.

[39] Linee guida per la Progettazione, l'Esecuzione ed il Collaudo di Interventi di Rinforzo di strutture di c.a., c.a.p. e murarie mediante FRP, 2009 - Guidelines for Design, Execution and Test of retrofit interventions for concrete and masorny structures using FRP.

[40] McKenna, F., 2011. OpenSees: a framework for earthquake engineering simulation, Computing in Science & Engineering, 13(4), 58-66.

[41] FEMA 356, 1997. Prestandard and Commentary for the Seismic Rehabilitation of Buildings, Washington (DC), 1997.

[42] Ancheta, T.D., Darragh, R.B., Stewart, J.P., Seyhan, E., Silva, W.J., Chiou, B.S.-J., Wooddell, K.E., Graves, R.W., Kottke, A.R., and Boore, D.M., 2014. NGA-West2 database. Earthquake Spectra, 30(3), 989-1005.

[43] Wen, Y.K., 2001. Reliability and performance-based design, Structure Safety, 23(4), 407-428.

[44] Vitiello, U., Asprone, D., Di Ludovico, M., and Prota, A., 2017. Life cycle cost optimization of the seismic retrofit of existing RC structures, Bulletin of Earthquale Engineering, 15.5, 2245-2271.

[45] Comerio, M.C., 2006. Estimating downtime in loss modeling, Earthquake Spectra, 22.2, 349-365.

[46] Ebrahimian, H., Jalayer, F., and Manfredi G., 2015. Seismic retrofit decision-making of bridges based on life-cycle cost criteria, in Proceedings, 5th ECCOMAS Thematic Conference on Computational Methods in Structural Dynamics and Earthquake Engineering, Crete, Greece, 25-27 May 2015.

[47] Jalayer, F., Asprone, D., Chiodi, R., Prota, A., and Manfredi, G., 2012. Seismic Retrofit Decision-Making based On Life Cycle Cost Criteria, in Proceedings, 15th Word Conference on Earthquake Engineering, Lisbon, Portugal, 24-28 September 2012.

[48] FEMA, HAZUS-MH., 2003. MR3 Technical Manual. Multi-hazard Loss Estimation Methodology Earthquake Model, Washington (DC), 2003.

[49] Jalayer, F., 2003. Direct Probabilistic seismic analysis: implementing non-linear dynamic assessments. Ph.D. dissertation, Stanford University, California.

[50] Jalayer, F., Elefante, L., Iervolino, I., and Manfredi, G., 2011. Knowledge-based performance assessment of existing RC buildings. Journal of Earthquake Engineering; 15 (3): 362-389.

[51] Jalayer, F., Iervolino, I., and Manfredi, G., 2010. Structural modeling uncertainties and their influence on seismic assessment of existing RC structures. Structural Safety; 32 (3): 220-228.

Chapter 7

CONCLUSIONS

The scope of this thesis is to propose a journey through probabilistic performance based assessment and retrofit design based on nonlinear dynamic analysis tools. The thesis aims to address the performance-based assessment paradigm by developing seismic fragilities and earthquake loss estimation. In the context of the "Performance-based earthquake engineering" (PBEE), an important focus in this thesis is dedicated to the estimation of the conditional probability of exceeding a damage measure DM expressed as critical the demand to capacity ratio throughout the structure and a given ground motion time-history and relating it directly to IM (by collapsing the intermediate EDP step). The conditional probability of exceeding a given level of DM given IM can be expressed as the structural fragility for a given performance level. In fact, the accurate identification of the level of performance through the assessment of analytic structural fragility for existing buildings is one of the fundamental steps in the modern performance-based engineering.

The central point of the thesis is related to the non-linear dynamic analysis procedure known as Cloud Analysis. This analysis is based on fitting a linear regression model in the logarithmic scale to the pairs of structural response parameter (e.g., maximum inter-story drift) and IM (e.g., first-mode spectral acceleration) for a suite of as-recorded ground motions. This method is well-known both for the simplicity of its underlying formulation and for the relatively small number of structural analyses required.

A functional variation to the original Cloud Analysis is presented in Chapter 3 in order to take into account the cases leading to structural collapse. Moreover, to reduce record-selection-dependence of the results, a Bayesian version of the Cloud Analysis considering the "collapse-cases" is presented in which the

uncertainty in the structural fragility model parameters is considered. This leads to a Robust Fragility estimate and a desired confidence interval defined around it.

The entire method is based on the adoption of a normalized demand to capacity ratio as the damage measure/decision performance variable. In particular, a normalized demand to capacity ratio coined as "critical demand to capacity ratio" and denoted as *DCR*, takes the structure closest to the onset of a prescribed limit state *LS*, is adopted. In fact, Cloud Analysis can lead to very good fragility estimates on two conditions: (1) the ground motion records are chosen carefully; and (2) a scalar *DCR* that is always equal to one at the onset of the limit state is adopted as the performance variable. Two simple rules are defined for records selection: (1) make sure that a significant portion of the records leads to *DCR* greater than one; and (2) make sure that the suite of records covers a wide range of seismic intensity levels. Satisfying the above-mentioned rules almost always entails the presence of records that lead the structure into collapse. Therefore, the original simple logarithmic regression fragility model is extended into a five-parameter fragility model, which is created analytically as a mix of linear logarithmic regression and logistic regression. These parameters are estimated through Bayesian inference adopting a Markov Chain Monte Carlo simulation procedure which leads to a "Robust" Fragility and its plus/minus k standard deviation confidence band (e.g., k=2) that consider the uncertainties in fragility parameters. Two different benchmarks are set: fragility obtained based on the IDA (the records are scaled) and fragility obtained based on MSA with variable conditional spectrum-compatible records per intensity levels (again scaling is tolerated within a certain limit). The methods are demonstrated using three frames representing shear-critical, shear-critical/flexure-dominated and flexure-dominated behaviour.

It is observed that the difference with IDA-based and MSA-based fragilities are almost always contained within the plus/minus two standard deviation confidence intervals. For the shear-critical and shear-critical/flexure-dominated frames, the Robust Fragility obtained from Cloud Analysis-based fragility is very close to that obtained based on MSA while IDA-based fragility seems somehow more distant. The MSA results picture the flexure-dominated frame as an almost invincible structure; a result that is obtained based on ground motion records that have not physically occurred. In this case, the Cloud Analysis results lie

somewhere in between the MSA and IDA results (that remain particularly conservative). Moreover, comparison of two sets of records containing 34 and 70 records further emphasizes the importance of populating adequately all intensity levels with data points. It is also worth mentioning that the Bayesian parameter estimation procedure based on Markov Chain Monte Carlo is particularly useful for providing the confidence intervals for the Robust Fragility curve and for capturing the correlation between various fragility parameters. This work, done for the limit state of Near-Collapse, can be performed for any other limit state/performance level.

The adoption of DCR_{LS} as performance variable is also central to a new nonlinear dynamic analysis procedure referred to as "*Cloud to IDA*" (presented in Chapter 4), that exploits the Cloud Analysis to perform IDA in a more efficient manner. This procedure is an efficient solution for performing IDA, based on the consideration that the intensity levels to scale should be chosen strategically to scaling in a strictly necessary manner the records. In particular, *Cloud to IDA* is proposed as an efficient procedure with limited scaling of ground motion records that exploits the results of a simple Cloud Analysis for carrying out incremental dynamic analysis (IDA). In general, the procedure is applicable when the adopted EDP is expressed in terms of a normalized *DCR* (in Chapter 4 the critical *DCR*) that is equal to unity at the onset of the limit state.

There is indeed a natural link between Cloud and IDA procedures. The Cloud data can be viewed as the first points on the various IDA curves. On the other hand, an IDA curve can be obtained theoretically with only two data points, consisted of pairs of intensity versus critical demand to capacity values, if the interval of values covered by the two points covers the demand to capacity ratio equal to one. In the *Cloud to IDA* procedure, the intensity levels to scale to are chosen strategically with the aim of performing the minimum number of analyses and minimum amount of scaling necessary. To this end, one can exploit the simple linear (logarithmic) regression predictions made based on the results of the structural analysis to the un-scaled registered records (a.k.a., Cloud Analysis) to choose landmark IM levels for scaling. Therefore, those records that are going to be potentially scaled up/down by a factor close to unity are identified from the pool of original records in order to avoid excessive scaling of the records (the *Reduced sets 1* and *2* in Chapter 4).

The results indicate that the risk estimates obtained based on the *Reduced sets 1* and *2* are very close to those obtained based on the Cloud Analysis considering the collapse cases and MSA based on varying suits of CS-compatible records (the "best-estimate" herein). The same observation holds when comparing the statistics of the corresponding fragility curves. This is while the IDA-based fragility reveals a slight shift to the left compared to the other more "scaling-conscious" methods. Nevertheless, the risk results obtained are in overall good agreement between the alternative dynamic analysis methods. Moreover, this work employs the Robust Fragility concept to consider the uncertainty in the estimation of fragility model parameters. The definition of an error margin for the estimated fragility makes it possible to quantify the difference between the fragility curves obtained based on alternative dynamic procedures in terms of the number of standard deviations. Moreover, it allows for mapping the confidence band for the fragility to the risk level.

In synthesis, the proposed *Cloud to IDA* procedure leads to results (in terms of risk) very close to the "best-estimate" MSA with varying suits of CS-compatible records, when specific attention is made to choose records that require limited scaling. On the other hand, the proposed procedure lead to results that are identical to IDA, when the same set of records are used. All of this is possible with a number of analyses that is sensibly lower (almost an order of magnitude) with respect to IDA and MSA. It is worth emphasizing that the use of DCR_{LS} as the performance variable directly is indispensable for the proposed *Cloud to IDA* procedure.

Chapter 5 deals with the quantification of the impact of structural modelling uncertainty on the seismic performance assessment for existing building. The modified version of Cloud Analysis, that considers the (eventual) cases of global dynamic instability, based on coupling the simple regression in the logarithmic space of structural response versus seismic intensity for a suite of registered records with logistic regression, is implemented to propagate both record-to-record variability and the structural modeling uncertainties. For each of the registered records within the suite of ground motion records, a different realization of the structural model is generated through a standard Monte Carlo Simulation procedure. Also here, the Bayesian version of the Cloud method, in which the uncertainty in the structural fragility model parameters is considered,

is implemented to have a Robust Fragility estimate and a desired confidence interval defined around it.

It is observed that, for the case study longitudinal frame of the Van Nuys Holiday Inn Hotel, Cloud-based Robust Fragility curve with the consideration of both record-to-record variability and structural modelling uncertainties leads to a reduction both in median and in the dispersion of the fragility curve with respect to the Cloud-based fragility considering only record to record variability. Moreover, the Cloud-based Robust Fragility curve is very close to the results provided by IDA-based LHS and MVFOSM fragility curves, while the computational effort is sensibly lower. These observations refer to the specific case study and additional comparisons needed to validate these results. Based on the site-specific hazard, it can be noted that the difference between the Cloud-based Robust Fragility curve and the IDA based fragility curves obtained using the LHS and the MVFOSM approach are more accentuated in the zone of very small hazard values. Thus, it can be noted that Cloud-based Robust Fragility curves (with 34 or 70 realizations through standard MC simulation or LHS sampling) with their plus/minus two standard deviation confidence bands provide reliable results in term of risk with respect to IDA-based LHS and MVFOSM fragility curves. Consequently, and with specific reference to the case-study frame, the Cloud-based Robust Fragility procedures provides --in an extremely efficient manner-- reliable risk estimates.

Finally, in Chapter 6, the PBEE methodology is implemented for the case-study building in order to choose the most appropriate seismic retrofit design that maximizes the utility (by minimizing the expected costs) and satisfies the safety-checking for three different performance levels. The case study nonductile longitudinal frame of the Van Nuys Holiday Inn Hotel is retrofitted based on different strategies, used to improve the seismic performance of the frame.

The moment resisting frame is modeled using structural elements with fiber cross sections. Particular attention is dedicated to the modeling of the flexural-shear-axial interactions. A suitable procedure is used to address critical modeling issues while predicting the response accurately and keeping overall computational process simple with easy implementation. This procedure has the goal to predict an envelope of the cyclic lateral response that includes the lateral displacement and corresponding strength predictions at the peak strength, onset of lateral

strength degradation, and loss of axial-load-carrying capacity. The model also considers the rigid body rotation of the column due to slip of column longitudinal bars from the anchoring concrete (not accounted for in flexural analysis). Deformations due to flexure, reinforcement slip, and shear are modeled individually using existing and new models. Specific rules have been set in order to predict the flexure critical, shear critical and flexure-shear critical failure mechanisms of the members. This model has the advantages to create a comprehensive and rigorous procedure in order to classify and analyse the structural members. In particular, the selected approach allows for explicit modeling of flexure-shear-axial load interaction based on simple sectional analysis. This is an accurate yet simple approach to model potential collapse and flexure-shear damage in nonductile columns.

A nonlinear performance based methodology is proposed to assess and compare different retrofit methods, considering hazard level, target performance levels, and also life cycle cost estimates. The methodology proposes the critical demand to capacity ratio for each performance level (DCR_{PL}) as structural performance parameter and requires nonlinear dynamic analysis (Cloud Analysis is used in this work) of the structures and development of fragility curves at the selected performance levels. A framework for probability-based demand and capacity factor design (*DCFD*) seismic safety evaluation is implemented in order to verify the structural performance and safety at each chosen performance level. It's to note that, for the case study longitudinal frame as the source of uncertainty, only the record-to-record variability, which is proved to be the dominant source of uncertainty, is considered herein. Based on the consideration that, for existing buildings, the structural modeling uncertainties might be able to shift the results in terms of which retrofit strategy would be optimal, this issue is briefly investigated at the end of Chapter 6 with reference to the case study transversal frame of the same existing building. It is showed how the consideration of the structural modeling uncertainties in addition to the record to record variability can give more accurate results.

Definitively, retrofit design criteria such as target drift capacity (adopted in this work) and target strength are very helpful in terms of feeding an intelligent "first guess" into the procedure. Such a first guess is going to be assessed based on performance-based criteria. In other words, the performance-based retrofit

assessment procedure rules out the proposed strategies that do not meet the code-based (or desirable) structural safety criteria. In fact, the whole performance-based procedure can be formalized as an optimization procedure that minimizes/maximizes a utility function (e.g., economic losses, functional benefits, etc.) and satisfies code-based (or desirable) safety constraints. Based on such a premise, the optimal retrofit strategy is chosen by comparing the expected loss during the service life of the structure for each retrofit option that satisfies structural safety requirements for a given set of performance levels. The only compatibility requirement among alternative retrofit solutions is a uniform definition of the onset of performance level(s). Amongst the viable retrofit designs that satisfy the risk-related safety-checking *DCFD* criteria, the one that corresponds to the minimum expected loss over the life cycle of the building is identified.